# Role of protein and DNA damage in biological response to radiation and aging

**Kuzmić, Mira**

**UNIVERSITY OF SPLIT**
**SCHOOL OF MEDICINE**

**MIRA KUZMIĆ**

# ROLE OF PROTEIN AND DNA DAMAGE IN BIOLOGICAL RESPONSE TO RADIATION AND AGING

**DOCTORAL DISSERTATION**

**Split 2018.**

**UNIVERSITY OF SPLIT**
**SCHOOL OF MEDICINE**

**MIRA KUZMIĆ**

# ROLE OF PROTEIN AND DNA DAMAGE IN BIOLOGICAL RESPONSE TO RADIATION AND AGING

**DOCTORAL DISSERTATION**

**Split 2018.**

**SVEUČILIŠTE U SPLITU**
**MEDICINSKI FAKULTET**

**MIRA KUZMIĆ**

# ULOGE OŠTEĆENJA PROTEINA I DNK U BIOLOŠKOM ODGOVORU NA ZRAČENJE I STARENJE

**DOKTORSKA DISERTACIJA**

**Split 2018.**

The doctoral dissertation was conducted in:

- The Mediterranean Institute for Life Sciences (MedILS) in Split, Croatia

- Institut de Radioprotection et de Sûreté Nucléaire (IRSN) in Cadarache, France

Supervisors:

Prof. Dr. Sc. Miroslav Radman and Dr. Sc. Sandrine Frelon

# ACKNOWLEDGEMENTS

*I am first and foremost indebted to my mentors, Prof. Miroslav Radman and Dr. Sandrine Frelon, for their proficiency and scientific contributions to this thesis. Also, they taught me an array in different scientific approaches, general and detailed ones, and for that I am deeply grateful. I must also thank Dr. F. Paquet, Dr. L. Blanchard, Dr. B. Bernard and Dr. C. Lecomte for very kindly revising my thesis; and Prof. M. Glavina-Durdov and Prof. D. Ljutić for their valuable help. I would like to thank especially A. Perger for proofreading my thesis. In addition, I am very grateful to Prof. S. Galas for some important directions during my thesis and to Dr. H. Javot for imparting, so kindly and effortlessly, her expert knowledge. I do not exaggerate when I say it was a blessing for my thesis, articles and scientific career. Finally, a very special thank you to my dissertation committee members, Prof. E. Vrdoljak, Prof. T. Zemunik and Prof. M. Merćep, for their immensely useful corrections and revisions of my thesis (subject and the dissertation).*

*In addition, I would also like to express my gratitude to many people who in their various ways helped me come to the end of this exciting academic journey. At MedILS in Croatia these are: Jelena, Irena, Željka, Prosper and Ljilja – thank you for always being so kind to me and for being there for me when I needed your help; Marjan, Anita, Fernando, Mladen, Romain, Marina, Lara, Tea, Steve, François-Xavier for giving me scientific advice and directions that were of crucial importance –although some of you are not at MedILS anymore, I am honored to have met you. At IRSN in France there are also many people who have been a significant part of my thesis and to whom I owe my gratitude: Jacqueline, who started the collaboration with Miro and opened the doors of IRSN to me; Catherine, Rodolphe, and Christelle for welcoming me so kindly at IRSN; all of my colleagues at IRSN (and forgive me if I forget to mention some of you): the ISATIS team with Cécile, Sébastien, Ingrid, and Rémi, and others: Antoine, Amine, Kewin, Lucy, Nico, Magali, François, Terramage and Clara– thank you for your kindness and help in difficult moments. Finally, I would like to thank the people from my doctoral study "Biology of Neoplasms" who administered this thesis from beginning to the end: Marita, Julija and Ines – thank you for being there for me. I must thank my wonderful colleagues: Nikolina, Srki, Gašpar, Mirko, Marija and others – you have been great companions to me on my journey and I am proud and grateful to call some of you my personal friends.*

*There are several more people from different institutions who have also contributed to this thesis with their support and depth of knowledge: MC. Thibaut at The French Alternative Energies and Atomic Energy Commission in Cadarache; A. Badache and P. Verdier-Pinard at the Cancer Research Center of Marseille in France; and M. Dolinar at The Faculty of Chemistry and Chemical Technology of the University of Ljubljana in Slovenia, whom I could never thank enough for his kind and helpful advice.*

*And last, a very special thank you to my family, friends and my boyfriend for their tremendous support and understanding during my journey. My little sister, Dr. M. Čikeš, has helped me with the abstract and made it wonderful; thank you, sis, for being so versatile in our mother tongue. There are no adequate words – and not enough space here – to express how grateful I am to my mother for all her love, support and strength. As for my father, I hope his frail health will serve him long enough to see his daughter become a "proper" doctor of science.*

# TABLE OF CONTENTS

# LIST OF FIGURES

# LIST OF TABLES

# ABBREVATION LIST

**D**

DBD-FISH – DNA breakage detection-fluorescence *in situ* hybridization

*D. radiodurans* – *Deinococcus radiodurans*

DNPH – 2,4-dinitrophenylhydrazine

DSBs – double strand breaks

DSC – dose-response curve

**C**

CEZ – Chernobyl exclusion zone

**E**

$EDR_{10}$ – dose rate that has 10 % effect on species

ELISA – enzyme-linked immunosorbent assay

**F**

FRTA– free-radical theory of aging

**G**

Gy – Gray

**H**

HPLC-MS – high performance liquid chromatography-mass spectrometry

**I**

IHC – immunohistochemistry

IR – ionizing radiation

**L**

LET –linear energy transfer

**M**

MMR – Mismatch repair

M9t – M9 buffer supplemented with $10^{-5}$ triton

mTOR – mechanism of target of rapamycin

**O**

OD – optical density

**P**

PC – protein carbonylation

PFA – paraformaldehyde

PFGE – pulsed-field gel electrophoresis

PTM – post-translational modification

**R**

ROS – reactive oxygen species

RRO – radiation-resistant organisms

**S**

SG II – SYBR Green II

SSBs – single strand breaks

Sv – Sieverts

**T**

tDr – time for DNA repair

TUNEL – terminal deoxynucleotidyl transferase dUTP nick-end labeling

**U**

UVR – ultraviolet radiation

# PART I: GENERAL CONTEXT

Discovery of DNA as the carrier of genetic information and its structure **[1]** transformed biology and biomedical research, and the latter became focused on a genome. It is now believed that through DNA sequence most or all can be diagnosed and treated **[2]**. Therefore, DNA mutation has been established as a diagnostic and prognostic biomarker, especially in cancer as one of the leading causes of morbidity and mortality **[3]**. Genotoxic effect of ionizing radiation was held as the primary cause of radiation-induced cell death and diseases **[4]**.

However, DNA is not the only biomolecule damaged by ionizing and UV radiation. Other key biological macromolecules are subject to oxidative damage by radiation, notably proteins **[5]**, lipids **[6]** and RNA **[7]**. In addition, epigenetics features as an important player in the expression of cellular phenotypes **[8]**. Proteins are functional molecules of the organisms and are sensitive to endogenous and exogenous damaging agents. However, there are few mechanisms of the clearance of damaged proteins, e.g. proteasomal degradation and autophagy of aggregated proteins (lysosome) **[9]**, whereas protein oxidative damage (i.e. carbonylation) was found to correlate with cellular aging and death **[10]**.

Protein carbonylation is an irreversible and irreparable oxidative damage **[11]** with deleterious biological consequences. In *E. coli*, lethal hit corresponds to 5 million protein carbonyls per cell **[5]**. Protein carbonylation has been used as a biomarker of oxidative stress and aging **[12]**. High UV doses lead to rapid aggregation of carbonylated proteins **[13]** and resistance to proteolysis. In spite of numerous protocols, highly oxidized aggregated proteins **[14]** make quantification of damaged proteins difficult. Recently, there was a significant methodological improvement yielding robust quantitative relationship between highly carbonylated proteins and high UV doses **[15]**. Nevertheless, quantification of protein carbonylation as a biomarker of aging and low-dose radiation damage still needs improvement. This thesis is a contribution to the methodological improvement of the monitoring of protein carbonylation and an attempt to tackle the question of causality versus correlation, in regards to biological and phenotypic consequences of radiation exposure, i.e. longevity modification and death.

# PART II: INTRODUCTION

# Chapter 1: Radiobiology

## 1.1. Background

### 1.1.1. Discovery and definition of radiobiology

Radiobiology was first introduced as a discipline in medical sciences in 1896 by Leopold Freund who conducted a therapeutic treatment of a hairy mole with X-rays (discovered in 1895 by Wilhelm Röntgen) **[16]**. Several weeks after Röntgen's discovery of X-ray, Ivan Romanovich Tarkhanov demonstrated deleterious effects of irradiated frogs and insects, which confirmed the birth of radiobiology **[17]**. In 1898 Marie Skłodowska Curie and her husband Pierre Curie discovered the radioactive polonium and radium. Marie Curie was a pioneer in the studies on radioactivity, which was discovered by H. Becquerel. In 1903 Pierre Curie suggested that radium that penetrates bone better than x-rays and induces deep flesh burns could be used in cancer treatment **[18]**. Finally, radiobiology is a dual scientific discipline (radiation physics and biology) that studies interaction of ionizing radiation (IR) with living matter and the biological consequences upon organisms **[19]**.

### 1.1.2. Radioactivity

IR separates from non-ionizing radiation at approximately 10 eV, which is the ionization energy of oxygen atom. Radioactivity represents the energy released and emitted from unstable atomic nuclei. This radiation decay leads to the re-balancing of unstable atoms (radionuclides) to a final stable native (electrically neutral) state. Ionization, on the other hand, is a process where the atom is converted into an ion(s) by removing electron(s). Therefore, diverse radionuclides have different nature and consequently different penetration capacity. Furthermore, IR quality is defined with linear energy transfer (LET), considering X-rays and gamma (γ) rays as low LET radiations, whereas high LET radiations are heavily charged particles, neutrons and protons **[20]**.

If radionuclide has excessive protons or neutrons, radioactivity emits alpha particles (α). α particle is equivalent to helium atom nucleus, which is composed of two protons and two neutrons. α particles can be released by uranium-238 (U-238) or americium-241 (Am-241). Since α is a large particle, it displays high reactivity with

material and low penetration capacity, where a sheet of paper or skin surface can stop them **(Figure 1) [21]**. However, beta particles (β) are electrons and positrons emitted from radionuclides that have a different number of protons and neutrons. According to their size, β particles are less reactive and more penetrable than α particles. For example, tritium (H-3) and nickel-60 (Ni-60) emit β particles that are blocked by aluminum foil **(Fig 1)**. In contrast, gamma rays (γ) are not energized particles and they belong to electromagnetic radiation. This photonic wave has low interaction with material and high penetration capacity. It takes thick blocks of lead to stop γ rays, emitted from e.g. cobalt-60 (Co-60) or cesium-137 (Cs-137) **(Fig 1) [21]**. However, emission of γ rays is usually produced along with α or β particles. When α or β particles are emitted from the nucleus, daughter nucleus might stay excited, whereas de-excitation lowers energy of daughter nucleus to the ground state and emits γ ray.

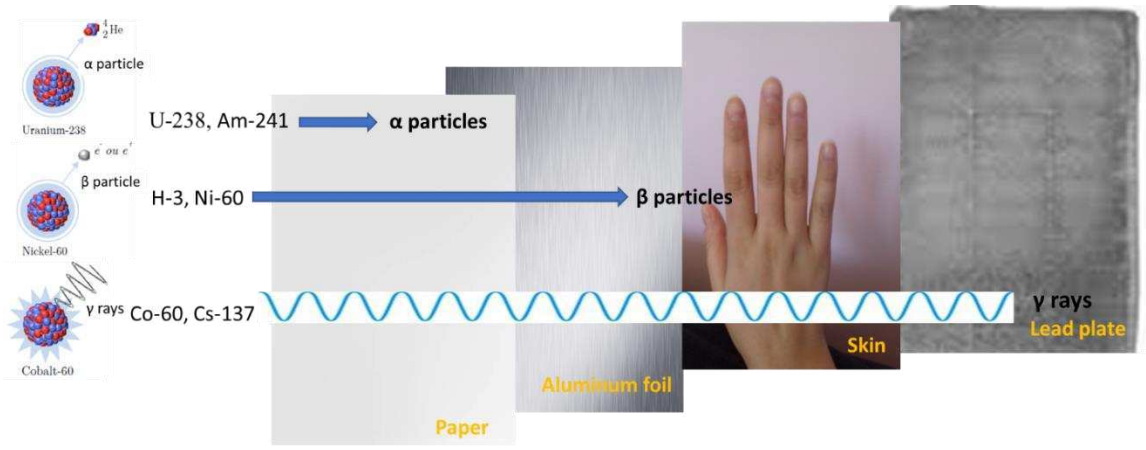


**Figure 1.** Defining ionizing radiation and its' penetration through the different surface.

## 1.1.3. Sources of ionizing radiation

There are two sources of IR origin, natural and artificial, but it is more often (in more than 50% cases) natural, e.g. cosmic rays. Consequently, living organisms are continuously exposed to IR from natural radiation. Artificial radioactivity is punctual with origins from health care (medical diagnosis and therapy **[22]**), nuclear power reactor accident and, in the past, from nuclear weapons testing. Accordingly, the average level of professional exposure is subjected to internationally recognized limits, which are approximately 10 times higher than the average exposure to natural radiation **[23]**.

### 1.1.4. Measuring ionizing radiation: absorbed and effective dose

As IR is a damaging agent, it was very important to establish measuring scale to enable measuring biological effects in correlation with IR. Therefore, absorbed dose expresses quantitative energy that is deposited per mass unit and the measuring unit is gray (Gy); the energy of 1 J/kg of tissue is equivalent to 1 Gy. In human radioprotection, effective dose is used instead of the absorbed dose because all types of radiation are not the same; therefore they do not cause the same biological effect and all biological tissues are not equally sensitive. Indeed, with a hypothesis on biological radiosensitivity (cellular repopulation and cycle), different tissues in mammals display different radiosensitivity **[24]**. Effective dose, which is expressed in Sieverts (Sv), is then the product of the absorbed dose and radiation weighting factor and tissue weighting factor.

### 1.1.5. Ionizing radiation-induced damage

IR might provoke cellular damage, regardless its type or source **[19]**. Namely, IR can damage cells directly (by ionizing/exciting the cell biomolecules through Coulomb interactions) or indirectly (radiation interacts first with other molecules, e.g. water) **(Figure 2)**. In fact, direct damage target can be DNA **(Fig 2)**, but also proteins and lipids **[25-27]**. Furthermore, low LET radiations mostly provoke indirect cell damage in following steps: (1) photon radiation induces (2) water radiolysis that generates (3) free-radicals which can induce (4) chemical DNA breaks and potentially cause (5) biological effect **[19]**. While first 4 steps are at a molecular level, the last one is macroscopic, as we can see biological effects. The last two steps are also of radiobiological interest **[28]** due to health effects of radiation to establish radioprotection.

In conclusion, according to the level of damage and repair, irradiation of cells can result in the following outcomes: no effect; division delay; apoptosis; reproductive failure; genomic instability; mutation; transformation; bystander effects and adaptive responses **[29]**. Finally, all of these outcomes are crucial for basic and clinical research.

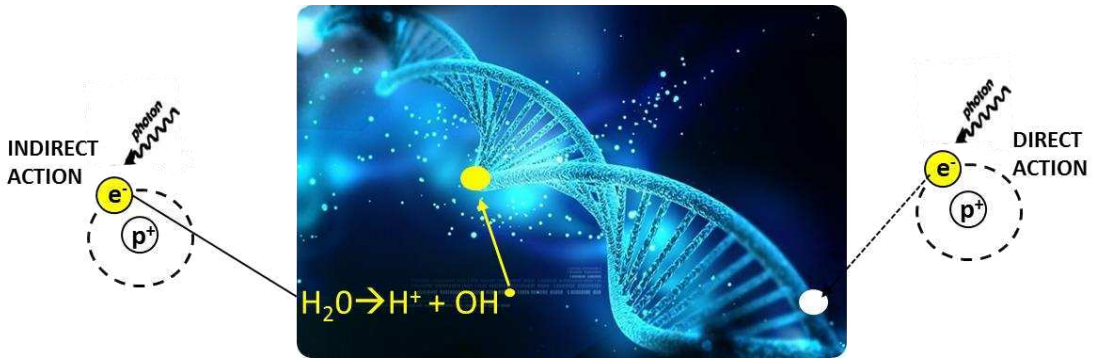


**Figure 2.** Direct versus indirect action of IR on DNA molecule.

## 1.1.6. Cellular consequences of radiation-induced molecular damage and the relationship to radiobiology

Depending on the type of damage and repair and cell fate, effects have been classified as deterministic (coming from no or weak repair) and stochastic (coming from bad repair yielding mutation) effects. Deterministic effects appear short term after exposure (hours to months) and do not occur below the certain threshold. Once the threshold has been exceeded, the severity of an effect increases with a dose, e.g. skin erythema/necrosis/epilation (2-5 Gy), radiation sickness, cataract (2-10 Gy), sterility (2.5-3.5 Gy) and teratogenesis/fetal death (>20 Gy). It is observed that high doses and high dose rates can cause different symptoms, e.g. radiation burns and hair loss **[19]**. Unlike deterministic effect, stochastic effects (cancer or hereditary effects) can appear up to 40 years after exposure and have no threshold dose; their incidence is more likely to occur with a higher dose and their severity is not dose-related. The most common model of stochastic effect is cancer. Different models exist to assess the relationship between doses and effects. In radiological protection, the linear non-threshold relationship is retained for risk assessment **[30]** but different models are proposed by opponents, e.g. threshold model and the hormesis model. **Figure 3** shows these different models. The LNT model is for a long time widely accepted by the majority of experts in radiology and epidemiology. This model assumes that risk of adverse effects, such as the incidence of tumors, increases linearly with dose even at low doses of radiation (<100 mGy) where the effects are not currently defined. On the other hand, the linear threshold model assumes there are no significant biological effects below a threshold dose. Finally, the hormetic model is based on the possibility that low ionizing radiations potentially induce a positive adaptive phenomenon of organisms. Threshold and hormetic models are now highlighted in the context of the risk assessment of exposure

to low doses of ionizing radiation. However, it is necessary to acquire experimental data specific to such exposures, in order to improve the assessment of radiological risk for environmental radioprotection.

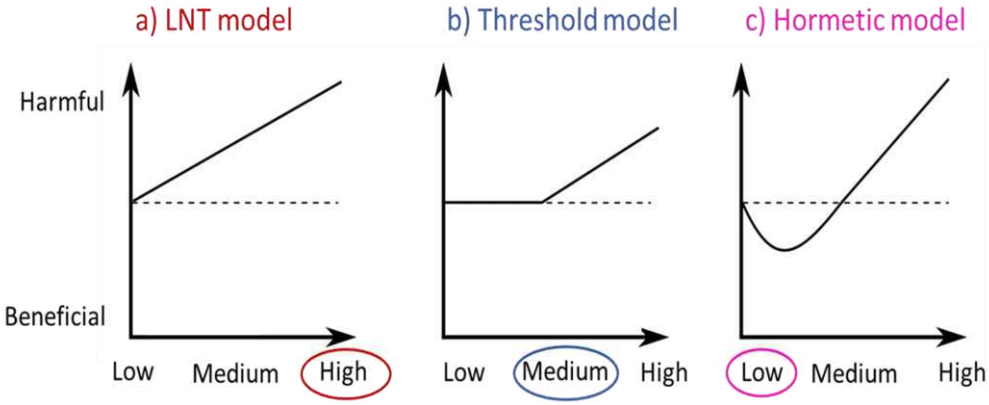


**Figure 3.** Typical dose-response curves (curves a, b and c). Dashed line indicates the natural incidence of the effect. Curve a) represents LNT; curve b) represents a linear relationship with a threshold, curve c represents radiation hormesis **[24]**.

## 1.1.7. Environmental radioprotection context

In addition to human radioprotection, environmental one also needs to deal with different organism radiosensitivity. The latter was first defined by lethal effects of high acute doses. Namely, radiosensitivity towards high acute doses is statistically correlated with the taxonomic group. In fact, primitive organisms (e.g. viruses, protozoa and bacteria with their cell wall) are more radioresistant than higher taxonomic groups (mammals, birds and amphibians) **[31, 32] (Figure 4)**. Biological radiosensitivity seems to be linked to organism's stage (early organism's stage appears to be more radiosensitive than its adult counterpart), the capacity of cellular reconstitution (differentiation and proliferation) and cell cycle. Later a study published in 2013 **[33]** showed, *via* the use of EDR10 (dose rate resulting in a 10% decrease of a physiological parameter in exposed organisms; here mainly reproduction), that the radiosensitivity of key environmental species covered more than five orders of magnitude, with an unknown mechanistic explanation.

Due to the increasing use of radioactive compounds worldwide, particularly for energy production, their impact on humans and ecosystems has become a major public, regulatory and scientific concern **[30, 34]**. In this context, a number of national and international projects have been developed, such as the European FASSET and ERICA

programs **[35, 36]**. The objective of these projects was plural: (i) the setting of a methodological framework for the assessment of the environmental impact of ionizing radiation (FREDERICA database **[37]**), but also (ii) control of the relevance of decisions on environmental issues with respect to exposure, effects and risks of ionizing radiation **[38]**. However, available data are still insufficient to establish an accurate estimate of radiological risk **[36]**, notably because of the number of species covered (mostly mammals, fish, higher plants, terrestrial and aquatic invertebrates **[37]**) and of the lack of data on chronic exposure **[39]**. In addition, radiological risk assessment should be assessed with sensitive and early parameters **[40]**, in view of the need to enhance our knowledge on radiation-induced damage cellular and molecular mechanisms, thus facilitating major scientific advances in the field of radio-toxicogenomic **[41]**. Indeed, the integration of subcellular markers, which are generally more sensitive and early than "macroscopic" markers (if not balanced with other mechanisms of controls and regulations), will help to predict the effects on the major physiological functions of morbidity, reproduction and mortality **[42, 43]**.

Regarding environmental species the conclusion is thus as follows: to reach the objectives of environmental radiation protection it now seems necessary to use integrated approaches to improve the understanding of the mechanisms involved at different levels of biological organization, to find sensitive markers of exposure and, ultimately, adequately protect the environment.

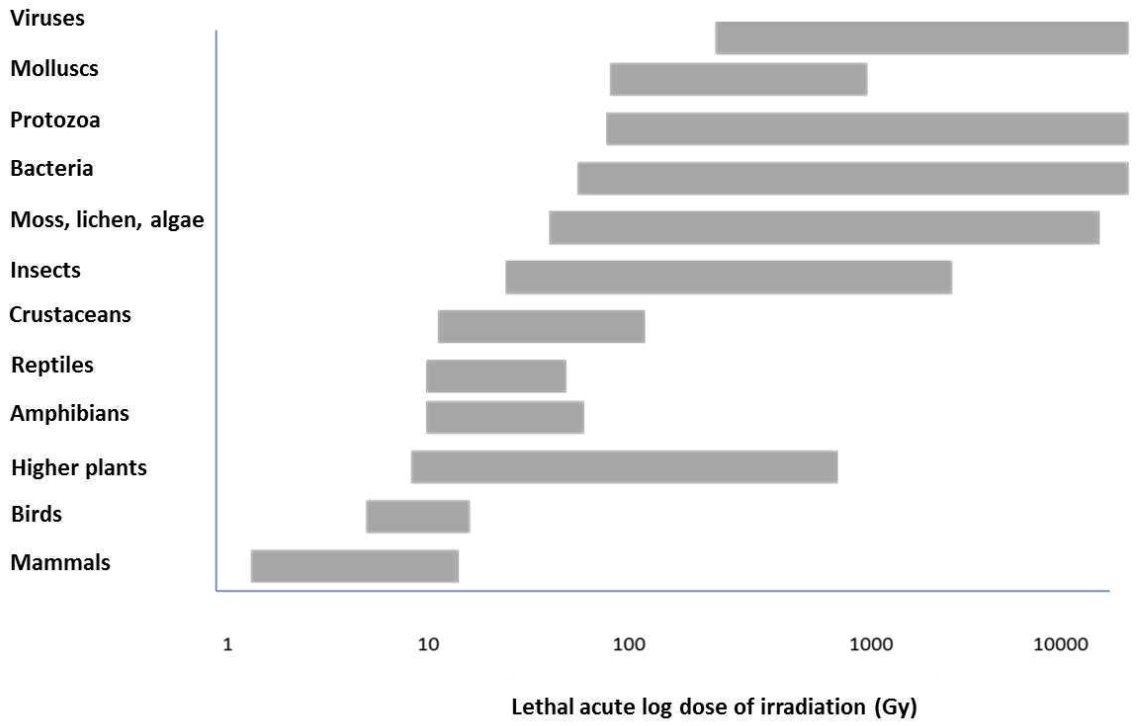


**Figure 4.** Acute dose ranges that result in 100% mortality in various taxonomic groups. Humans belong to the most sensitive mammals and are, therefore, among the most sensitive organisms **[31]**.

## 1.1.8. Conclusion

In order to achieve a reliable and representative radiological risk assessment of the populations, it is important to integrate a multi phylum approach (including human) and take into account more or less radiosensitive environmental species. In most environmental studies conducted on radioprotection chronicity, reproduction has been shown as the most radiosensitive macroscopic biological parameter with respect to mortality, morbidity and longevity, regardless of the species considered (invertebrates mainly). However, whereas the molecular signature of aging is widely studied **[44]** and the link between reproduction and lifespan is stressed in several studies **[45]**, few studies have been conducted accurately and carefully on the chronic radiation exposure molecular effects on lifespan and aging of organisms.

## 1.2. Ionizing radiation and aging

### 1.2.1. Theories of aging

Biological reasons for aging are nowadays better understood **[46]**, but until recently aging was not considered to be an actively regulated process **[47]**. Schrödinger believed that negative entropy is a source of life, meaning that energy is essential to maintain the complex structures **[48]**. One could say that aging is a metabolic process of multifactorial stochastic events based on loss of molecular fidelity and gain of entropy (disorder) at the levels of molecules, cells, tissues and organs **[46]**. There is also that known analogy with a car; an old vintage car can be maintained indefinitely, but at a huge financial cost, since with time defects increase and repair budget goes up. To rephrase in biological terms, soma could be maintained indefinitely, but with continually increasing expenses of resources **[46]**. Furthermore, Hayflick had suggested taking a cellular senescence as a biomarker of aging. Indeed, a replicative cellular potential is correlating with a lifespan of different species **[49]**. The point of this theory is that organs and body age because cells are shutting down, i.e. cells are senescing. On the other hand, cellular senescence could be anti-neoplastic effective mechanism that cells are using to avoid cancer **[50]**.

Aging is acknowledged as a multifactorial stochastic mechanism with bottom-up affection from biomolecules to organs. Energy resources are of crucial importance for biomolecular fitness that slows down the process of aging. Therefore, an energetically expensive investment, such as reproduction, has a profound shortening effect on the lifespan. This is represented with the aged phenotype that leads to senescence and ultimate death **[46]**.

There are numerous theories of aging which can be divided into three general groups: biochemical, physiological and psychosocial. Their description is presented in **Table 1**. Psychosocial theories (disengagement and activity postulate) are built on social interactions during aging, while activity conjecture came as opposed to disengagement theory. The physiological theory comes from endocrinal hormonal imbalance and owns it its name, i.e. neuroendocrine theory. Regarding biochemical theories, they are all involved in metabolism, either *via* aerobic oxidative metabolism (free-radical theory) or membrane changes (membrane theory of aging) or declining production of ATP (mitochondrial decline theory) or cross-linking of proteins and glucose.

**Table 1.** Different theories of aging and their definition. Only one reference, among numerous, which represents each one of them is given.

| Type of aging theory | Name of aging theory* | Description of the theory | Reference |
|---|---|---|---|
| Psychosocial theory | Disengagement theory | Psychosocial theory in the field of gerontology that describes distancing from society and change in relationships as people age. | **[51]** |
| | Activity theory | Healthy aging includes staying active in physical and social sense. | **[52]** |
| Physiological theory | Neuroendocrine theory | Aging is induced by neuronal and endocrine (hypothalamic-pituitary-adrenal axis) hormonal imbalance. | **[53]** |
| Biochemical theory | The free-radical theory* | Aging is effective stochastic mechanism based on aerobic metabolism and redox state which leads to the programmed deficiency in reliability of biomolecular constructs. | **[54]** |
| | The membrane theory of aging* | Aging results from changing in membrane composition, electrical potential and semi-permeability. | **[55]** |
| | The mitochondrial decline theory* | Aging comes from declined production of ATP, mitochondrial DNA and mRNA. | **[56]** |
| | The cross-linking theory | Aging results from crosslinking reaction which link proteins between themselves or with glucose which makes proteins functionally inactive. | **[57]** |

*Theories that may share a common mechanism of action (i.e. radical production) with ionizing gamma radiation.

## 1.2.2. Free-radical theory of aging

The most popular aging theory is called "free-radical theory of aging" (FRTA) **[55]** and its author is Denham Harman **[58]**. FRTA is based on free-radical induced oxidative damage **(Table 1)**. Moreover, it has been known to share some mechanisms of action with IR **[59]**. FRTA and IR are both mediated by reactive oxygen species (ROS) which induce different biomolecular modification, e.g. oxidative stress, DNA mutations and shorter telomere formation **[60]**.

## 1.2.3. Acute and chronic impact on aging

It was postulated that acute radiation and aging share some similar mechanisms of action, and synergy could result in accelerated aging **[61, 62]**. Depending on irradiation mode (acute or chronic radiation), lifespan was reported to be prolonged **[63]** and shortened **[64]** in response to IR. High acute exposure to 4 Gy was observed to

shorten mouse lifespan, while low dose rates (70 or 140 mGy per year) of chronic radiation extend the lifespan of mice for 23% **[63, 65]**. The possible explanation of this phenomenon may be attributed to different radiobiological mechanisms under those two modes of irradiation. Presumably, chronic exposure with a low dose rate (70 mGy per year) can set up the adaptation *via* up-regulation of anti-oxidative and repair mechanisms so-called hormetic effect **[63]**. This is not the case with acute gamma dose (4 Gy), because it induces different stress signaling pathways, where life-shortening happened especially with irradiation of young mice **[64]**. When it comes to people, irradiation at doses higher than 1.5 Gy of gamma irradiation, life expectancy tends to be reduced due to cancer occurrence **[66]**. However, chronic radiation impact on aging is not fully investigated yet. On one hand, it was reported that chronic radiation induces premature cellular senescence **[67]**, but on the other hand, chronic radiation prolongs the lifespan **[65, 68]**.

### 1.2.4. Conclusion

We do not yet know enough about the effects of chronic gamma irradiation on aging **[67, 68]** and corresponding molecular damages. Therefore, further research on common mechanisms between chronic gamma irradiation and aging is necessary.

# 1.3. Model *Caenorhabditis elegans* (ionizing radiation and aging)

## 1.3.1. Discovery, anatomy and the life cycle of *C. elegans*

*Caenorhabditis elegans* (*C. elegans*) is a self-fertile nematode that was first isolated from the soil in 1900 by Émile Maupas **[69]**. The name has been changed and finally derived from Greek *caeno* - recent, *rhabditis* - rod-like and Latin *elegans*– elegant. *C. elegans* represents non-parasitic, transparent soil roundworm, with the length of 1 mm and 959 post-mitotic cells, without any respiratory or circulatory system **(Figure 5, adult)**. Most of them are hermaphrodites **[70]** that reproduce within 3 days and live *circa* 25 days. The life cycle begins with *ex utero* egg hatching at 20 °C and is followed by development through larval stages **(Fig 5,** from L1 to L4 stage**)** which last for 2.5 days **(Fig 5) [71]**. During development nematodes enlarge in size 500 times. Sexual maturity is reached on 3$^{rd}$ day and lasts till 10$^{th}$ day **[70]**. However, when it comes to drastic changes, extrinsical or intrinsical, *C. elegans* can form an alternative dormant stage, which is resistant to desiccation and the anus and mouth are closed. This dormant stage is called dauer and is pheromone driven; the pheromone is constitutively expressed in worms and is modulated by temperature and food presence. For this reason, in case of high caloric restriction, larvae after hatching are arrested in development and cannot reproduce nor move much until they have food and/or water in their environment **[50]**. Finally, dauer is a reversible long-lived resistant nematodes' stage that was a solid base to study metazoan plasticity that leads to shifts in behavior and metabolism, accompanied by changes in development, growth, and reproduction **[72]**. Genes that are notably involved in the development of this alternative stage are: *age-1*, *daf-2* and *daf-12*. Their role will be defined in the following parts **(part 1.3.2. and part 5 – resuls – aging study) [50]**.

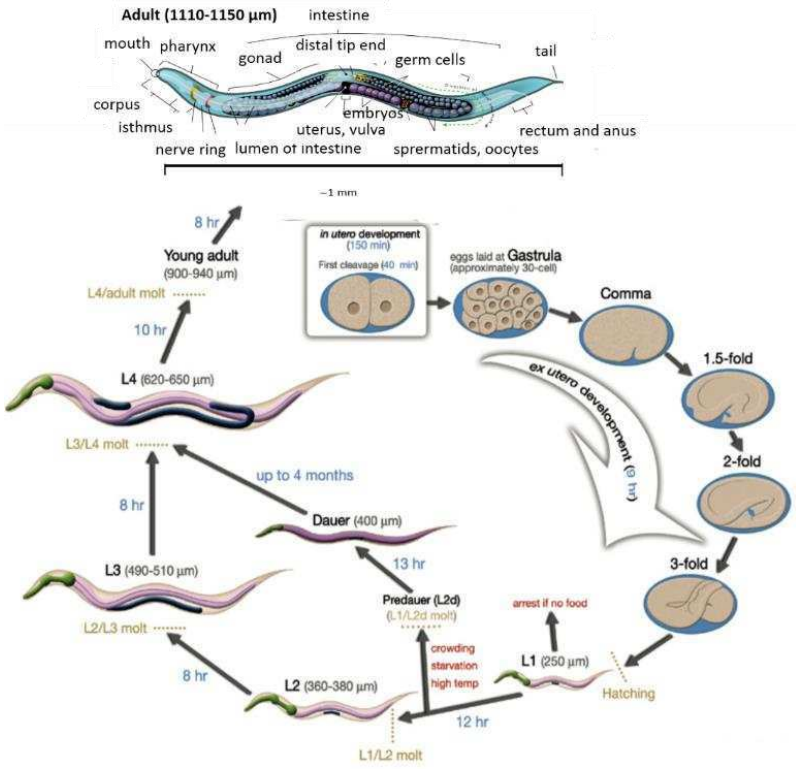


**Figure 5.** Anatomy and life cycle of *C. elegans* **[71]**.

## 1.3.2. *C. elegans* as a model of aging

Nematode *C. elegans* ages rapidly **[73]** and was the first multicellular organism to have its whole genome sequenced. From 2012 it is the only organism with completed connectome ("neuronal wiring diagram") **[74, 75]**. On the genetic basis, *C. elegans* has emerged as one of the first model systems for aging research **[76]**. Among all studies on the topic, several pathways have been found critical for lifespan duration and are briefly reviewed here. Dauer stage, described in the previous paragraph **(part 1.3.1)**, was considered an ageless organism (it was thought to improve its chances of survival and reproductive success), on which numerous studies of aging were made **[76]**. In addition, DAF-2 pathway was extracted as a pathway that impacts lifespan from dauer stage **[76]**. Indeed, DAF-2 function is crucial for the development of nematodes to adulthood (*daf-2* mutants form dauers constitutively), and DAF-16 activity is required for dauer formation (*daf-16* mutants cannot form dauers). Cloning of *daf-2*, *daf-16* and *age-1* genes revealed the crucial role of insulin/insulin-like growth factor-1 signaling (IIS) pathway in the regulation of nematodes' development and aging **[77]**. Another key modulator of aging, which is also involved in development and growth, is the mechanistic target of rapamycin (mTOR). Rapamycin was found to extend the lifespan

in budding yeast, mice, fruitflies and nematodes **[78]**. Finally, dichotomy was observed regarding rapamycin co-dependency of *daf-16* in enhancing longevity in *C. elegans* **[79]**. On the other hand, a biological genetic clock was also set up in nematodes; it involves 4 different "clock genes", i.e. *clk* and *gro* genes (independent of dauer genes) **[80]**, among which *clk-1* slows down aging if mutated. Finally, some theories explain how redox signaling may be involved in aging and provide some examples of ROS functions and signaling in *C. elegans* metabolism **[81]**.

However, aging study requires maintaining synchronously aging populations (without mix stages). Frequently germline ablation is used as a method of choice to obtain synchronously aging populations. However, most of the germline ablations induce lifespan extension *via* increased proteasome activity, fat accumulation and autoregulation of lipid metabolism through DAF-16 and SKN-1 detoxification **[82]**. Another technique, performed in the early aging studies, consists in using 5-fluorodeoxyuridine drug (FUdR is the inhibitor of DNA synthesis) in *C. elegans* plates to maintain synchronous cultures of aged animals **[83]**. However, FUdR needs to be used under strictly controlled conditions **[84]** because it can induce side effects if not used properly, e.g. larvae morphology abnormalities, contamination with progeny or slight lifespan prolongation **[85]**. Another option to produce sterile nematodes are widely accepted mutants, e.g. *glp-1* mutant which reproduces normally at the lower temperature (15 °C) but turns into sterile phenotype at the higher temperature (25 °C) **[85]**. *Glp-1* mutant contains partial loss of function e2141 whereas Glp-1 regulates somatic and germline growth and differentiation **[86]**. *Glp-1* nematodes are the excellent model to understand the signaling network, mechanisms of aging and radiation effects, in order to discuss the most popular theory of aging (FRTA) **[87]**.

In conclusion, aging on *C. elegans* has been studied from different angles and it has been shown that several pathways – e .g. IIS **[77]** and mTOR pathways **[79]**, reproduction and different post-translational modifications – could potentially share some part of the signaling cascades, acting either synergistically or antagonistically.

### 1.3.3. Radiosensitivity: acute and chronic radiation of *C. elegans*

Since nematodes are more radiosensitive than viruses and less than amphibians, there are frequently used as a laboratory model in acute and chronic irradiations **(Table 2)**.

Following acute exposure, nematodes' survival has been shown to decrease, while lifespan expectancy is dramatically reduced; doses delivered were extremely high (cumulative dose of 1000 Gy with the dose rate of 27 $Gy.min^{-1}$). In addition, acute doses such as 30 and 120 Gy on L4 stage yielded a decline of reproductive function (decrease of spawning and hatching capacity, respectively) **[88, 89]**. It was also recorded that young stage *C. elegans* (L3 stage) was more radiosensitive than adult nematodes (8 days old) **[62]** and that sensitivity of gametes to acute irradiation is related to developmental stage **[90, 91]**. Indeed, embryos are – to the point when it threatens their survival – more radiosensitive in diakinesis/early embryogenesis (from 40 Gy) than in pachytene (from 100 Gy) **[90]**. Meanwhile, only one study investigated the impact of acute exposure on *C. elegans* growth and shown that L1 stage was affected from 10 Gy **[92]**.

Regarding the molecular damage, cell cycle arrest at doses of 60 and 120 Gy and apoptosis of pachytene germline have been observed **[93]**, which could explain partly the decrease in hatching capacity. Indeed, cell cycle arrest is specific to mitotic cells (germline and somatic lineage) in *C. elegans*, whereas apoptosis is typical only for meiotic cells, i.e. germline. Irradiation could promote the expression of *egl-1* and *ced-13* that bind CED-9 and release CED-4 to induce apoptosis. In addition, an increase in protein carbonylation at 200 Gy was found to be correlated with the decrease of hatching success **[91]**, whereas no major protein carbonylation has been found at lower doses **(Dubois et al, 2018 submitted)**.

For the moment, the impact of chronic irradiation was observed only to impair the reproductive function of *C. elegans*, without evident affection on somatic cell lineage. In addition, studying chronic exposure during nematodes' developmental stage (during 65 h, from egg to L4/young adult stage) showed no impact on nematode growth parameters whatsoever. However, there was an impact on spawning capacity (from the dose rate 52 $mGy.h^{-1}$ **(Dubois et al, 2018 submitted)**), as well as the dose-depended significant decrease in egg-laying with a transgenerational effect (over 3 generations). Not only that, in non-irradiated generations which came after parental exposure there was a decrease in the number of larvae per individual (from the dose rate 7.1 $mGy.h^{-1}$). Nevertheless, hatching capacity was not affected whatever the chronic dose rate (between 7.1 and 337 $mGy.h^{-1}$) or the generation. Regarding the molecular damage, a decline in spawning capacity was associated with a cell cycle arrest in spermatozoa of exposed generation, and to a lesser degree with apoptosis. For non-irradiated generations placed in control environment after parental exposure, only the decrease in

the number of spermatozoa is associated with the effect on reproduction. This could be potentially explained by direct *in utero* embryonal exposure or by transgenerational maternal effects **[94]**. The protein carbonylation level has also been studied after chronic exposure of *wt C. elegans*, but no relationship between this level and the reproduction impairment has been emphasized in that conditions **(Dubois et al, 2018 submitted)**.

To conclude, reproduction is so far the most radiosensitive studied parameter (especially spawning capacity), after acute and chronic irradiation, affecting growth and survival of nematodes **[90, 93, 94]**.

**Table 2.** Radiotoxicity of ionizing radiation on *C. elegans*.

| Regime of IR | Dose (Gy) | Monitored affected cells | Biological (d)effect | Radiotoxicity biomarker | Reference |
|---|---|---|---|---|---|
| low chronic ɣ $^{137}$Cs | 6 | germline | transgeneral reproduction | DNA damage-apoptosis | **[95]** |
| low chronic ɣ $^{137}$Cs | 0.5-6.5 Gy | germline and somatic cells | reproduction | PC-proteasomal activiy | **(Dubois et al, 2018 submitted)** |
| acute ɣ $^{137}$Cs | 0.5-200 Gy | germline and somatic cells | reproduction | PC-proteasomal activiy | **(Dubois et al, 2018 submitted)** |
| acute X-rays | 40 | germline | reproduction and hatchability | DNA damage-apoptosis | **[90]** |
| acute ɣ $^{137}$Cs | 60-120 | germline and somatic cells | reproduction | DNA damage-apoptosis | **[89]** |
| acute ɣ $^{137}$Cs | 60 | germline and somatic cells | growth delay and phenotype | DNA damage | **[92]** |
| acute ɣ $^{137}$Cs | 60 | germline | reproduction | DNA damage (DSB) | **[93]** |
| acute ɣ $^{137}$Cs | < 200 | germline | hatching | PC | **[91]** |
| acute ɣ $^{137}$Cs | 100-300 | somatic cells | prolong the lifespan | ? | **[62]** |
| acute ɣ $^{137}$Cs | > 1000 | somatic cells | accelerate aging | ? | **[62]** |

# Chapter 2. Photobiology

## 2.1. Background

### 2.1.1. Discovery and definition of ultraviolet radiation

In 1801 Johann Wilhelm Ritter discovered fast-tanning reaction of silver chloride-soaked paper exposed to the sun. He filtered sunlight through a glass prism to obtain each light of the spectrum and measured the rate of silver-chloride reaction in each color of the spectrum. There was a weak reaction in the red light and strong reaction in the end of the violet light. Finally, he placed silver-soaked paper just beyond the violet light where there was no visible sunlight. That reaction was the most intense and he called the light "deoxidizing rays"; that was in fact UV light **[96]**. This was the first proof of the existence of invisible light beyond violet spectrum. Therefore, official name "ultraviolet" was derived from Latin *ultra* - beyond. Ultraviolet radiation (UVR) falls in the category of non-ionizing light; the spectrum is somewhere between X-rays and visible light. Among the crucial focuses of UVR effects is genotoxicity, e.g. mutagenic effect of UVR, was revealed in 1960 **[97]**. Consequently, a scientific field of photobiology opened up to study the effect of non-ionizing radiation on living organisms, e.g. UVR effects and photosynthesis **[98]**.

### 2.1.2. Ultraviolet subtypes of radiation

Major subtypes of UV light are UVA, UVB and UVC **(Figure 6)**. Furthermore, it was observed that shorter UV wavelength (UVC light) **(Fig 6)** was more dangerous than longer ones, due to higher energy. On the other hand, UVC is the least penetrable from all UV spectra. UVC is fully absorbed by ozone, UVB mostly (90%), whereas UVA passes almost completely through the atmosphere **(Fig 6)**. Skin barrier represents the similar protective function as ozone, i.e. it is highly efficient towards UVC light, enabling only an affection of epidermis with photo-lesions and mutations which are efficiently repaired **(Fig 6) [99]**. However, repair efficiency depends on UVC dose, where only unrepaired damages are potentially lethal **(Cvjetan et al, unpublished communication)**.

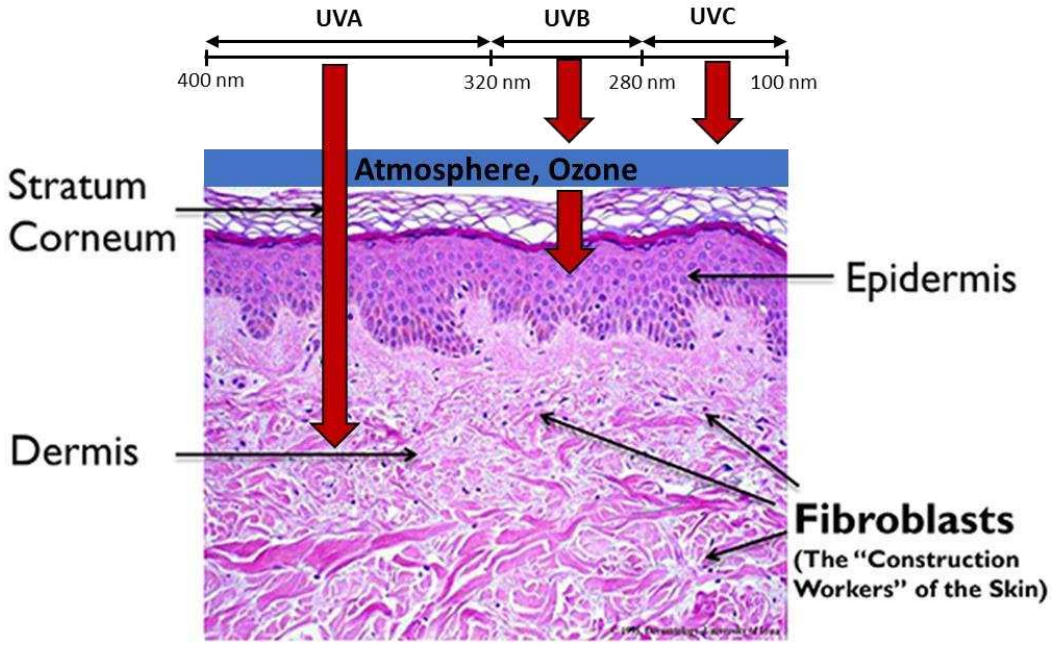


**Figure 6**. Solar UV radiation, its permeability through atmosphere and skin **[100].**

## 2.1.3. Sources of ultraviolet radiation

UV light has natural (10% of sunlight) and artificial sources (mercury, tanning lamps and black lights). Nowadays, the cosmetic industry is frequently using UV light, especially for nail treatment and tanning treatment (frequently prohibited). However, different subtypes of UVR set up different hazard ratio. Furthermore, solar UVR is extremely dangerous in countries with low ozone coverage, e.g. Brazil. All of this has resulted in increased incidence of skin cancer **[101, 102]**. Subsequently, different organizations, including governments, are trying to impact public awareness of photoprotection behavior **[102]**.

## 2.1.4. Ultraviolet radiation-induced damage

Since UVA is fully penetrable and UVB partially penetrable, UV radiations introduce DNA damage, respectively **[100]**. Ultimately, UVR has specific molecular signature regarding damaging DNA, which is pyrimidine dimer **[97, 103] (Figure 7)**. Furthermore, if this photoproduct is not repaired it can introduce DNA mutations **[100]**. Recent findings indicate that proteins also express damage induced by UVR, i.e. protein carbonylation **[5, 104]**.

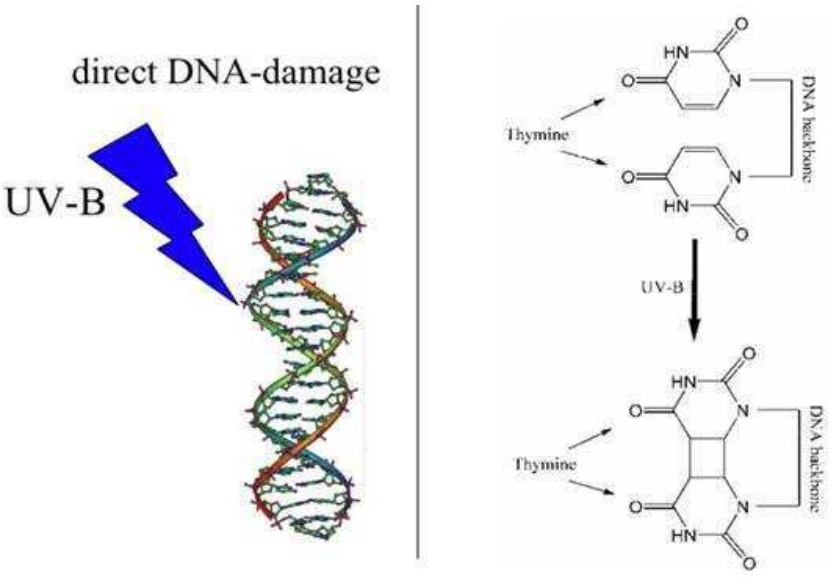


**Figure 7.** Photoproduct formation after UVB induced direct DNA damage.

## 2.1.5. Measuring ultraviolet radiation: absorbed and equivalent dose

As UV can cause biological damage, ambient UVR measurements can be expressed in physical and biological units **(Table 3)**. The physical unit of UVR is joule per square meter ($J.m^{-2}$). On the other hand, biologically effective UVR unit is constructed as erythemal response function (MED, SED). In addition, solar UV index shows the level of UVR at Earth's surface **[105]**. Finally, it is important to have different standard measurements of UVR in order to set the threshold and classification of UV for different biological damage induced by UVR.

**Table 3.** Different ways to measure the effects of ultraviolet radiation. This UVR is in the solar range from 280 to 400 nm and artificial range from 250 to 400 nm.

| |
|---|
| MED: UVR dose that produces minimal erythema and is equivalent to 200 $J.m^{-2}$ |
| SED: UVR dose that produces standard erythema and is equivalent to 100 $J.m^{-2}$ |
| Solar UV index: UVR in $W.m^{-2}$ multiplied by 40. |

## 2.1.6. Threshold

UV is classified as carcinogenic, derived from its mutagenic and non-specific damaging actions. The most common classification of skin types for UVR sensitivity is the Fitzpatrick scale **[100]**. Moreover, UV is the most important environmental risk factor for skin cancer and other skin disorders. Finally, all of those classifications represent a serious threshold warning which should be observed and heeded, especially

due to the fact that there are huge variations of UV doses across the globe (in some places the dose is four times as big as in others) **[106]**. The maximum acceptable dose (threshold dose) for the human is 2.2 $kJ.m^{-2}$ for UVR 300 nm to avoid the development of cataract **[107]**.

## 2.1.7. Photoprotection: photosensitivity and dose-response curves

Photoprotection is a protective mechanism of an organism for UVR induced molecular damage. Since phototrophs (including plants) use the sunlight for photosynthesis, they own the most sophisticated photoprotective mechanisms. Usually, UVR is used for water disinfection against microorganisms. Different microbes display different photoprotection. Namely, bacteria species has 10 times higher photosensitivity than virus and protozoa species **[108]**. To correlate UVR with microbial inactivation, different dose-response models are used **(Figure 8)**. Effect of shouldering is used under low doses, while tailing model is used at higher doses reaching plateau **[109]**. For medium doses a standard linear relationship is used.

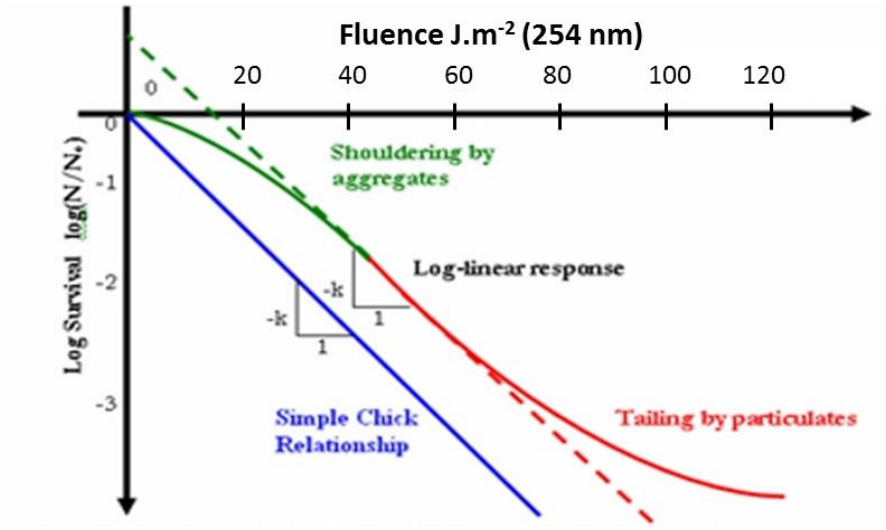


**Figure 8.** Typical dose response survival curves of microbes under UVR **[109]**.

On the other hand, people have the lowest photoprotection of all organisms. Furthermore, skin is one of the most photosensitive tissues. Therefore, UVR overexposure can lead to cancer (point A, **Figure 9a**) *via* carcinogenesis (DRC, **Fig 9b**). Carcinogenesis is following a linear relationship. Unlike gamma rays, where high doses of UV can cause damage and cancer, lack of UV exposure can lead to osteomalacia and osteoporosis due to lack of vitamin D (point C, **Fig 9a**). Therefore, minimum risk in terms of health requires some UVR (point B, **Fig 9a**) **[110]**.

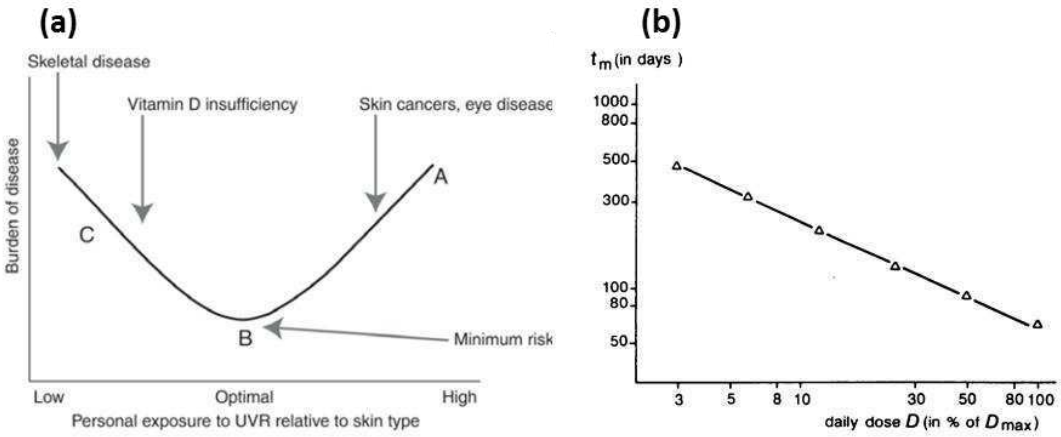


**Figure 9 - (a).** Illustration of the potential correlation between UVR exposure and the burden of disease **[110]**. **(b)** The dose-effect relationship for carcinogenesis by UV radiation in hairless albino mice **[111]**.

## 2.1.8. Conclusion

Overexposure to UVR can induce carcinogenesis and lethal effects. However, lack of UV exposure is also hazardous due to vitamin D deficiency. To conclude, UV has an ambiguous status, since it is, in moderate doses, necessary for a healthy life, but potentially lethal in excessive doses. Cancer and osteoporosis are good examples of the opposite biological effects of UVR over and sub-exposition, respectively.

## 2.2. Radiation-resistance (UV radiation and cell death)

### 2.2.1. UV-induced damage

Aside from direct DNA damage (e.g. pyrimidine dimer), UVR promotes also indirect damage *via* ROS generation, which affects all biomolecules, e.g. DNA, proteins and lipids (membrane) **[112]**. Among the biomarkers of UVR are protein carbonylation (PC), lipid peroxidation **[5, 104, 113, 114]**, but also direct and indirect DNA lesions **[115]**. PC seems involved in radiation-induced bacterial death (*D. radiodurans* and *E. coli*), but a much higher irradiation dose is required for radiation-resistant species to obtain the same amount of PC compared to radiation-sensitive species **[5, 116]**. UVR is inducing two types of DNA lesions, i.e. cyclobutane pyrimidine dimer and pyrimidine-pyrimidone (6-4) photoproduct **[117]**. While photoreactivation (*via* photolyase) and nucleotide excision repair are repairing photoproducts **[117]**, PC, on the other hand, has no classic repair system, but rather degradation mechanism *via* proteasome and autophagosome **[118, 119]**, which are very efficient systems of degradation.

### 2.2.2. Organism's resistance to radiations

High radiation-resistant organisms (RRO) belong to extremophiles which are rare among eukaryotes and prokaryotes. Radioresistant bacterial model is *Deinococcus radiodurans* (*D. radiodurans*) that resists high doses of IR (5000 Gy, **[5, 120]**), UVR (1000 $J.m^{-2}$, **[5]**) and desiccation (85% viability after two years in the presence of less than 5% humidity **[121]**). Organism's resistance to UV radiation was studied on RRO and photosensitive organisms. Since bacterial genome is compacted into a nucleoid formation, it was observed that radioresistant bacterial species display higher density of nucleoid as opposed to radiosensitive bacteria **[122]**. In addition, the frequency of UV induced DNA damage (photoproducts) is the same in resistant and sensitive organisms **[123]**. Radioresistance has been found partially encoded in small cytosolic molecules and different proteins, e.g. manganese ions, peptides, 2',3'-cyclic phosphodiesterase and DdrB protein (single-strand binding protein) **[5, 124-127]**. These molecules act as the anti-oxidant shield which reacts with most of ROS and the modulation of their level changes radioresistance of different organisms **(Figure 10) [5, 125]**. Indeed, it is suspected that resistant organisms have a higher level of protection than sensitive ones, particularly proteome protection. Extreme resistance to UV (and

other agents) in the model bacterium *Deinococcus* involves globally the same DNA repair proteins as in sensitive bacteria like *E. coli*, although additional *Deinococcus*-specific proteins may also contribute (e.g. DdrB). The induced expression (controlled by IrrE/DdrO) of some of the DNA repair proteins (modulated by gene like *uvrA*, *uvrB*, *recA*) following irradiation is required for resistance. The deinococcal DNA repair proteins may have some specific properties or different expression levels (compared to *E. coli*), and, in particular, they may perform better because of much better protection against oxidative damage **[128]**. Although ribonucleoprotein particle Ro function is not precisely defined, an ortholog of ROP-1 is also involved in resistance to UVR **[129]**.

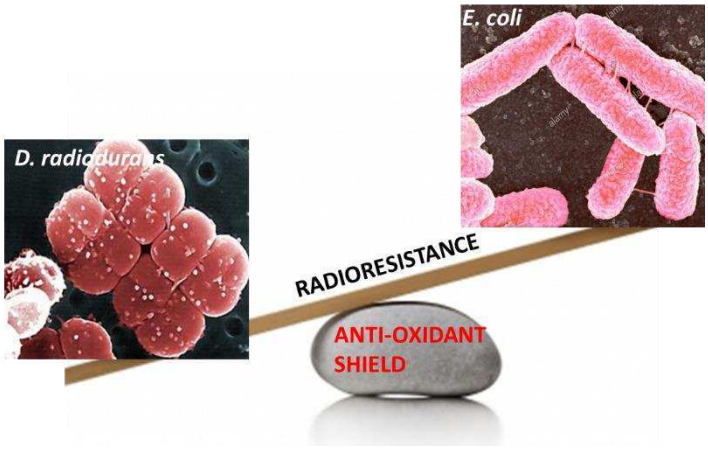


**Figure 10.** Radioresistance of different species is following anti-oxidant shield.

## 2.2.3. UV-induced cell death: mechanism of action

All subtypes of UVR are potentially lethal to different organisms, e.g. from prokaryotes (bacteria) to eukaryotes (plants, animals and people) by photodynamic reactions (mutagenic and oxidative effect on biomolecules) **[130]**. The lethal effects of UVR are well known, especially in shortwave UV spectrum **[131]**. Nevertheless, two types of cell death are involved in UVR, i.e. apoptosis (programmed cell death) and necrosis (autolysis) **[132]**. In bacteria, it was proposed that UVR also initiates programmed-like cell death **[133]**. Apparently, oxidative stress is inducing this type of death *via* caspase-like (metacaspase) program.

Since UV produces photoproducts, the immediate following intermediate in the repair pathway is DSB. Furthermore, DNA repair can last for a few hours **[131]**. On the contrary, from a protein point of view, PC is not significantly increased just after UVR.

In that condition, while DNA is undergoing repair, carbonyl anabolism is ongoing following irradiation. Finally, at the same time, most of DNA is repaired, whereas PC has reached its anabolic maximum **(Cvjetan et al, unpublished communication)**. Therefore, lethal UVR reveals PC as an important biomarker of bacterial cell death **[5]**.

## 2.3. Model *Escherichia coli* (UV+ death)

### 2.3.1. Discovery, structure and life cycle of *E. coli*

In 1885 German pediatrician Theodor Escherich first described the bacterium *Bacterium coli* commune; later it was named after him and is now known as *Escherichia coli* (*E. coli*) **[134]**. *E. coli* is a Gram-negative bacterium, oxidase negative, catalase positive and lactose positive. Its diameter is from 1.1 to 1.5 µm with a length of 2.0 to 6.0 µm. In biological classification it belongs to the family *Enterobacteriaceae* **[135]**. Antigen signature of the family *Enterobacteriaceae* is complex and it involves following antigens: capsular (K), somatic (O), flagellar (H) and fimbriae (F) antigens (**Figure 11a**). Furthermore, family *Enterobacteriaceae* lives in the digestive tract of mammals, birds, reptiles and even humans **[135]**.

Therefore, *E. coli* is a part of gut microbiota in the gastrointestinal tract, particularly in the blind gut and colon. The intestinal microbiota is protecting against carcinogenic substances from food and pathogenic bacteria **[136]**. It also has a very important role in digesting food, producing a wide range of vitamins (vitamins B including B12 and vitamin K), hormones and enzymes.

Asexual reproduction of *E. coli* by binary fission is prevalent compared to sexual reproduction by conjugation ("the transfer of genetic material through a sex pilus"). Binary division at 37 °C is beginning with DNA replication followed by DNA attachment to the membrane. This induces membrane invagination and finishes with cell wall synthesis and its division **(Fig 11b)**. During exponential growth, the generation time of *E. coli* lasts approximately 20 minutes. Finally, a life cycle of *E.coli* depends on genome size, sequence and habitat **[137]**.

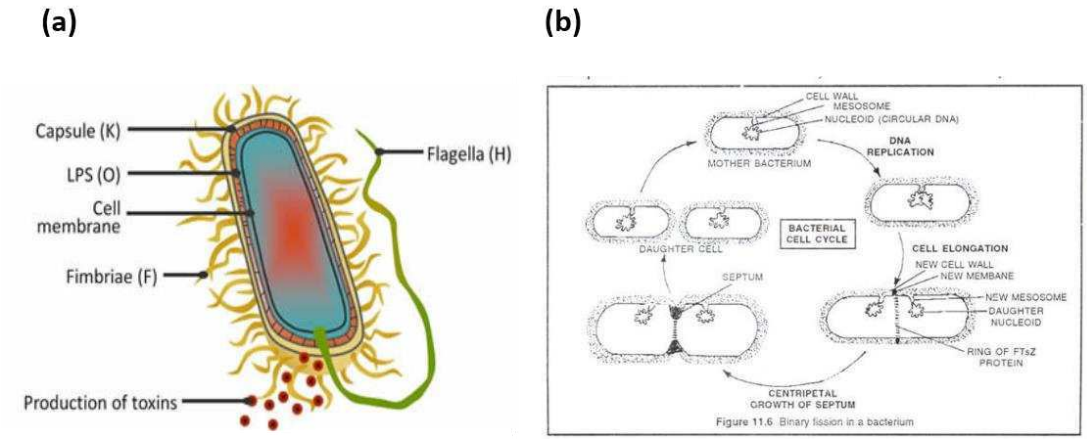


**Figure 11 - (a).** Structure and antigen composition of *E. coli*; **(b)** Cell cycle of *E. coli* at 37 °C.

## 2.3.2. *E. coli* as a model organism

*E. coli* has appeared prominently as a model of choice in molecular biology onset. As a result, a lot is known about it: its genetic code and its regulation, DNA replication, transcription, a life cycle of different viruses, etc. **[138]**. Becoming the most comprehensive organism on Earth, the genome of *E. coli* was fully sequenced in 1997 **[139]**, which uncovered its remarkable genome plasticity **[138]**. Genome plasticity describes genotype changes as a response to different microenvironment which resulted in less than 40 % of common genes among different *E. coli* strains. In conclusion, *E. coli* is the most researched organism due to easy maintenance and manipulation through short life cycle **[138]**. Therefore, *E. coli* is an excellent model for studying radiation-induced biomolecular damage.

### 2.3.3. UV-induced damage in *E. coli*: death

As already mentioned, UV induces DNA damage in form of photoproducts, **(Fig 6b)** with different mechanisms of creation and repair that require a good biological response from membrane and proteome, as proteins are in charge of DNA repair and sustention **[116, 140]**. Radiation research on prokaryotes showed that DNA lesions can be repaired but protein lesions are not so amenable to repair. From all UV spectrum, UVC radiation range is the most lethal for *E. coli* (around 254 nm) and the corresponding lethal dose (single hit) is 360 $J.m^{-2}$ **[5]**. UV dose-response survival study on *D. radiodurans* and *E. coli* showed that death correlates with dose and protein carbonylation simultaneously **[5]**, but mechanisms need to be further investigated to understand the processes of death better.

### 2.3.4. Conclusion

It is far from clear why, how and precisely when the life of irradiated cells irreversibly ceases. However, huge sensitization effects of DNA repair mutants show that only unrepaired, residual DNA damage is lethal **[121]**. Protein damage reduces the efficacy and precision of vital cellular processes resulting in high mutation rates and functional degeneracy **[141]**. Therefore, direct and indirect radiation effects that damage proteome (in charge of genome repair, replication and expression) should determine genome and cell fate **[5]**.

# Chapter 3. Molecular tools to assess effects of radiations

## 3.1. Background

### 3.1.1. DNA damage

Multiple molecular tools are available to assess the effects of irradiations. These tools can be classified into different biomolecular categories, including – among others – methods to detect DNA and protein damage. As already stated, radiations induce different DNA damage, e.g. DNA strand-breaks (with IR, SSBs or DSBs) and photoproducts (with UVR). In case of UVR, photoproducts during the process of repair are excised and subsequently generate a strand break (DSB). Afterwards, deficiently repaired DNA damage may introduce DNA mutations. Therefore, a multitude of markers associated with this repair of DNA breaks (SSBs and DSBs), such as gamma-H2AX and DNA mutations, represent standard biomarkers of radiation-induced DNA damage.

### 3.1.2. DNA repair

Mechanism and time necessary to repair DNA damage are crucial for cell vitality. The most usual time for DNA repair (tDr) after radiation is between 2 and 4 hours for different types of mammalian cells (epithelial, neocortex, bone marrow cells, etc.) and radiation types (gamma, X-rays, UV radiation, etc.) **[142-144] (Table 4)**. Moreover, the most accurate estimation of DNA damage is to follow its reparation in real time, since tDr is rather rapid.

**Table 4.** Comparative properties of time for DNA repair measured on different models and different types of radiation.

| Model | Radiation type | Time for DNA repair | Reference |
|---|---|---|---|
| biophysical cell model | gamma | 24 h* | **[145]** |
| mouse corneal epithelial cells | gamma | 4 h | **[144]** |
| tumor cells from albino mice | UVC | 4 h | **[143]** |
| mammalian nerve cells | gamma | 2 h | **[146]** |
| mouse bone marrow cells | X-rays | 3-4 h | **[142]** |
| mammalian cells | UV | few h | **[147]** |
| *E. coli* | UVC | 2 h | **[148]** |

*h stands for hours.

## 3.1.3. Protein damage

Proteome degeneracy induced by IR has been underestimated for a long time but recently it has been acknowledged that proteome inevitably carries out cellular function. Due to the protein radiosensitivity, it is important to reconsider protein damage induced by IR to explain mechanisms of radiotoxicity. Depending on protein function and biological period, protein damage can induce deleterious cellular consequences. Namely, cellular proteins targeted by IR, change their expression, activity and redox post-translational modification (PTM) status **[4]**, e.g. *in vivo* IR of mouse increased PC level and induced neurotoxicity **[149]**. PTMs influence structural and functional properties of protein *via* conformational changes, protein degradation and enzymatic activity **[4]**. Potential radiotoxicity triggered by proteome changes occur already at 1 Gy, inactivation of redox enzyme from 2 Gy and increase in PC at 6 Gy (presented in **Table 5**). Among oxidative damage to protein, carbonylation is one of the most important; it is already considered as a biomarker in several conditions of stress and aging **[5, 150]**.

**Table 5.** Comparative properties of IR induced radiotoxicity.

| IR dose | Radiotoxicity | Reference |
|---|---|---|
| 1 Gy | intestine and brain: ↑ phosphoglycerate kinase 1 and ↓ transaldolase 1, respectively | **[151]** |
| 6 Gy | neurodegeneration: disruptions of PTMs and increased PC level | **[4]** |
| 2-8 Gy | inactivation of redox enzymes : catalase, SOD, GPx, etc. | **[152]** |
| < 10 Gy | proteome changes: cyclooxygenase 2 expression | **[153]** |

↑ and ↓ stand for upregulation and downregulation, respectively.

## 3.1.4. Carbonylation

Carbonylation is a posttranslational oxidative modification with irreversible and unrepairable nature **[11]** that targets all biomolecules **[104]**. However, proteins are the most susceptible to carbonylation among major biomolecules (nucleic acids, proteins and lipids) after UVR. Direct protein carbonylation is happening on 4 amino acids: Lys, Arg, Pro and Thr **[11]** *via* acyl-modified amino acids **[154]**. The possibility of PC occurrence is predetermined with prior protein oxidative status and protein structure. Oxidative status is defined as protein covalent modifications introduced by oxidative stress, whereas protein structure describes its spatial conformation driven by numerous non-covalent interactions. Finally, each carbonylation event influences protein oxidative status and protein structure, which makes the protein more susceptible to the following carbonylation **[11, 155]**. However, unlike DNA repair, there are no

as yet defined exact mechanisms of carbonylation repair **[156]** other than degradation system *via* proteasome and autophagosome **[9]**. Finally, some basic information on PC still needs further investigation, e.g. carbonyl metabolism after different stress including irradiation.

## 3.2. General methods for detection of DNA damage

### 3.2.1. Background

Historically, numerous methods were used to reveal DNA damage and some of them are presented in **Table 6**. They can be divided into direct and indirect methods. Detection of DNA strand breaks (SSBs and DSBs) was made mainly using direct methods. Standard methods for strand breaks are comet and FISH. The FISH method enables visualization and improves resolution of nucleic acids, multiplex targeting, quantification and life cell imaging. Comet, on the other hand, is known as single-cell gel electrophoresis that enables DNA strand breaks detection, UV-induced pyrimidine dimers, oxidized bases and alkylation damage on a cellular level **[157]**. However, their limitations (e.g. limited resolution and irreproducibility) led to hybrid methods, e.g. comet-FISH assay **[158]**. The method of choice for measuring modified DNA bases is high performance liquid chromatography-mass spectrometry (HPLC-MS) **[159]**, but due to expensive limitations this method was not routinely implemented. As for indirect methods, immunological methods were used for quantification of DNA damage against DNA oxidation and modification (ELISA and IHC) **[157]**. Immunological methods have some problems with cross-reactivity, while DNA repair proteins were used successfully as molecular markers for visualizing and quantifying mutations (FCM and *in vivo* MMR) (**Table 6)**. Fluorescent *in vivo* system enables detection of mutations and (possible) repair **[160]**. Therefore, some of these methods will be detailed more precisely with deeper insight on mismatch repair system and *in vivo* DNA damage detection method **[160]**.

**Table 6.** Distinct types of DNA lesions are adopted from review **[157]**. Corresponding methods, description and limitations are used to evaluate each type. Only MMR method is extracted from another article **[160]**.

| DNA damage detection | Method | Description | Limitation |
|---|---|---|---|
| **DIRECT** | | | |
| DNA strand breaks | comet | single-cell gel electrophoresis: gold standard method | limited resolution (10–800 kb) |
| site-specific breaks in DNA regions | comet-FISH | detect repetitive DNA sequence with intercalating probes | DNA loss, damage that misled probes to intercalate DNA |
| SSBs and DSBs | FISH | detection of chromosomal, genetic and genomic aberrations | reproducibility and signal discontinuation |
| DNA strand breaks | DBD–FISH | quantitative detection of SSBs and DSBs from a single cell | irregularity of signal and high autofluorescence |
| DNA fragmentation: apoptosis | TUNEL | TdT dUTP nick-end labeling | sensitivity, specificity, not self-sufficient method |
| DNA oxidation and photoproducts | HPLC-MS | the method of choice for measuring modified DNA bases | high cost and expertise for accurate measurement |
| **INDIRECT** | | | |
| DNA oxidation and modification | ELISA, IHC | immunological methods for quantification of DNA damage | cross-reactivity of the antibodies with usual DNA bases |
| DNA strand breaks | FCM | quantitative detection of DNA DSBs *via* H2AX molecules | reaction kinetics and cell cycle phase |
| DNA mutation | *in vivo* MMR | introduced mutations are tagged with MutL foci | rapid repair and dilution of mutation effect |

The following acronyms are used: MMR, mismatch repair; comet, single-cell gel electrophoresis; TUNEL, terminal deoxynucleotidyl transferase dUTP nick-end labeling; HPLC-MS, high performance liquid chromatography-mass spectrometry; DBD-FISH, DNA breakage detection-fluorescence *in situ* hybridization; IHC, immunohistochemistry; ELISA, enzyme-linked immunosorbent assay.

## 3.2.2. Usual methods for DNA damage detection

A very useful method to reveal and quantify DNA strand breaks is called DNA breakage detection–fluorescent *in situ* hybridization (DBD–FISH) **[161]**. DBD-FISH is an alternative FISH method that potentiates the detection and quantification of DNA strand breakage (SSBs and DSBs) from a single cell **[157]**. It displays high sensitivity to ionizing radiation, e.g. the minimal dose inducing damage is 0.1 Gy. It is also successful in making X-ray high dose response, where DBD-FISH signal increases linearly with dose, without reaching saturation **[162]**. A linear dose response was previously problematic due to non-adequate chromosomal phase and high level of its damage that led to (methodological) saturation in high doses **[161]**.

Another version of FISH method is comet-FISH method that is used to detect repetitive DNA sequence **[161, 163]** with intercalating probes. This method is on a cellular level and it detects DNA damage and repair in total and in specific regions. This technique is useful for detection of site-specific breaks in DNA regions which are relevant for the development of different diseases **[164]**. It was also made in combination with single-gel electrophoresis to detect telomere repeated sequence. Due to its damage (e.g. photoproducts, DNA crosslinking with another DNA **[165]**, SSBs), DNA can be less available for intercalating agents. Since probes of interest are intercalating agents, they do not have the full access to intercalating DNA and detection is limited. In addition, DNA might also be lost, especially from the tail, by diffusion. Finally, direct and indirect methods display different advantages and disadvantages **(Table 6)**; some methods are more appropriate for certain experiments than others.

A good example of appropriate indirect diagnostic methods following IR exposure is the visualization of phosphorylated forms of variant histone in eukaryotes (e.g. as γ-H2AX foci) **[166]**. First and foremost, upon DSB formation, DNA reacts with recruiting phosphorylation of thousands of variant histones. γ-H2AX foci that are used as a biomarker of DNA damage are thought to represent DSBs in a 1:1 manner **[167]**, although this has become questionable in the case of a cluster of DSBs that are represented by one large γ-H2AX foci **[168]**. Afterward, at sites of DSBs, detection of massive phosphorylated histones is mediated by antibody and can be visualized by immunofluorescence and/or western blot *via* secondary antibodies. Accordingly, maximal level of γ-H2AX is 30 minutes after IR **[169]**. The linear dose response was obtained 24

and 48 hours after irradiation in blood and skin cells, respectively **[170]**. Notably, γ-H2AX can also be recruited by UVR **[171]** or DNA crosslinkers, e.g. mitomycin C **[172]**.

### 3.2.3. Mismatch repair and *in vivo* DNA damage detection method

An indirect method that follows DNA mutations in real time *in vivo* was created using mismatch repair (MMR) machinery **[160]**. MMR is a highly conserved mechanism in prokaryotes and eukaryotes by which cells detect and correct all base-base mispairs but C-C, which is an extremely rare error **[173]**. Hemi-methylation of adenine in 5'GATC sequence is controlling and strand-directing MMR in *E. coli*. Four proteins, MutS, MutH, MutL and MutU (UvrD), are specifically involved in this process **[174]**. MMR system enables detection of DNA mutations *in vivo* by labeling MutL protein with GFP/YFP, so that only unrepaired mismatches will cause fluorescent focus formation. When chemical modifications (e.g. base alkylations, oxidations and base analogs) cause base-pair mismatching, such DNA damages are also detected using this method **[160]**.

## 3.3. General methods for detection of protein carbonylation

### 3.3.1. Background

The following paragraphs are taken from our publication **[104]**: "Measurement of PC was initiated by Stadtman and coworkers as a biomarker of aging **[12]**. Quantification of protein carbonylation includes biochemical and immunological assays (ELISA, Western blot, dot blot and *in situ* carbonylation), spectrophotometric and chromatographic techniques and mass spectrometry analysis (MS).

### 3.3.2. Usual methods for carbonyl detection

Previously, carbonyl detection was performed mostly indirectly (with Western blot and ELISA) **[175, 176]**) using 2,4-dinitrophenylhydrazine (DNPH) **[177]**. Since DNPH reacts in a non-selective manner **[178]** it can give false positive results which are not-reproducible **[179]**. In addition, direct DNPH detection in UV spectrum displays low sensitivity which was partially improved by indirect detection of DNPH with antibodies that carry fluorophore **(1$^{st}$ approach, Figure 12)**. Therefore, new reactants were necessary in the methodological field, e.g. fluorescent labeled aminooxy and hydrazide. These new reactants that are already labeled with fluorophores can be detected directly in gel electrophoresis, without any blotting whatsoever. Therefore, fluorescence difference gel electrophoresis was highlighted in carbonyl detection in so-called 2D-DIGE methodology **[180, 181]**. Since hydrazide carries fluorophore when it binds carbonyls, accuracy, sensitivity and reproducibility (of carbonyl level) increase, compared to DNPH-used techniques **[15, 180] (2$^{nd}$ approach, Fig 12)**. This was a welcomed advance in carbonylation methodology. Nevertheless, it has revealed other problematic points in PC quantification.

Indeed, results that were obtained from the multi-center study showed the incompatibility of modern methods to measure high PC levels **[14]**. Notably, highly carbonylated protein can aggregate *via* protein cross-linking **[13]**. Those aggregates display resistance to proteolysis and are presumably detergent-insoluble **[182, 183]**. Therefore, protein extraction was a critical step in obtaining highly carbonylated proteins **(3$^{rd}$ approach, Fig 12)**. However, this was improved recently with compatible solubilization buffer that reveals the high linear correlation between severely carbonylated proteins and high UV doses **[15]**, unlike previous research **[14]**. Nevertheless, it is important to develop a complementary method which does not include any

protein extraction whatsoever, e.g. optical method, to localize all carbonyls within organism or cell. Finally, optical methods enable *in situ* localization of biomolecules as well as their damage, e.g. *via in situ* hybridization **[184]** and immunohistochemistry **[185]**.

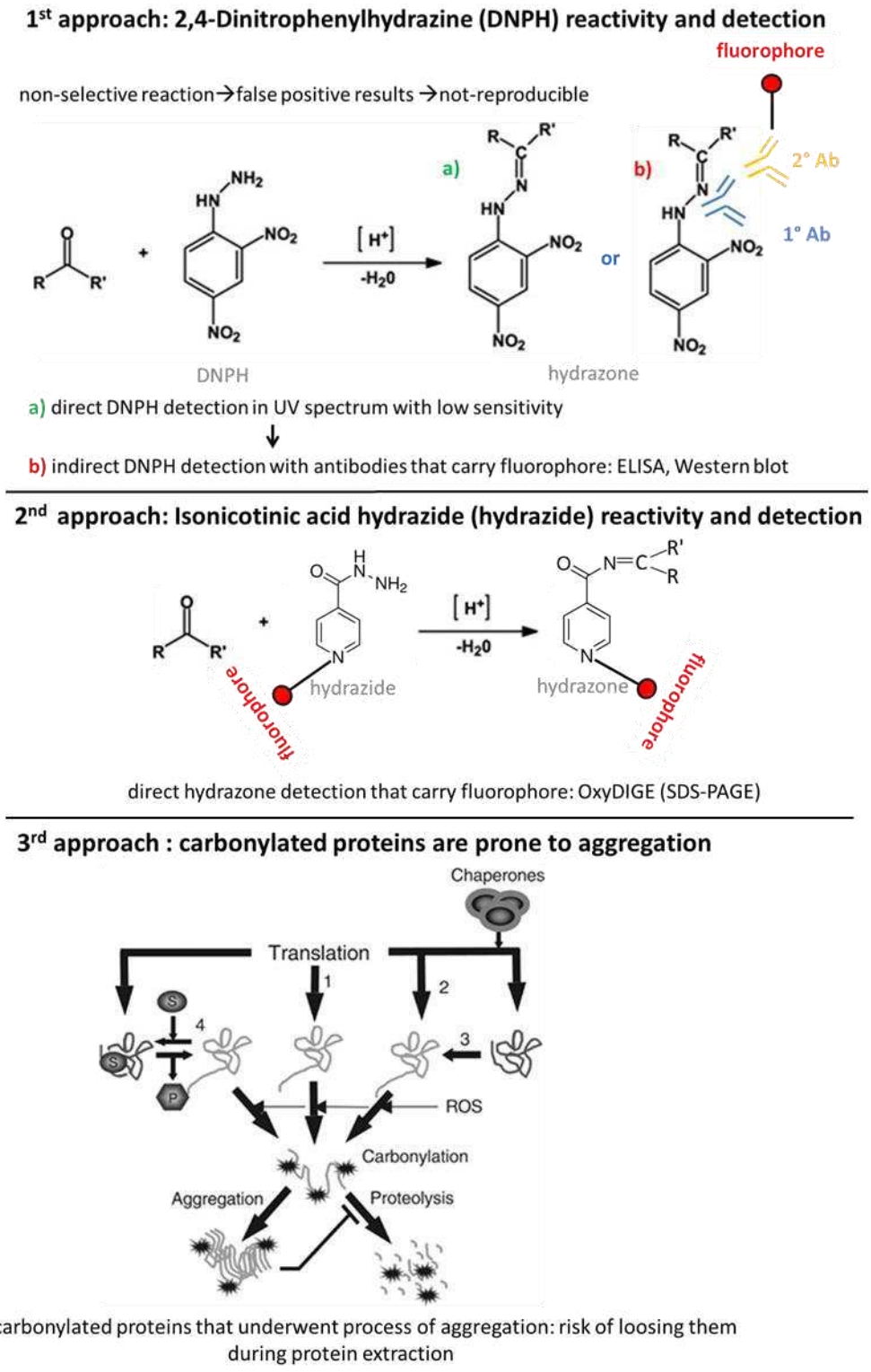


**Figure 12.** Different problematics and partial solutions in the detection of PC. DNPH and hydrazide reactivity with carbonyl groups and examples of its detection are presented in 1st and 2nd approach respectively. Since severe carbonylation is prone to aggregation (photo adopted from **[11]**), it can be lost during protein extraction (3rd approach).

### 3.3.3. *In situ* carbonyl detection methods

As previously stated, all biomolecules contain a certain level of carbonyls (either as natural keto groups or as oxidative modification), whereby the content can increase due to oxidative stress **[5]**. Actual methods for *in situ* detection of carbonylation are rare, especially for DNA carbonylation **[186-192]**. *In situ* carbonylation that was performed on *C. elegans* could not reveal carbonylation in eggs because of disabled DNPH penetration through eggshell **[193]**. In addition, while several biological molecules can be carbonylated, e.g. nucleic acids, lipids, proteins, only total carbonylation was reported without distinguishing the molecular origin of these carbonyls. Although some of those drawbacks (e.g. sensitivity) were sidestepped in the recent study using hydrazide **[192]**, most of those studies used paraformaldehyde (PFA) as organisms' fixator. The problem is that PFA has aldehyde origin with reactivity towards DNPH **[194]** and subsequently introduces false positive signal. Therefore, *in situ* carbonylation methodology needs to be improved to assess carbonyl metabolism within an organism to monitor this damage in time."

# PART III : RESEARCH AIMS AND HYPOTHESIS

The first step of this project is to establish new *in situ* method (without any extraction step) for measuring carbonylation and quantitating biomolecules likely to be carbonylated, i.e. DNA, lipids, proteins and RNA in *C. elegans* after UV exposure (part I). The second step is using this methodology in different models to show the importance of protein carbonylation as a potential biomarker of (i) bacterial death (part II) and (ii) nematodes' aging and damage by ionizing radiation (part III).

(i) Since carbonylation has become a suspected cause of mortality, the kinetics of protein carbonylation, DNA mutations and membrane integrity were monitored in *E. coli* after lethal UV-exposure.

(ii) Some of the consequences of aging and ionizing radiation appear to be shared. To address the question of mechanisms of action in both cases, protein carbonylation level was determined in *C. elegans* after aging and/or chronic exposure to gamma radiation. Simultaneously the lifespan of *C. elegans* has been followed. Mutant *glp-1 Caenorhabditis elegans* has been used because of its conditional sterility which enables the study to be conducted over its entire life cycle.

Hypotheses:

Hypothesis 1: Current methods for measuring highly carbonylated proteins suffer from partial loss during protein extraction, which leaves this highly carbonylated protein fraction undetected: a development of an *in situ* approach can help to obtain total carbonylation signal that also includes previously undetectable fraction.

Hypothesis 2. Protein carbonylation is one of the biomarkers of bacterial cell death after UV exposure that correlates with membrane permeability.

Hypothesis 3: Protein carbonylation and change in lipid metabolism is a faithful marker of aging after exposure to gamma radiation.

# PART IV: MATERIALS AND METHODS

# Research structure

We have started the research in the fundamental radiobiology (at MedILS, Croatia) on the most thoroughly studied and simplest biological model, *E. coli*. We wanted to investigate the biochemical basis of radiation-induced cell death by following cellular damage. As we were also interested in the molecular chemistry of aging, we started to use *C. elegans* as a suitable model of aging, trying to simplify the enormous complexity of human aging and age-related diseases. We wanted to mimic aging by radiation with a notion that it was already proved that radiation can reduce organismal lifespan. Therefore, we have started collaboration with IRSN in France, to investigate the influence of the low-chronic gamma irradiation on *C. elegans* organismal damage and aging. My thesis is the result of this collaboration (IRSN, France and MedILS, Croatia).

# Research outcome

Research outcomes were deduced from research aims in **Table 7**.

**Table 7.** Research outcomes and quantitative outcome measures.

| Research outcome | Quantitative outcome measure |
|---|---|
| UV induced carbonylation (Part I) | UV dose [$J.m^{-2}$]; carbonylation levels [LOF*]; *in situ* assays for nucleic acids and proteins [LOF]; colocalization of biomolecular carbonylation [Pearson's coefficient] |
| Death study (Part II) | UV dose [$J.m^{-2}$]; Survival after UV**; monitoring DNA damage and mutation rate**; carbonylation levels [LOF]; biomolecule levels [LOF] |
| Aging study (Part III) | Gamma dose [Gy]; Kaplan Meier estimation of lifespan [counting and modelling]; carbonylation levels [LOF] and [nmol carbonyls/mg proteins]; colocalization [Pearson's coefficient] |

*LOF is level of fluorescence and ** is counting

# Ethical principles

Research on *Escherichia coli* and *Caenorhabditis elegans* do not require ethical approval.

# Research design

Experimental study was performed under the collaboration of IRSN, France* and MedILS, Croatia**. The design is described in research flowchart.

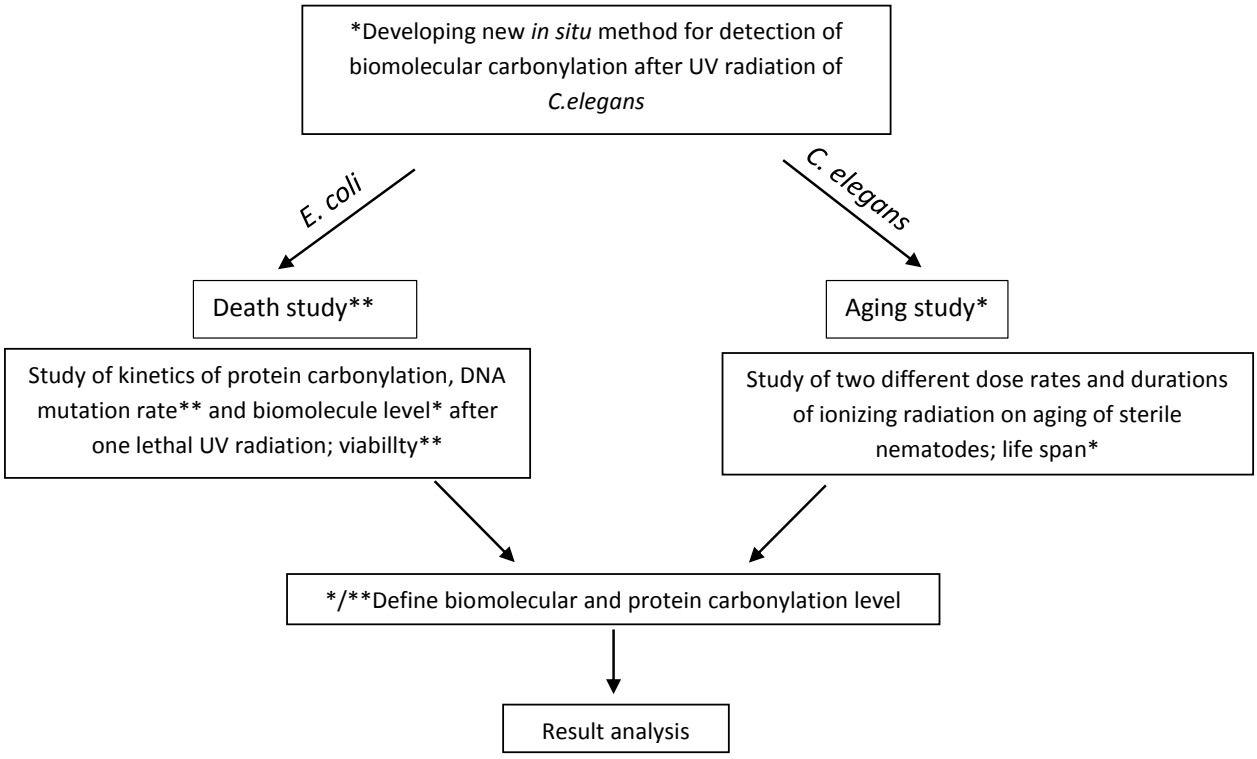

# Research methods

## a) Research model systems

- ***E. coli*: death study**

*E. coli* laboratory strain MG1655 strain that was used for death study (hypothesis 2) is provided by Marina Elez. *MutL* was deleted from chromosome, followed by *E. coli* transformation with the plasmid that contains *mutL –yfp* gene under the control of *lac* inducible promoter. Cells were cultivated in LB medium, supplemented by 1 % of 0.1 M IPTG overnight at 37 °C and 200 rpm. In the morning cells were diluted 100 x in fresh LB medium and supplemented by 1 % of 0.1 M IPTG, followed by 2 hours of incubation at 37 °C and 200 rpm until it reached exponential growth phase ($OD_{600}$ ~ 0.2).

### Viability assay

The viability of *E. coli* was quantified by plating (in 5 µl, 7 serial dilutions) all different treatments, including control, on LB plates followed by incubation on 37 °C overnight. Viability was estimated the day after by counting colony forming units (CFU). Every condition was plated in 5 technical replicates within 3 biological replicates.

- ***C. elegans***

### *In situ* study

The wild-type (*wt*, Bristol N2) and *glp-1* sterile mutant *C. elegans* strains were purchased from Caenorhabditis Genetics Center (CGC, MN, USA). Nematodes were maintained on nematode agar (NGM), fed with *E. coli* OP50 at 18 °C or 15 °C in the dark with 70% humidity, according to standard method **[195]**. N2 (*wt*) animals at young stage were used to set up a new *in situ* method for measurement of carbonylation level (hypothesis 1). *E. coli* bacterial strain OP50 was prepared under the standard procedure **[195]** and seeded on NGM plates, followed by UVC bactericidal exposure (during 20 min with 200 $\mu W.m^{-2}$ at 254 nm, lamp Bio-LinkCrosslinker). Nematodes were collected from NGM plates, washed with M9 medium 3 times (to remove bacteria from *C. elegans*) and aliquoted in 50 µl in Eppendorf tubes. This is non-treated control

for labeling of carbonyls and biomolecules **[104]** but it needs to be frozen prior to labeling in order to enable labeling of carbonyls in embryos (freezing enables penetrating eggshell once it is de-frozen). Therefore, samples were quick-frozen in liquid nitrogen, followed by usage, or stored at −20 °C until usage.

### Aging study

*Glp-1* sterile nematodes for aging study (hypothesis 3) and IR were prepared in 3 steps. All steps were carried out at 15 °C, with 70% relative humidity and in darkness, and were constantly controlled by HOBO **[196]**. All NGM plates which were used for this experiment were seeded with 10 x concentrated bacteria (*E. coli* OP 50) to prevent the starvation and metabolic changes. The first step is transferring 100 gravid worms with worm picker on 10 NGM plates (9-cm diameter plates), followed by 5 days incubation at 15 °C to stimulate the reproduction. The second step is the 1$^{st}$ synchronization at fifth day, where plates were rinsed with M9 buffer and the worms were cleansed 3 times in M9 buffer in glass tubes with centrifuge speed of 400 g during 2 minutes. Cleansed samples were then subjected to bleaching (20 % NaOH, 10 % hypochlorite and 70 % $H_20$) for 5 minutes in order to release eggs from worms' uterus. Fast centrifuge was necessary to prevent eggs' degeneration (800 g for 1 minute followed by removal of a maximum of supernatant). Again, the samples were cleaned 3 times. The number of eggs was counted under the binocular in 1 µl of M9. The volume which contained 5000 eggs was then transferred to 20 NGM plates, followed by 5 days of incubation, as stated above. And finally, on the last day, the procedure of synchronizing the plates was carried out. The rinsing and washing process was the same as in the second step. Samples were passed through the saccharose gradient (3 and 7%), in order to separate only gravid worms whose eggs from uterus should be synchronized over 3 hours (internal communication). Bleaching was carried out on gravid worms, followed by counting the eggs, as in the second step. The volume (which corresponds to 3000 eggs) was then transferred on 50 6-cm NGM plates that fit the $^{137}$Cs source, and 50 eggs were transferred to 15 6-cm NGM plates to follow the lifespan.

#### *Lifespan*

There were approximately 50 worms on 6 cm plate to follow their lifespan. Lifespan was monitored in biological triplicates for every condition. Furthermore, 4 different radiation treatments were at least for 64 hours irradiated. The effects mentioned above are the following: normal aging (control), cumulative radiation (from eggs to old stage with 7 and 52 mGy.h$^{-1}$) and

recovery effect (radiation from eggs to young stage and recovery). The time points for following the lifespan under binocular are every second or third day during radiation, and afterwards every day except weekends. It is important to note that when radiations were finished and eradiated plates were transferred to control incubators without radiation, they were separated from the control plates by a piece of lead and a shell to prevent bystander effect. Bystander effect phenomenon is mirror-like effect induced by radiation. Finally, non-irradiated cells showed the phenotype of damaged irradiated cells that were in the near proximity of irradiated cells **[197]**.

## b) Radiation treatments

Radiation treatments and sample sizes of all models are presented in **Table 8 and 9**. Details of each treatment are described below.

**Table 8.** Sample size of each experiment.

| Methods | *In situ* microscopy | OxyDIGE | Lifespan nematode / viability |
|---|---|---|---|
| ***C. elegans*** | 3 rep*, 15 nematodes | 3 rep, 6000 nematodes | 3 rep, 150 nematodes |
| ***E. coli*** | 3 rep, 1000 bacteria | 4 rep, $10^9$ bacteria | 4 biological rep, 8 technical rep |

*rep is replicate.

**Table 9.** Radiation treatments of each experiment.

| Model | Stage | Type of radiation | Dose rate and time | Condition |
|---|---|---|---|---|
| N2 *C. elegans* | young adult | UVC, 254 nm | 99.99 $J.m^{-2}$ $s^{-1}$, 30' | M9 buffer, 25 °C |
| *E. coli* MG1655 | exponential phase | UVC, 254 nm | 1 $J.m^{-2}$ $s^{-1}$, 100'' | 0.01 M $MgSO_4$, on ice |
| *glp-1 C. elegans* | synchronized embryos | gamma, $^{137}Cs$ source | 7 and 52 mGy $h^{-1*}$ | 6-cm Petri dish, 25 °C |

* Duration of gamma radiation is 2.5 and 19 days.

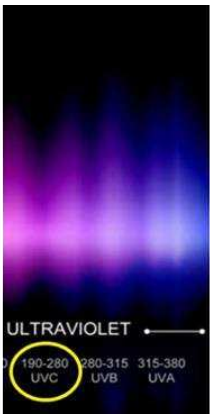


**Figure 13.** Used spectra of UV light.

### 1. UVC radiation

UVC radiation **(Figure 13)** was used on *C. elegans* and *E. coli* for *in situ* method and death study, respectively.

- N2 (wt) *C. elegans*: *in situ* study

Positive control for carbonyl labeling *in situ* was conducted with UVC irradiation at young stage of N2 *C. elegans* **[104]**. UVR of nematodes was performed in 1 ml of M9 buffer, supplemented with $10^{-5}$ triton (Triton X-100, Sigma Aldrich Co, St. Louis, Missouri, USA) (M9t) within a glass plate (petri dish with diameter of 3 cm) during 5 different times/doses (5, 10, 20 and 30 min) with constant dose rate of 99.99 $J.m^{-2}$ $s^{-1}$. *C. elegans* were collected from the plate and washed with M9t medium 3 times, followed by aliquoting in 50 µl, quick-frozen in liquid nitrogen and stored at - 20 °C until usage. Those UV-treatments were used for quadruplex labeling, followed by quantification of carbonylation. The highest dose (UVR during 30 min) represented positive control of carbonyl labeling and was used for confocal imaging, followed by quantification of colocalization between carbonyls and biomolecules.

- *E. coli*: death study

With 100 J.m$^{-2}$ of UVC radiation, we induced 90% to 99% of death in *E. coli* compared to control sample. Initially we measured the kinetics of cell killing and DNA mutation rate, but finally we took 2 relevant time points after radiation to measure all parameters. The first time point is immediately after irradiation, while the second is 2 hours after radiation. Cell survival after irradiation was counted the day after on LB plates in 4 replicates.

Bacteria were cultivated as described above until exponential growth phase, washed 3 times in 0.01 M $MgSO_4$ and concentrated 5 times in 0.01 M $MgSO_4$ (OD ~ 1). UVC irradiation (at 254 nm) was performed at the dose rate of 1 J.m$^{-2}\cdot$s$^{-1}$ during 100 seconds on ice. Viability was estimated as mentioned above. Cell counts of *E. coli* were estimated by plating serial dilutions on LB plates overnight at 37 °C. Half of the irradiated cells of *E. coli* were harvested and washed 3 times in 0.01 M $MgSO_4$ immediately after irradiation. Another half was also harvested but resuspended in LB medium to OD ~ 0.2, followed by incubation for 2 hours at 37 °C and 200 rpm. After 2 hours of incubation, cells were harvested and washed 3 times in $10^{-2}$ M $MgSO_4$. Everything was prepared in 4 biological replicates. *E. coli* was frozen instantly in liquid nitrogen and stored at -80 °C until usage.


**Figure 14.** Used $^{137}$Cs source for IR.

## 2. Ionizing radiation: aging study

Ionizing radiation was used on sterile *C. elegans* to study aging. Plates were placed perpendicular to the $^{137}$Cs source (**Figure 14)** with 1 to 3 RPL (Radio photoluminescent) dosimeters placed on the back of the container to check the stability of the dose rate during the experiment. Irradiation was conducted at 25 °C and with 70% relative humidity in the darkness. IR was started at egg stage at different dose rates provided by a $^{137}$Cs source in an incubator (**Fig 14)**, where the temperature and humidity were controlled by HOBO **[196]**.

There are four irradiation designs during two different time exposures and two different dose rates (**Figure 15)**: in the first irradiation groups worms were irradiated from egg stage to

L4 stage (during 65 hours) with 7 and 52 mGy.h$^{-1}$ reaching 0.5 and 3.3 Gy, respectively; in the second irradiation groups they were irradiated from egg stage to "old" stage (during 19 days) with the same dose rates reaching 3.3 Gy and 24 Gy, respectively (**Fig 15)**. After each treatment was completed, samples were washed with M9 3 times and quick-frozen in grinder tube (minimal volume). Samples were stored at -80 °C until usage.

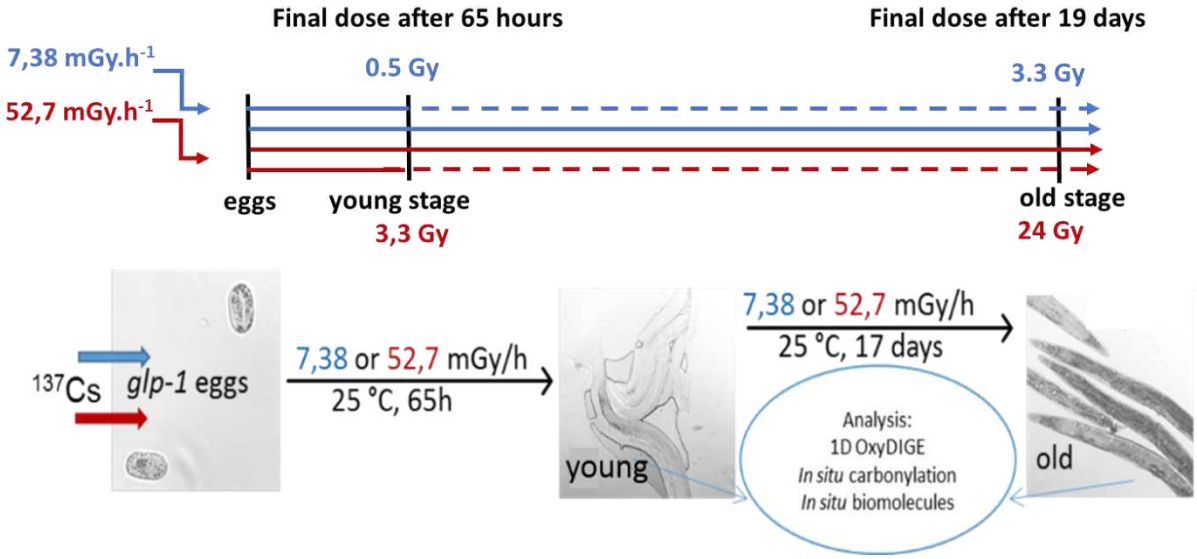


**Figure 15.** There are 4 radiation designs with 2 dose rates (blue and red line, 7 and 52 mGy.h$^{-1}$, respectively). All radiations started at embryo stage (synchronized sterile *glp-1* mutant over 3 h) and stopped either at young stage (65 h=1day of the adulthood) or old stage (19 days=17days of the adulthood). Nematodes that were subjected to IR until young stage were left in recovery until old stage (dashed line). All conditions (including non-irradiated control) were sacrificed at old stage (19 days).

Although the study focused on the young and old stage of worms during radiation and aging, its goal was also to follow their biomolecule level between young and old stage. The biomolecules of interest were: carbonyls, proteins, lipids and nucleic acids. In the experimental design presented in **Figure 16**, different effects were monitored every 2 or 3 days, while HOBO data were also undertaken. Plates were again washed with M9 for 3 times, as mentioned above. After the worms were washed, they were transferred to fresh 6-cm NGM plates with 10x concentrated bacteria to avoid starvation. The samples for biomolecular labeling were collected from all replicates, i.e. 10 worms from 10 replicates were taken and quickly frozen in 100 µl of M9. Aging, radiation and recovery effects were followed from young stage to old stage, whereas dose and dose rate effects were observed within the same stage. Aging effect is normal control without any radiation treatment (first horizontal line in **Fig 16**). Radiation effect is long-term radiation (from egg stage to old stage) with either of chosen dose rates, 7 and 52 mGy.h$^{-1}$ and

corresponding cumulative doses are presented in third and fifth horizontal line **(Fig 16)**, respectively. However, recovery effect is short-term radiation, where nematodes were irradiated during developmental period from egg stage to young stage with both dose rates (7 and 52 mGy.h$^{-1}$, second and fourth horizontal line, respectively), and afterwards there were left to recover until old stage. Dose rate effect compares two different dose rates but the same final dose, i.e. 7 and 52 mGy.h$^{-1}$ at old stage (last vertical line, third and fourth points). Finally, dose effect represents all different doses at the same stage, including the control which represents zero dose. In the first vertical line **(Fig 16)**, there are 3 doses to compare: 0 (control, first point), 0.5 Gy (second and third points) and 3.3 Gy (fourth and fifth points).

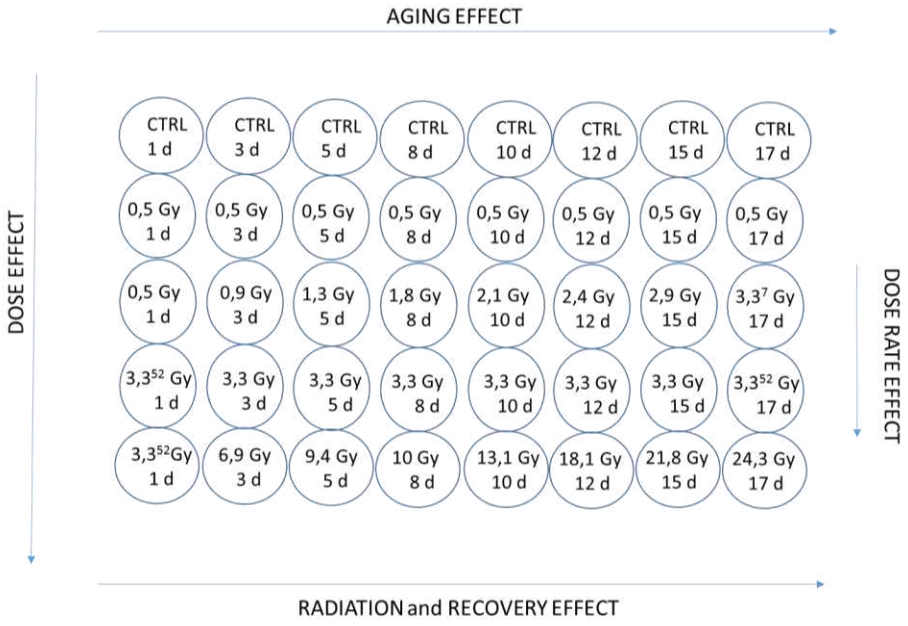


**Figure 16.** Experimental design of *in situ* experiments of *glp-1* mutant. "d" stands for days; "1d" stands for the 1$^{st}$ day of the adulthood, equivalent to 65 h and fix the zero point of the time scale; "0.5 Gy" stands for short term radiation (3 days) with a final cumulative dose of 0.5 Gy and a dose rate of 7 mGy.h$^{-1}$; "3.3$^{7}$ Gy" stands for long term radiation (19 days) with a final cumulative dose of 3.3 Gy and a dose rate of 7 mGy.h$^{-1}$; "3.3$^{52}$" Gy stands for short term radiation (3 days) with a final cumulative dose of 3.3 Gy and a dose rate of 52 mGy.h$^{-1}$; "24.3 Gy" stands for long term radiation (19 days) with a final cumulative dose of 24.3Gy and a dose rate of 52 mGy.h$^{-1}$.

# c) Protocols

## *In situ* labeling

### *In situ* study: *in situ* carbonylation

The following paragraphs are taken from our publication **[104]**: "Chemoporation of all samples was performed with 150 µl of 40% isopropanol (2 -Propanol, SIGMA-ALDRICH Co., St.Louis, Missouri, USA), vortexing and holding for 3 min on ice. followed by centrifugation for 1 min at 19000g at RT and removing maximum of the supernatant (RMS). Cy5 Hz (Cy™5 Mono Hydrazide, GE Healthcare Life Sciences, Buckinghamshire, UK) working solution is 2 $\mu g.ml^{-1}$ in 40% isopropanol. Carbonyls were labeled by placing 150 µl of working solution in chemoporated samples, and these were then incubated for 30 min at RT at 500 rpm. The nematodes were washed with M9t and proceeded with 3 bouts of centrifugation with RMS. The reaction of Hz dye was stopped with 1 ml 0.2 M $NaBH_4$ (each time freshly prepared in water with heating until $H_2$ starts to release) by vortexing and incubating for 15 min. $NaBH_4$ was removed by centrifugation for 1 min on 19000g at RT and RMS.

### All studies: Multiplex labeling for carbonyls, proteins, DNA and lipid fraction

Chemoporation was as described above. Carbonyls were labeled with Cy5 hydrazide, by the protocol mentioned above, followed by 3 washings and RMS **(Figure 17)**. The second labeling was for proteins by placing 150 µl of Cy3 NHS (Cyanine3 NHS ester minimal dye, Interchim, Montluçon, France) working solution, followed by incubation for 15 min at RT at 500 rpm. Washing 3 times and RMS. Third labeling was for DNA by placing DAPI (Vectashield mounting medium for fluorescence with DAPI, Vector Laboratories, Burlingame, California, USA) working solution in chemoporated samples, followed by 30 min incubation at 500 rpm at RT. No washing was done after this step, only centrifugation for 1 min at 19000g at RT and RMS. The last labeling was for lipid fraction by placing 150 µl of BODIPY 505/515 (BODIPY 505/515, Molecular Probes ThermoFisher Scientific, Eugene, Oregon USA) working solution in samples, followed by incubation for 15 min at RT at 500 rpm. Nematodes were washed with M9t, followed by 4 bouts of centrifugation with RMS. $NaBH_4$ and Tris were excluded from quadruplex labeling as this was successive staining, and both of those buffers can change the affinity of binding for other dyes.

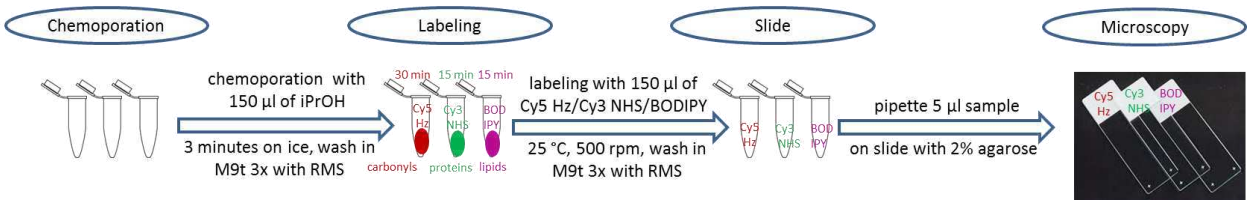


**Figure 17.** Protocols for *in situ* carbonyl, protein and lipid labeling in *C. elegans*.

## *In situ* study: Cy5 Hz and SYBR Green II double labeling of carbonyls and RNA

RNA carbonylation was labeled by chemoporation and DNase I (RNase-Free DNase Set, QIAGEN, Hilden, Germany) treatment, followed by 3 washings in M9t and RMS **[104]**. The first labeling was for carbonyls, with Cy5 hydrazide by the protocol mentioned above, followed by 3 washings and RMS. The second labeling was for RNA by placing 150 µl of SYBR Green II (SG II) working solution, followed by incubation for 30 min at RT at 500 rpm. Washing for 3 times in M9t and RMS **(Figure 18)**.

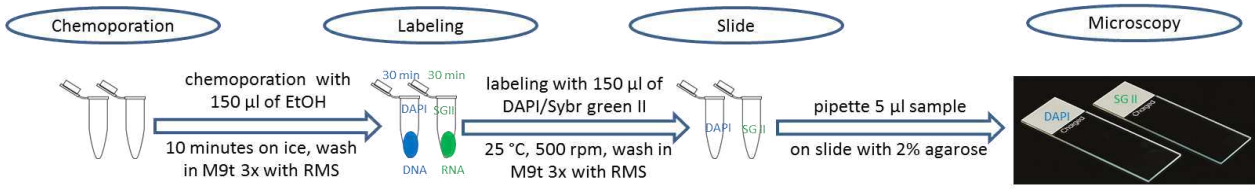


**Figure 18.** Protocols for *in situ* DNA and RNA labeling in *C. elegans*.

## Slide preparation

### *In situ and aging study*

For microscopy, after labeling was finished, slides were prepared by pipetting (with cleaved tip which is pre-coated with M9t to prevent the worms from adhering to the tip) 5 µl of each sample onto a slide with 2 % agarose (Agarose, Type I, SIGMA-ALDRICH Co., St. Louis, Missouri, USA) **(Fig 17 and 18)**. The slides were covered with cover glass."

### *Death study*

For microscopy, cells from exponentially growing cultures were inoculated onto a slide with 2% agarose, supplemented with sugar and IPTG.

## Fluorescence quantification

### *In situ and aging study*

The following paragraphs are taken from our publication **[104]**: "Integrated fluorescence of the slides was quantified using a Typhoon scanner (Typhoon FLA 9500) in LF glass plate stage for signal quantification. Between 81 and 111 worms per condition were analyzed. Each slide with approximately 30 nematodes at the young adult stage was analyzed with the fluorescence mode of scanning, using parameters (excitation/emission and filter) for Cy3 (protein signal, excitation at 532 nm) and Cy5 (carbonyl signal, excitation at 635 nm) detection. Pixel resolution was 10 µm. Both signals were then integrated using IQTL, specific software, in its "colony counting" mode. Integration started with Cy3 protein signal, and continued with Cy5 carbonyl signal, in the same colony as for Cy3. Then the average intensity (intensity normalized by integrated area) of each nematode was considered; the mean and standard deviation was calculated per condition and per replicate. Normalization of 5, 10, 20 and 30 min UVC samples to control samples (no UVC) was finally calculated to express the induction of carbonyls. The carbonyl signal was also quantified by confocal microscopy. 9 worms per condition were analyzed.

## Confocal microscopy imaging

### *All studies*

Images were obtained with an LSM 780 confocal microscope (Carl Zeiss, France) using a 10× dry (N.A. 0.45) and 20× dry (N.A. 0.80) or 63× oil immersion objective (N.A. 1.4) with a pinhole setting of 1.31 A.U. and 8 or 12 bits images.

*Imaging*

Cy5 was excited with the red HeNe laser (633 nm), and emitted light was collected between 643 and 696 nm. Cy3 was excited with the yellow-green laser (561 nm), and emitted light was collected between 554 and 589 nm. DAPI and BODIPY were excited with the blue diode laser (405 nm), and emitted light was collected between 411 and 625 nm. DIC (differential interference contrast) images were collected simultaneously with the fluorescence images, using the transmitted light detector. Comparison of control/treated samples was carried out, using the same conditions of gain, offset and resolution (with a zoom set to 1).

*Imaging of double-labeled samples*

For double labeling with DAPI and SG II, dyes were excited simultaneously with 2 lasers: 405 nm (0.6% power) and 488 nm (0.2% power). Images were acquired in channel mode, using the filter MBS 405/488. For quantitative colocalization SG II and Cy5, dyes were excited simultaneously with 2 lasers: 488 nm (0.2% power) and 633 nm (10% power). Images were acquired in channel mode, using the filter (MBS 488/633). Zoom factor was 3.1 for worms and eggs. Images were taken at objective 63× for worms and eggs.

*Imaging of multiplex labeled samples*

For multiplex labeling with Cy5 Hz, Cy3 NHS ester, DAPI and BODIPY, dyes were excited simultaneously with 3 lasers: 405 nm (2.5% power), 561 nm (0.18% power for worm and 0.10 % power for the egg) and 633 nm (10.0% power). Images were acquired in spectral mode (using the filter MBS 405/488/561/633), and the signal was collected from 411 to 696 nm using a GaSP spectral detector. Zoom factor was 1.1 for the worm and 2.1 for the egg. Images were taken at objective 20× (for the worm) and 63× (for the egg). For quantitative colocalization dyes were excited simultaneously at objective 63× with 3 lasers 405 nm (1.8% power), 561 nm (0.6%) and 633 nm (10% power). Images were acquired in spectral mode (using the filter MBS 405/488/561/633), and the signal was collected from 411 to 696 nm using a GaSP spectral detector. Zoom factor was 3.1 for worms and eggs. Reference emission spectra were recorded for each dye (using their corresponding laser excitation). In addition, a reference spectrum was also recorded on unstained samples for each individual laser excitation (autofluorescence references). A complete set of these reference spectra was recorded for each objective. Spectral separation, using these reference spectra, was applied on multiplex images with linear un-mixing (with or without using the autoscale function) **[198]**, resulting in 4 separate dye channels and 3 background channels. For quantitative colocalization, linear un-mixing was done without autoscale, although autoscale does not change colocalization coefficients. Images were acquired in 8 bits (channel mode) or 12 bits (channel and spectral mode) and were processed using Zen black software (Zen black 2012 SP2 Version 11.0) and Adobe Photoshop CS2 version 9.0.2 (Adobe systems). For quantitative colocalization 12 bits imaging in a spectral mode was used."

***Death study***

*E. coli* cells were visualized with a 100 objective on an Axiovert 200 inverted microscope (Carl Zeiss), equipped with a Photometrics CoolSNAP camera (Princeton Instruments) and a temperature-controlled incubation chamber. Foci were counted manually on 1000 of cells in 4-time points after radiation: 0, 1 h, 2 h and 3 h. Time-lapse was taken every 5 minutes for 24 h, but we presented only until 2 h because most of the mutations have been repaired within 2 h. Images were taken and analyzed by MetaMorph software. Focus fluorescence was calculated by subtracting the background fluorescence of the cell from the maximal pixel intensity of the focus. Imaging of quadruplex labeling was performed as in previous publication **[104]**.

## d) Statistical analysis

### *In situ* study

The following paragraph is taken from our publication **[104]**: "Statistical analyses were done using the statistical software SPSS version 24 (IBM). Before each analysis, the normality (Shapiro - Wilk test) and homogeneity of data variance (Levene's test) were tested. This was repeated after data transformation, when these assumptions were initially not confirmed (log10-transformation). When these assumptions were confirmed, parametric tests were used. In all other cases nonparametric tests were used. Student's t-test, a parametric test, was used to compare the competitive assay with and without Tris for protein labeling, and to compare Pearson's correlation coefficient for colocalization of carbonyls with proteins, DNA, RNA and lipid fraction. Friedman's test was used to assess the relationship between UV-light exposure time and mean fluorescence intensity. When differences were significant ($p < 0.05$), Wilcoxon tests with Bonferroni correction (i.e. resulting in a significant level set at $p < 0.005$) were used to determine where the differences occurred. Following the Friedman tests, when a significant effect of UV-light exposure time on mean fluorescence intensity was found, Spearman's correlations and simple linear regressions were run to further explore the relationship between these two variables."

### Death study

Statistical analyses were calculated by unpaired, two-tailed Student's t test or one-way ANOVA with Tukey post analysis pairwise comparison in GraphPad Prism.

### Aging study

Statistical analyses were calculated in GraphPad Prism. Prior to analysis, Shapiro-Wilk and Levene's test were calculated, followed by parametric (one-way ANOVA with post-hoc Tukey test) or nonparametric analysis (Kruskal-Wallis statistic with Dunn's multiple comparison test). Statistical analyses of the lifespan data were made with XLSTAT-life statistical software. Survival data by the Kaplan Meier method and differences in survival are calculated using the Log-Rank test with 99% confidence. Three statistical parameters were calculated: Log-rank, Wilcoxon and Tarone-Ware.

# PART V: RESULTS

# *In situ* study

## Approach

The following paragraphs of *in situ* study are taken from our publication **[104]**: "As already stated, accurate measurement of carbonylation level is essential in terms of defining its biomarker potential of aging, age-related diseases, radiation induce stress, etc. It is also important to define which biomolecules are the most prone to carbonylation (proteins, RNA, DNA or lipids). None of the previous studies co-localized carbonyls and molecules likely to be carbonylated. Therefore, we improved fluorescent staining and optimized *in situ* labeling of carbonyls, along with labeling of the main potential targets of carbonylation, e.g. proteins, DNA, RNA and lipids. UV dose-response curve was made in correlation with the fluorescence of carbonyl signal. The simultaneous quadruplex labeling of nematodes and eggs (total carbonyls/proteins/DNA/lipids) allows visualized localization of four fluorescent signals.

For quadruplex staining, the chosen fluorophores coupled with Hz and NHS ester are Cy5 and Cy3. BODIPY 505/515 was chosen for lipid labeling in quadruplex staining because Nile red has a wide spectrum, overlapping with Cy3 and Cy5. However, RNA labeling was slightly different than other biomolecules due to Sybr green II non-specific nucleic acid labeling. Since it labels DNA and RNA, nematodes were pretreated with DNase, followed by RNA labeling.

Due to DAPI's wide emission spectrum and some overlapping between Cy5 and Cy3 dyes, BODIPY and Cy3, spectral separation on multiplex images was applied with linear un-mixing (with or without the use of auto-scale function) **[198]**. We checked for autofluorescence of *C. elegans*. With chosen fluorophores, autofluorescence is not significant, except at DAPI wavelengths, where the high autofluorescence below 450 nm requires the use of background un-mixing. Since Sybr green II is overlapping Bodipy spectra, RNA carbonylation was tested separately from other biomolecules (DNA, proteins and lipids).

We also optimized respective concentrations of dyes and laser intensities to obtain homogeneous quadruplex signal without saturation or masking of any dye overlapping with another. The optimal concentrations of Cy5 Hz and BODIPY 505/515 were 2 $\mu g.ml^{-1}$, of Cy3 NHS ester 1 $\mu g.ml^{-1}$and DAPI 0.4 $\mu g.ml^{-1}$ **(Table 10)**. In addition, to minimize the degradation of the previous label by the following one in quadruplex labeling, alcohol medium was chosen as a

solvent of all dyes. Selected chemoporation and labeling were thus carried out, in a test tube (see Materials and Methods section), in isopropanol (Cy5 Hz, Cy3 NHS ester and BODIPY 505/515) and in ethanol (DAPI) instead of usual fixation of the animal with paraformaldehyde, followed by labeling. Finally, labeled biomolecules (lipid fraction, proteins and DNA) and carbonyls have been studied separately, combined by pairs (DNA/carbonyls, proteins/carbonyls and lipid fraction/carbonyls) and combined all together.

**Table 10.** Comparative properties and kinetics of the dyes **[104]** ("h" stands for hours and "d" stands for days) used for total molecular labeling of carbonyls, proteins, DNA and lipids in this and previous research. The concentration of the dye is denoted with "Dye [C]". "Kit" stands for the papers that used the kit for carbonyl labeling and did not mention the concentration of DNPH. Papers on DNA(#) and lipid(*) labeling are numerous, only one representative has been cited. The concentration of SYBR Green II is given with 5X (commercial solution given in 10000X). **High specificity for RNA labeling with SYBR Green II is only when DNase pretreatment is used.

| Molecule | Dye | Fixation | Medium | Dye [C] (µM) | Time | Specificity | Sample and reference |
|---|---|---|---|---|---|---|---|
| Carbonyls | Cy 5 Hz | No | Isopropanol | 2 | 0.5 h | High | *C. elegans* (This paper) |
| | Coumarin Hz | Yes | PFA | 200 | 2 h | Medium | Fibroblasts **[192]** |
| | DNPH | Yes | PFA | Kit | 2 d | Low | *C. elegans* **[193]** |
| | Coumarin Hz | No | Cell medium | 20 | 0.5 h | High | Prostate carcinoma and lung cancer cells **[191]** |
| | DNPH | Yes | PFA | Kit | 1 d | Not shown | Renal cells **[189]** |
| | DNPH | Yes | PFA | $5{,}05 \times 10^3$ | 1 d | Low | Fibroblasts **[190]** |
| | DNPH | Yes | PFA | $5{,}05 \times 10^3$ | 1 d | Low | Neurons **[188]** |
| | DNPH | Yes | PFA | $5{,}05 \times 10^3$ | 2 d | Low | Muscle cells **[187]** |
| | DNPH | Yes | PFA | $5{,}05 \times 10^3$ | 2 d | Low | Brain tissue and cells **[193]** |
| Proteins | Cy 3 NHS ester | No | Isopropanol | 1.7 | 0.25 h | High | *C. elegans* (Only this paper) |
| DNA | DAPI | No | Ethanol | 1.4 | 0.5 h | High | *C. elegans* (This paper) |
| | DAPI | Yes | PFA | 5.4 | 0.5 h | High | *C. elegans* **[195]** # |
| Lipids | BODIPY | No | Isopropanol | 8 | 0.25 h | High | *C. elegans* (This paper) |
| | BODIPY | No | M9 | 27 | 0.33 h | High | *C. elegans* **[199]*** |
| | Nile red | No | Isopropanol | 9.4 | 0.5 h | High | *C. elegans* **[200]*** |
| RNA | Sybr green II | No | Ethanol | 5X | 0.5 h | High** | *C. elegans* (Only this paper) |

## *In situ* carbonylation

**Figure 19 a and b** shows that *in situ* carbonylation increases with UVC dose, visually **(Fig 19a)** and quantified by Typhoon scan **(Fig 19b)**, progressively from 5 to 30 min of irradiation. There were significant differences between all UV-light exposure times and a positive correlation between UV-light exposure and mean fluorescent intensity **(Fig 19b)**, in contrast to results obtained with Oxy-techniques **[14]**. There were significant differences between all UV-light treatments, except in 5-10 minute treatment. Therefore, slide scanning enables a rapid assessment of carbonylation simultaneously for many worms. Similar results were found by applying the advanced OxyDiGE method to the samples after extraction of proteins and use of the specific buffer of protein extract solubilization **[15]**. We used the same UV doses and obtain the same carbonylation induction trend as in previous research **[15]**.

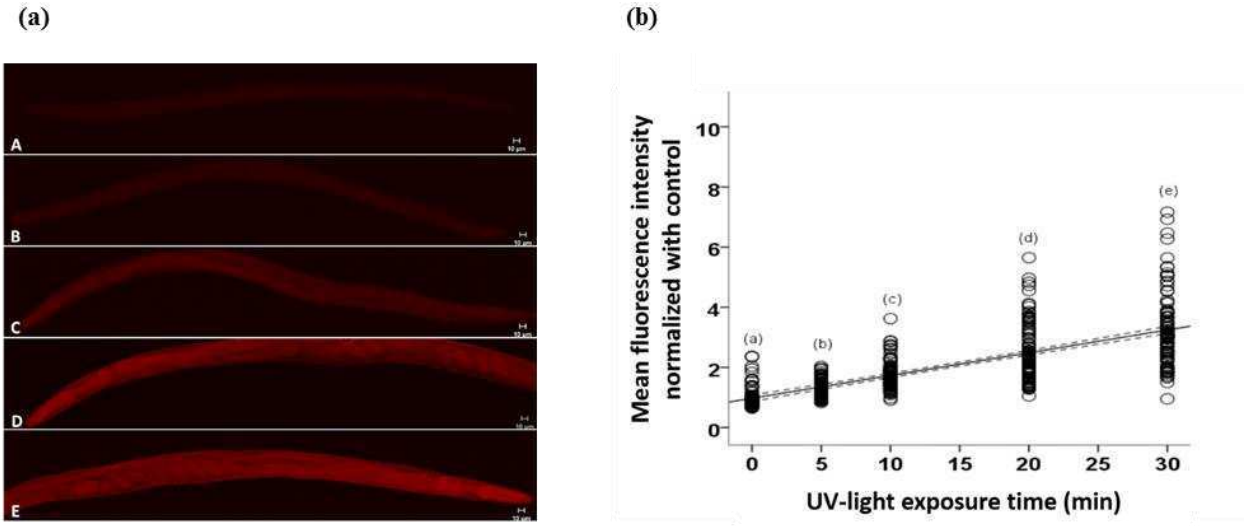


**Figure 19 – (a).** Confocal images of *in situ* detection of carbonylation in *C. elegans* **[104]**. The dose rate was 99.99 $J.m^{-2}s^{-1}$ and UV irradiation durations are 0, 5, 10, 20 and 30 minutes in A, B, C, D and E, respectively. Images are representative of two independent experiments performed in triplicates. Scale bar = 10 µm. **(b)** Integration of the signal from the experiment performed in triplicate with Typhoon scan of slides with 100 worms per condition. Values are normalized to control and plotted in relation to time of UV exposure. Treatments with dissimilar letters are significantly different (post hoc analysis with Wilcoxon tests with a Bonferroni correction applied; $p < 0.005$). Full line represents simple linear regression with 95% confidence intervals (dashed line). Mean fluorescence intensity = 0.975 + (0.076 × UV-light exposure time, $r^2 = 0.542$).

## Biomolecular carbonylation

We successfully labeled all biomolecules regardless of the life stage (from egg stage to adult worms). Quadruplex labeling in the worm and in the egg is shown in **Figure 20**. However, the order in quadruplex labeling is important. For instance, labeling with all dyes at once results in complete binding of Cy5 Hz to DAPI. Therefore, Cy5 Hz carbonyl derivatization should be done first, Cy3 NHS ester protein labeling second, DAPI DNA labeling third and finally BODIPY lipid labeling. Finally, reaction kinetics of all dies (with specific molecular targets) is similar, resulting in homogeneous staining (at employed concentrations, chosen to avoid saturation of one signal relative to others).

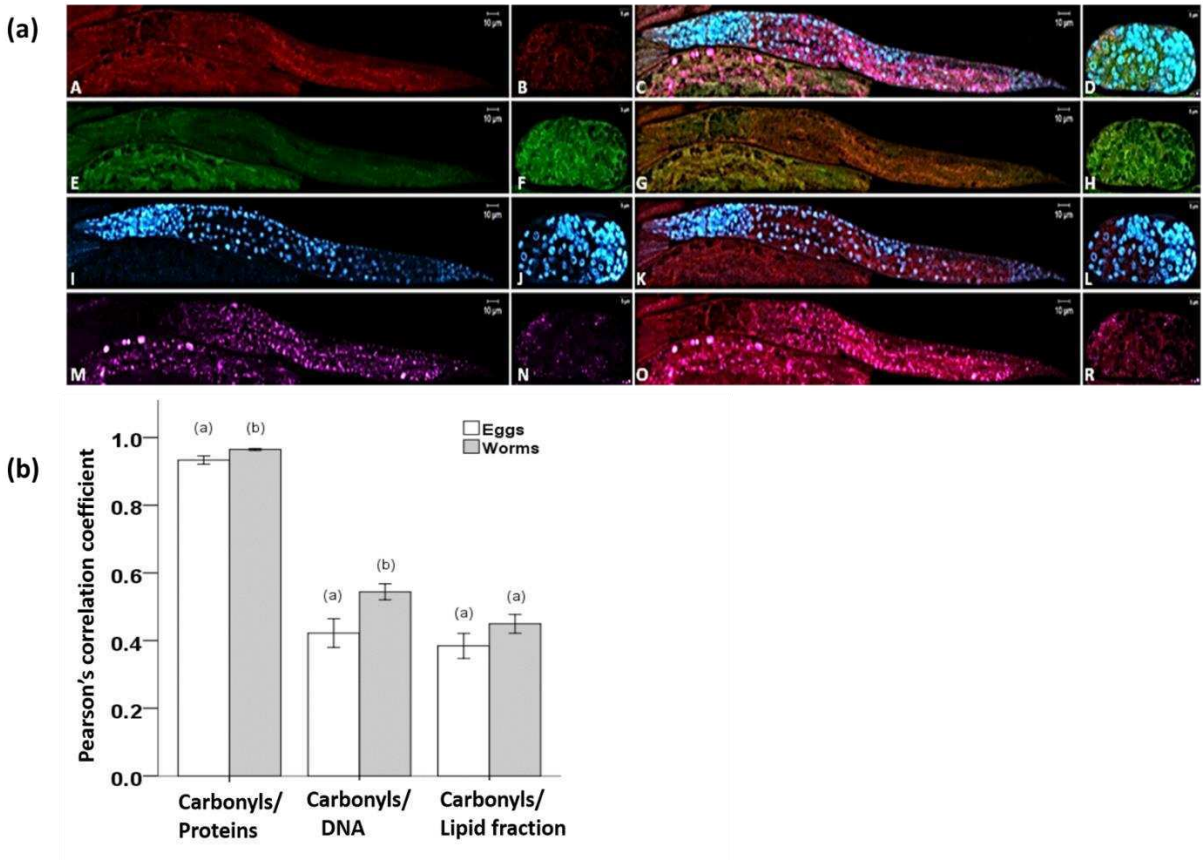


**Figure 20 – (a).** Confocal images of UV exposed *C. elegans* and egg **[104]**: single labeling of carbonyls (A and B), proteins (E and F), DNA (I and J) and lipids from hypodermal cells and on acidic compartments (LRO), (M and N) in worms and egg, respectively. Quadruplex labeling of carbonyls and biomolecules (proteins, DNA and lipid fraction) in worm (C) and egg (D). Double labeling between carbonyls and proteins (G and H), carbonyls and DNA (K and L) and carbonyls and lipid fraction (O and P) in worm and egg, respectively. Images are representative of three independent experiments performed in triplicates. Scale bar for the worm and egg are 10 µm and 5 µm, respectively. **(b)** Colocalization of carbonyls and biomolecules with ImageJ software using the JACoP plugin *via* Pearson's coefficient calculation. Mean ± SE, n = 15. Proteins, DNA and Lipid fraction colocalization with Carbonyls were considered as individuals statistical groups. Within each group, treatments with dissimilar letters are significantly different (Student's t-test; $p < 0.05$).

On the other hand, both nucleic acids (DNA and RNA) display similar colocalization with carbonyls in worms **(Figure 20 vs 21)**. Pearson's coefficient between carbonyls/proteins and carbonyls/DNA was significantly lower in eggs than in worms. On the other hand, there is significantly higher signal of RNA carbonylation in eggs than in worms **(Fig 21 b)**. However, lipid fraction/carbonyls colocalization does not show any significant difference between eggs and worms whatsoever.

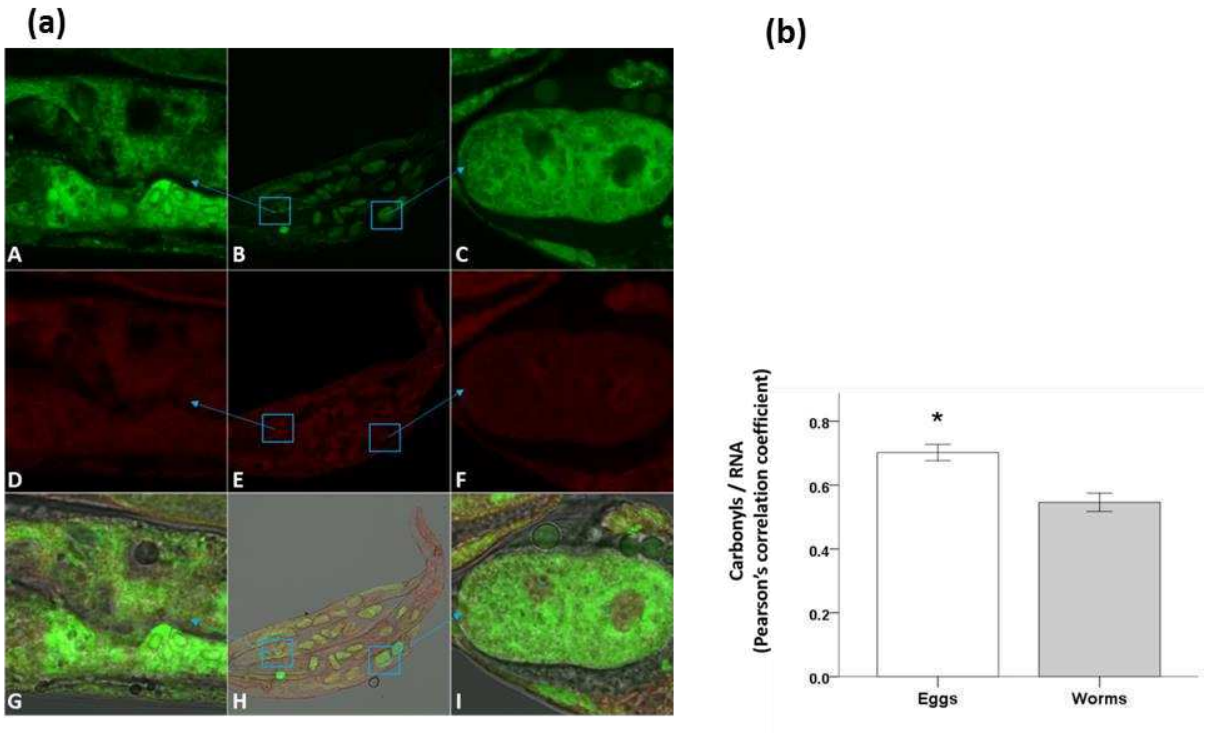


**Figure 21 – (a).** Confocal images of UV exposed *C. elegans* **[103]**: Images of the worm (A, D and G) and the egg (C, F and I) came from zooming the blue squares (B, E and H). Single labeling of RNA (A, B and C) and carbonyls (D, E and F), in worm (A, D) and egg (C, F), respectively. Duplex labeling of RNA and carbonyls is merged with DIC image (G, H and I) in worm (G) and egg (I). Images are representative of two independent experiments performed in triplicates. Scale bar for the worms (B, E and H) is 10 µm, while for the zoomed worm (A, D and G) and zoomed egg (C, F and I) is 5 µm. **(b)** Colocalization of carbonyls and RNA with ImageJ software using the JACoP plugin *via* Pearson's coefficient calculation. Mean ± SE, n = 15 (for eggs and worms). In eggs, there is significant higher colocalization of RNA and carbonyls than in worms (* Student's t-test; $p<0.05$).

Once this new methodology has been set up, we have decided to use it in studying the molecular mechanisms of radiation-induced bacterial death and *C. elegans* aging, as presented in the general context.

# Death study

## Approach

It is not clear why, how and precisely when the life of irradiated cells irreversibly ceases. Here we have explored the time sequence of the integrity of DNA, proteins and cell membrane (the latter is the diagnostic of cell death) by comparing the timing of DNA repair, protein carbonylation and biomolecule levels. Time of cell death is usually detected by membrane disintegration **[200]**. Recent studies of bacterial and animal cell death, following exposure to IR or UVR, found a remarkable correlation between cell killing and the incurred oxidative protein damage, but not with the radiation-inflicted DNA damage **[5]**. Extreme radiation resistance of some bacteria **[201]** and animals seemed to occur mostly by proteome protection systems, but not DNA, even if DNA protection mainly takes place by using proteins. This indicates that proteome rather than genome is the prime target in cell killing by radiation **[5]**. In these studies, however, protein damage (carbonylation) was measured immediately after radiation, whereas survival was determined one day (for *E. coli*) after irradiation by counting colonies. The question is what happens with these colonies in one day. Hence, the focus of this paper is the cell metabolism of *E. coli* exposed to lethal UVC radiation, by monitoring post-irradiation DNA repair, oxidative protein damage (PC) and biomolecule level (proteins, lipids and DNA).

## Viability

UVC radiation dose 100 $J.m^{-2}$ (with dose rate 1 $J.\ m^{-2}s^{-1}$) was used to irradiate *E. coli* in exponential phase (optical density (OD) between 0.2 and 0.4). The viability was counted on (LB) plates the day after, showing that this dose induces 90 to 99% of death in *E. coli* (**Table 11**). Bacteria were plated at different time points after UV radiation to measure the viability, and the longest one was 24 h. We have observed that after 24 h of UV radiation there are more cells than they are in control prior to radiation. This is probably due to 1 to 10% of surviving cells which continue normal division, i.e. radiation effect was diluted with divisions of surviving cells. Therefore, the decision was to take 2 time points after irradiation to measure the survival, immediately after radiation (UV 0 time) and 2 h after radiation (UV 2 h) (**Table 11**). 2 h after UVC radiation there is an increase in the number of bacteria, meaning that the recovery of surviving cells has already occurred.

**Table 11.** The viability of *E. coli* before and after UVC radiation (dose 100 J.m$^{-2}$ with dose rate 1 J. m$^{-2}$s$^{-1}$), measured by colony forming unit (CFU) count of *Escherichia coli* MG1655 on LB plates the following day.

| Sample name | Viability % |
|---|---|
| Control | 100 |
| UV 0-time | 1 % |
| UV-2 h | 10 % |

## Monitoring of DNA repair

A method was developed to detect visually, in living and dead bacterial cells, in real time, all unrepaired mismatched base pairs, including up to 3 non-matched bases, to which the mismatch repair protein MutS binds **[160]**. The foci of a functional MutL-YFP, which accumulates around the mismatch-bound MutS, signal mismatched or non-matched bases, i.e. regular replication errors and DNA damage that cause the loss of Watson-Crick base pairing. MutL foci were followed up to 3 h after irradiation on the agar slide by confocal microscope in time lapses of 5 minutes.

UVC damage and mutations start at approximately 1.2 MutL-YFP foci per cell immediately after radiation, and reduce to 0.08 per cell 2 h after radiation (**Figure 22**), which means that DNA repair is almost completed within 2 h after radiation. MutL foci require MutS to detect mutations/lesions, otherwise they are artefactual aggregates **[160]**. In *mutS* deficient strain all eYFP-MutL foci are abolished from the beginning of radiation, meaning that the foci we see are there due to DNA damage and base-pair mismatches. It has already been shown that MutL foci have a lifetime at least 200 minutes **[160]**.

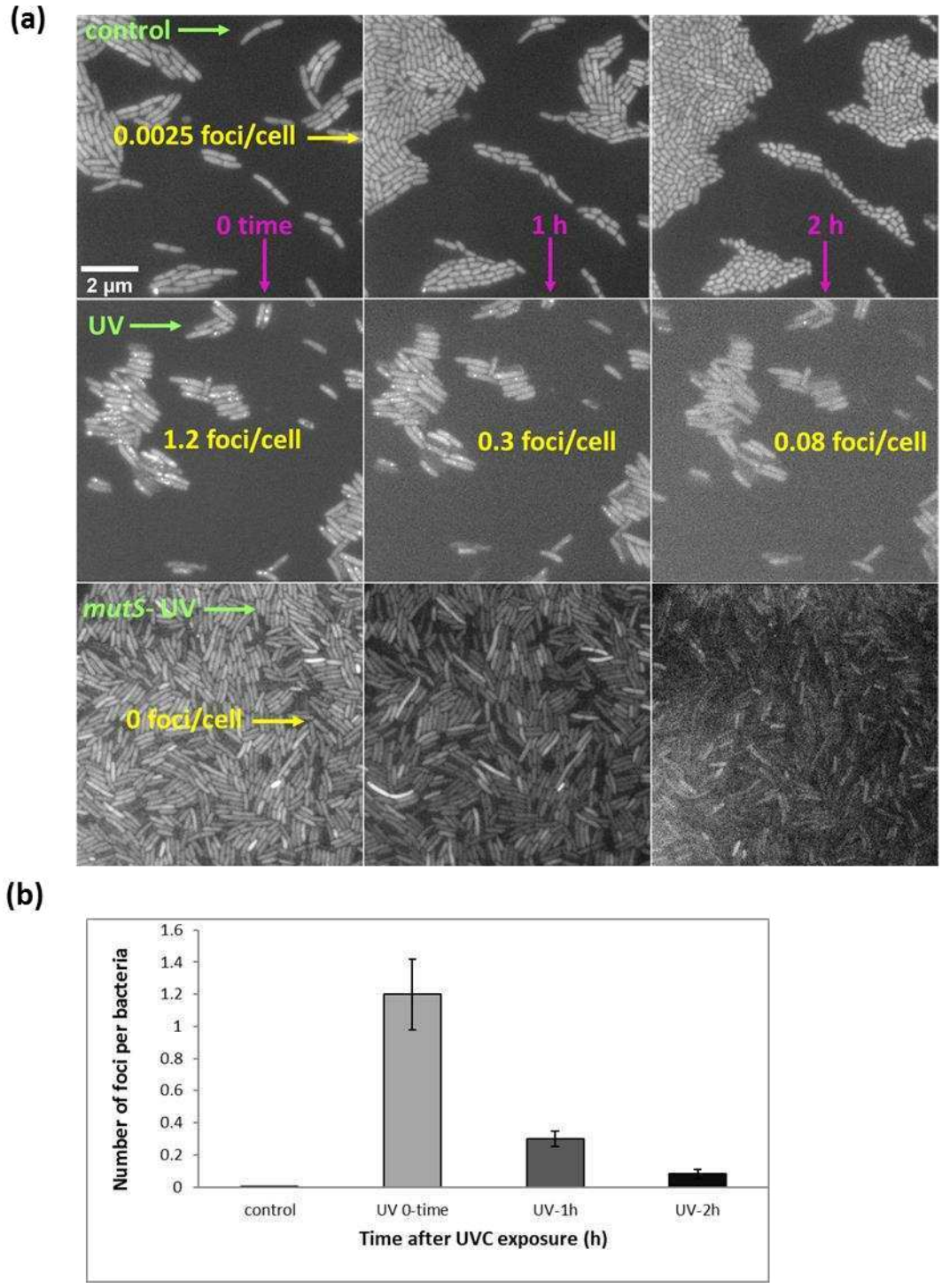


**Figure 22** – **(a)**. Loss of UVC-induced DNA base-pair mismatches after UV irradiation, monitored by eYFP-MutL foci **[160]**. Time points observed after radiation are: immediately after radiation (0 time); 1 and 2 hours after radiation (1 h and 2 h, respectively). At the same time points also control and irradiated *mutS*- strain were monitored. The number of MutL foci per cell is indicated for all conditions, whereas it was already known that *wt* has 0.0025 foci per cell and *mutS*- strain has no foci but random aggregates **[160]**. The experiment was done 3 times with 4 replicates. Scale bar is 2 µm. **(b)** Quantification of foci in UV-irradiated *E. coli* was counted manually on 1000 cells per condition in 3 denoted time points.

## Detection of macromolecules and carbonyl groups in permeabilized cells

Membrane integrity prevents internalization of diagnostic drugs; therefore it can be used for the quantification of cell death and, if the drug carries a hydrazide group, also for the assessment of intracellular carbonylation in dead cells **[200]**. Herein, all cells are permeabilized to monitor the levels of proteins, DNA and lipids as well as carbonylation in all cells **[104]**. Biomolecule labeling was done along with carbonyl labeling, according to the recent procedure **[104]** in **Figure 23** and signal quantification **(Fig 23b)**. Experiments were carried out on untreated *E. coli* (control), immediately after UV radiation (UV 0-time) and 2 h after radiation (UV-2 h).

Immediately after UV irradiation (100 $J.m^{-2}$ with dose rate 1 $J.\ m^{-2}s^{-1}$, UV 0-time), there was a small effect on protein and carbonyl levels compared to control. However, the more significant difference was observed on lipid level in UV 0-time compared to control **(Fig 23)**. On the other hand, DNA showed decreased level immediately after UV irradiation, compared to control (although not significantly), presumably due to DNA fragmentation or change in DNA supercoiling **(Fig 23)**. Indeed, DAPI is a highly specific DNA stain, preferentially binding to AT-rich regions of DNA molecule **[202]**, regions that expectedly contain cyclobutane pyrimidine dimers (CPD), in particular after UV irradiation **[203]**. We observed ~25% decrease in DAPI labeling, following UV radiation **(UV 0-time, Fig 23)**. Quadruplex labeling at UV 0-time reveals even more this decreased fluorescent labeling of DNA, compared to control **(Fig 23a)**.

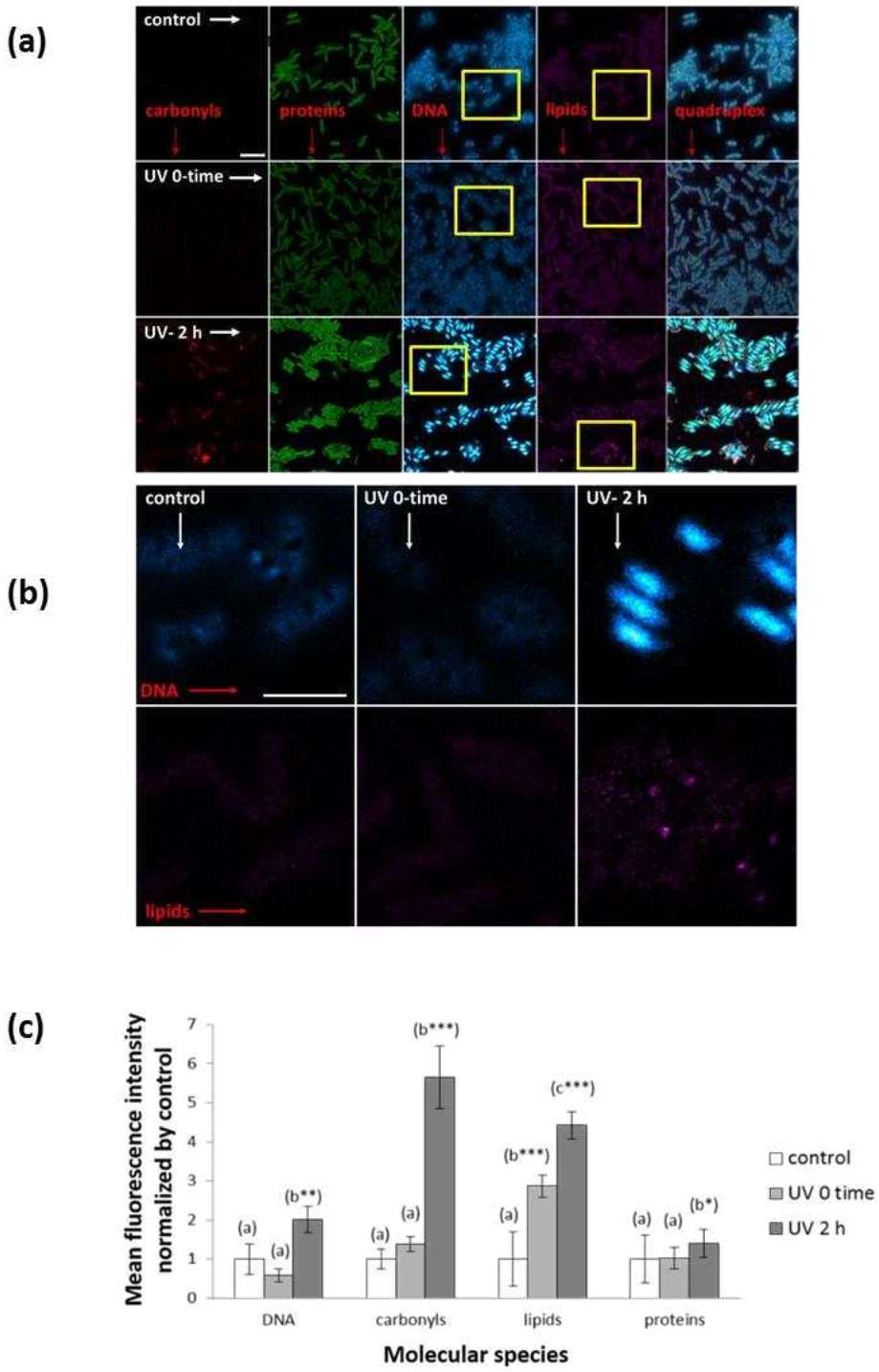


**Figure 23 – (a).** Confocal images and quantification of biomolecules and carbonylation in *E. coli* control and after UVC radiation (UV 0-time and UV-2h), showing single labeling of carbonyls, proteins, DNA, lipids and quadruplex labeling of carbonyls along with proteins, DNA and lipids. Images are representative of 3 independent experiments, carried out in triplicates. Scale bar is 5 µm. **(b)** Images of zoomed regions delineated with yellow squares **(a)** of DNA and lipids in all conditions. Scale bar is 2 µm. **(c)** DNA, carbonyls, lipids and proteins were considered as individual statistical groups: mean value ± SE, n=10. The experiment was done 3 times with 4 replicates. Treatments labeled with starred letters are significantly different (one-way ANOVA with Tukey post analysis; * < 0.05, **<0.01 and ***<0.001).

In the course of our investigation of the effects, a significant difference was observed on biomolecule level 2 h after UV radiation (UV-2 h), compared to control and UV 0-time (**Fig 23)**: signal for the levels of all biomolecules was increased. Since a high increase in global carbonylation at 2 h after UVR is the most significant result, we verified *in vitro* labeling of protein carbonyls that was normalized to protein, where the increase in protein carbonylation 2 hours after UVR was confirmed **(Figure 24)**. This excludes an artefactual signal increase for protein carbonylation.

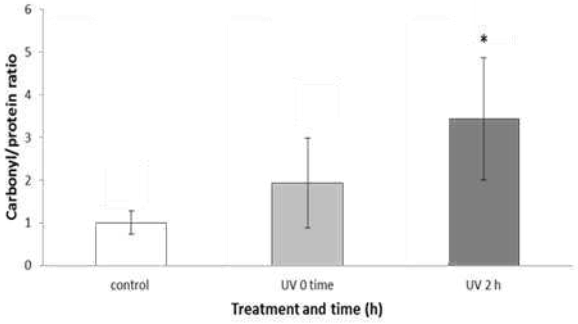


**Figure 24.** Protein carbonylation in *E. coli* after UVC radiation - Image J quantification of OXYBLOT and SDS-PAGE. Different conditions were considered as individuals statistical groups: Control- *E. coli* MG1655 without treatment; UV 0-time; MG1655 radiation without post-irradiation incubation; UV 2 h - MG1655 radiation with 2 h post-irradiation incubation. The experiment was done 3 times with 4 replicates. Treatment with the star is significantly different (unpaired, two-tailed Student's t test; $p < 0.05$).

In addition, DNA also shows increased signal in UV-2 h compared to control and UV 0-time **(Fig 23 a, b and c)**. This is consistent with our results that nearly 90% of DNA lesions recognized by the MutS/MutL proteins are repaired during 2 h after UV radiation **(Fig 22)**. The signal is more central and more intense in DNA UV-2h sample than in control and UV-0 samples. Some immunofluorescent microscopic observations revealed that genome in *E. coli* is compacted more in the final round of the stationary phase **(Fig 23 b, right panel)**, unlike few compacted bodies (nucleoids) in exponential phase **(Fig 23 b, left and the central panel) [204]**. In stationary phase, the nucleoid becomes more condensed **(Fig 23b, DNA, UV- 2h compared to control and UV 0-time)** presumably to protect DNA from damage **[205]**, resembling *D. radiodurans* radioprotection mechanism of condensed nucleoid **[122]**. Nevertheless, increased labeling of DNA should also be confirmed with another appropriate method, e.g. pulsed-field gel electrophoresis (PFGE). This approach has already been used in another research and shown that bacterial DNA was repaired after irradiation **(Cvjetan et al, unpublished communication)**.

Protein level was also increased apparently *in situ*, which requires additional confirmation *in vitro* to validate this finding. If protein level is truly increased 2 hours post-irradiation, this is in agreement with the observation that protein neosynthesis takes place at 1 to 3 h UV post-irradiation depending on UV dose **(Cvjetan et al, unpublished communication)**.

Being consistent with other biomolecules, UV irradiation also increases lipid level, which also needs further proof, e.g. with electron microscopy **(Fig 23)**. Moreover, lipid distribution also seems affected by irradiation, especially after 2 hours **(Fig 23)**. Lipid droplets (LD) are more uniformly distributed with potentially "small dotted pattern" in control. Although we are not at high magnification to confirm "small dotted pattern" of LDs, there is still a difference between UV 0-time and UV-2h regarding pattern, distribution and intensity. Moreover, UV-2 h seems to have disorganized this uniformed LD distribution (LDd) compared to UV 0-time (and control). Change in lipid distribution of UV 2-h is seen *in situ* as "dot-like effect" **(Fig 23b, lipids, UV-2h),** compared to more uniform lipid labeling in control and UV 0-time **(Fig 23b, lipids, control and UV 0-time)**.

Our next challenge is to see if lipid level and pattern are also altered due to aging and/or ionizing radiation of *C. elegans*.

# Aging study

## Approach

Although there might be multiple causes of aging, they converge to a few key mechanisms that affect the lifespan **[129]**. As already mentioned **(part 1.3.2)**, germline ablation **[82]**, mTOR pathway **[206]** and IIS pathway **[47]** are influencing aging. Moreover, another gene-block is known to regulate worms' development, phenotype and lifespan, e.g. clock genes (*clk-1*, *clk-2*, *clk-3* and *gro-1*). Numerous mechanisms, which also influence aging, influence these genes, e.g. autophagy and proteostasis control **[47]**. In addition, during aging there is an exponential increase of oxidative protein damage in very diverse animal species **[207]**. It has been suggested that also modification of lipid membrane plays a major role in aging **[208]**. Recently, it was shown that epigenetic drift, mediated by different PTMs such as DNA methylation and histone modification, impacts gene expressions and biomolecular interactions which finally affect aging **[46]**.

An old theory **[209]** posits that, through similar mechanisms, ionizing radiation accelerates aging **[61]**. Indeed, gamma irradiation and aging exert their effects *via* ROS. However, results in lifespan vary depending irradiation regimen. As nature provided environmental chronic ionizing radiations which can be overexpressed by nuclear accidents, e.g. Fukushima **[210]**, experimental exposure mimicking such accidents needs to be done to assess chronic risk **[38]**. As elaborated in the introduction **(part 1.3.3)**, reproduction is the most radiosensitive biological parameter, also for nematodes **[90, 93, 94]**. As germline ablation has a strong impact on a lifespan, radio-induced reprotoxicity could also have an impact on the longevity. Therefore, the primary interest of this research is to verify if low dose/dose rate chronic gamma irradiation influences the longevity of sterile *C. elegans* mutant (suitable for lifespan studies).

## Model system: thermosensitive sterile mutant *glp-1*

There is a constant tradeoff between investment in somatic maintenance and reproduction. *C. elegans* is a good experimental model to elucidate how germline and reproduction affect the longevity. It is known that germline ablation increases the lifespan. Some of transcription factors that are involved in lifespan extension by germline elimination are DAF2, DAF-12 and DAF-16, and are involved in IIS pathway **[45]**.

G*lp-1* sterile mutant facilitates the study radiation effect of *C. elegans* cohort that does not reproduce. G*lp-1* mutant reproduces normally at the permissive temperature (15 °C) but is sterile at the restrictive temperature (25 °C) **[85]**. Completely sterile nematode (without any progeny) can be obtained when *glp-1* eggs are placed at 25 °C **(Figure 25)**. At restrictive temperature, *ex utero* development of *glp-1* eggs to young adult sterile nematodes, lasts for 64 hours **(Fig 25)**.

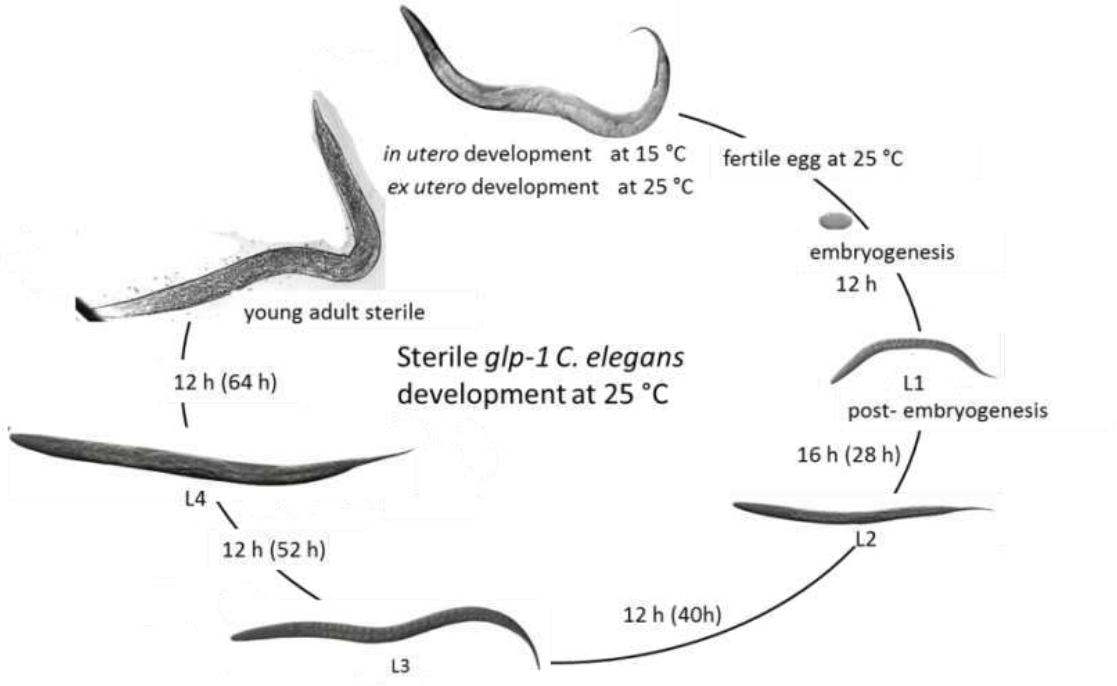


**Figure 25.** Development of thermosensitive mutant *glp-1* at the restrictive temperature, 25 °C. Scheme represents *ex utero* development of *glp-1* mutant.

## Impact of low-dose chronic gamma irradiation on the lifespan

Chronic gamma radiation was delivered at 2 different dose rates, i.e. 7 and 52 mGy.h$^{-1}$, during 2 different periods, i.e. from eggs to young adult stage (64 h); and from eggs to old stage (19 days). 64 h and 19 days in this experiment is equivalent to 1$^{st}$ and 17$^{th}$ day of the nematodes' adulthood, which we denoted as 1 d and 17 d, respectively, in materials and methods. This was accompanied by non-irradiated control to follow normal aging. Lifespan and some biomolecule levels were followed in all of these conditions. The maximum lifespan of sterile *C. elegans* observed was around 40 days – twice that of the normal nematode – as reported in the literature **[211] (control, Figure 26a)**. Lifespan data were processed with Kaplan-Meier estimator (work performed with Prof. S. Galas, Montpellier University, France). Low chronic gamma irradiation significantly reduces the lifespan of *glp-1 C. elegans* (at both dose rates, final doses and the duration of radiation) **(Fig 26b)**

($p<0.0001$). The "long-term radiation" (which lasted for 19 days) at 7 $mGy.h^{-1}$ shortened lifespan the most, as compared to controls **(Fig 26a)** and to the other treatments **(Fig 26b)**. Indeed, "long term radiation" with higher dose rate (52 $mGy.h^{-1}$) is not significantly different from other treatments **(Fig 26b)**. Finally, "recovery treatments" (radiation from eggs to young stage, followed by recovery until death) also failed to show any difference among treatments, whatever the different dose rates (7 and 52 $mGy.h^{-1}$) **(Fig 26)**. In previous studies some development stages of nematodes appeared more sensitive to irradiation **[62]** and that lower doses of gamma rays can be more detrimental than predicted effect assessed from linear dose response **[212]**. To investigate the underlying mechanisms and better understand the results, we performed assays at microscopic levels.

**(a)**

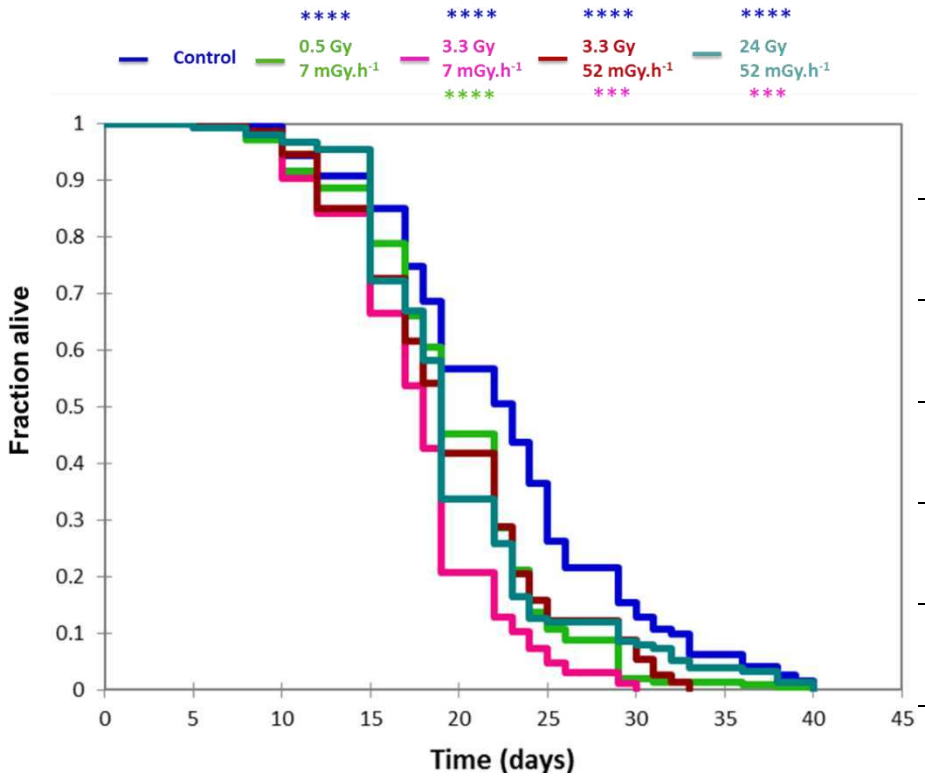


**(b)**

| **Dose**<br>**Dose rate**<br>**Condition** | **0.5 Gy**<br>**7 mGy.h$^{-1}$**<br>**Recovery** | **3.3 Gy**<br>**7 mGy.h$^{-1}$**<br>**Radiation** | **3.3 Gy**<br>**52 mGy.h$^{-1}$**<br>**Recovery** | **24 Gy**<br>**52 mGy.h$^{-1}$**<br>**Radiation** |
|---|---|---|---|---|
| **0**<br>**0**<br>**Control** | <0.0001 | <0.0001 | <0.0001 | <0.0001 |
| **0.5 Gy**<br>**7 mGy.h$^{-1}$**<br>**Recovery** | / | <0.0001 | 0.984 | 0.9 |
| **3.3 Gy**<br>**7 mGy.h$^{-1}$**<br>**Radiation** | <0.0001 | / | 0.000 | 0.000 |
| **3.3 Gy**<br>**52 mGy.h$^{-1}$**<br>**Recovery** | 0.984 | 0.000 | / | 0.484 |

**Figure 26 - (a).** Kaplan-Meier estimation of the lifespan of *glp-1* mutant after gamma radiation. Different conditions were considered as individuals statistical groups: Control (blue line)- *C. elegans* without radiation treatment; 0.5 Gy (green line)- γ radiation from eggs to L4 stage with 7 mGy.h-1 and recovery until death occurs; 7 mGy/h (pink line)- γ radiation from eggs to old stage with 7 mGy.h$^{-1}$ and recovery until death occurs; 3.3 Gy (red line)- γ radiation from eggs to L4 stage with 52 mGy.h$^{-1}$ and recovery until death occurs; 52 mGy.h$^{-1}$ (turquoise line)- γ radiation from eggs to old stage with 52 mGy.h$^{-1}$ and recovery until death occurs. The experiment was performed in triplicates. Treatments with stars are significantly different (Kaplan-Meier method; ***<0.001 and ****<0.0001). **(b)** In this table there is a statistical summary (XLSTAT-life statistical software) of survival data by the Kaplan Meier method and differences between survivals calculated using the Log-Rank test with 99% confidence. Log-rank statistical parameter is denoted in the table. Statistical significance is < 0.001.

## Impact of aging, radiation and recovery after radiation upon key macromolecules and their colocalization

The levels of biomolecules and their visualization in young and old nematodes (with and without radiation) are presented in **Figure 27**. Labeling of biological macromolecules is carried out according to recent optimized *in situ* procedure **[104]** in order to be able to study quantification and colocalization of carbonyls and biomolecules.

Young stage nematode is usually a "fit and fast" worm, endowed with fast coordinated movements, while old ones are "large and slow" **[213]**. Comparing 1d and 17d nematodes, aging significantly increases carbonyl level (2.5-3 fold) whatever the conditions (control and irradiated) **(Fig 27c; top and bottom left)**. In contrast, chronic gamma irradiation reduces carbonyl level in young (2-3 fold) and old (1.5-5 fold) stage, whatever the dose rate, final dose or duration of radiation **(Fig 27c; top and bottom left)**. Chronic irradiation decreases the level of carbonylation, while aging increases carbonylation in unirradiated and irradiated nematodes. In addition, carbonylation at this magnification seems to be decreased in the intestine compared to other parts of *C. elegans* body, whatever age or radiation **(Fig 27a)**.

Regarding lipid level, our results showed a high level of lipids compared to previous N2 *wt* nematode (data not shown). This is in agreement with the literature **[82]**. In addition, lipid level trends with aging and/or after irradiation are similar to carbonylation. Namely, lipid level increases 1.7-fold with age of unirradiated nematodes and 2.25-fold for chronically irradiated nematodes (7 $mGy.h^{-1}$ but not 52 $mGy.h^{-1}$ dose rate). Irradiation itself decreases lipid levels at young (3.75-7.5 fold) and old stages (3-13 fold) **(Fig 27c, middle top and bottom)**. Moreover, lipid distribution along the nematode body appears impacted by aging and irradiation **(Fig 27a, lipid panel)**. However, only a few worms were observed per condition and need to be verified with visualization of lipids and their distribution, e.g. with electron microscopy. At young stage (L4 stage), lipid droplets (LD) seem distributed along nematodes' body in two parallel lines in "dense small dotted pattern", separated visibly by the digestive system. LDs at control young stage give the symmetrical appearance **(Fig 27a, lipid panel, control and Fig 27b, control young nematode)**. Chronic gamma irradiation during developmental stage (from eggs to L4 stage) seems to disorganize this uniformed LD distribution (LDd) and digestive system becomes difficult to discern **(Fig 27a, lipid panel, 0.5 and 3.3 Gy young and Fig 27b, irradiated young nematode)**, unlike the control young nematodes **(Fig 27a, lipid panel, control and Fig 27b, control young nematode)**. On the

other hand, in aging (old stage at 17$^{th}$ day of the adulthood) nematodes LDs seem to go out of the inner body to the sides, compared to young stage, and the size of LDs is changed **(Fig 27a, lipid panel, control old compared to control young)**.

Interestingly, protein level is not significantly changed either by aging or irradiation **(Fig 27a)**. However, it seems that protein staining is more homogeneous in young nematodes compared to old ones **(Fig 27a, protein panel, old compared to young nematodes)** which could be due to protein aggregation.

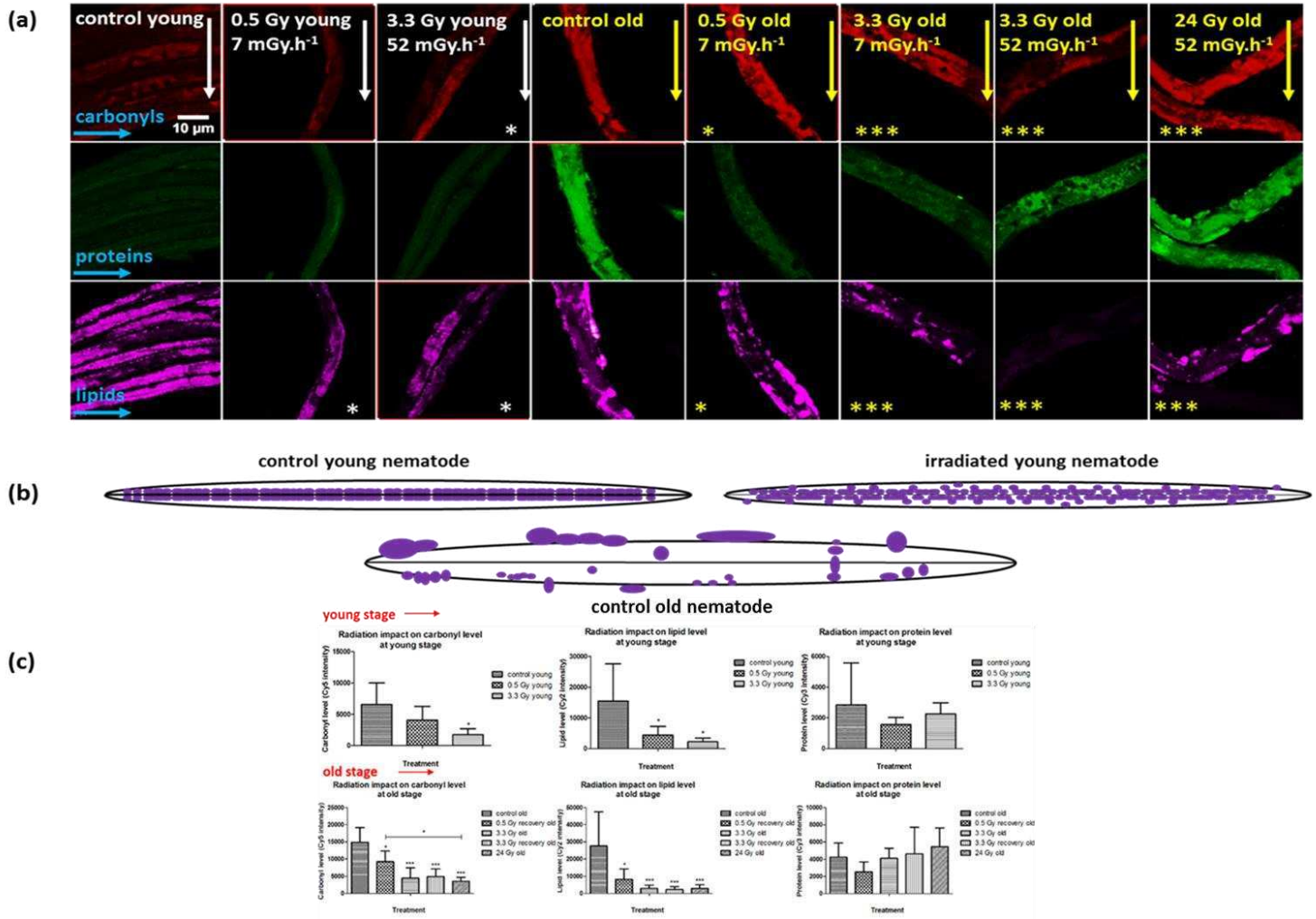


**Figure 27 – (a).** Impact of aging, radiation and recovery after different radiation treatments on biomolecule levels of *C. elegans*. Biomolecules were visualized *in situ* with the confocal microscope. Mean ± SE, n=15. **(b)** A simplified version of LDd (violet dots) in young and old nematodes made upon observation of few nematodes per condition. In addition, old nematodes display similar LDs with or without radiation. Therefore, only old control nematode was illustrated. **(c)** Biomolecular levels were measured *in situ* and quantified with ImageQuantTL on two stages, i.e. L4 and old stage. Mean ± SE, n=3, 3, 6 (young: control, 0.5 and 3.3 Gy), n=9, 6, 6, 9, 6 (old: control, 0.5 Gy, 3.3 Gy, 3.3 Gy recovery and 24 Gy). Treatments with stars are significantly different (Tukey and Kruskal-Wallis tests; * < 0.05; **<0.01; ***<0.001).

The levels of key macromolecules and their colocalization were followed from young stage (3rd day of nematode life) to old stage (19th day of nematode life), using specific differential staining **[104]** and dedicated software for signal analysis **[214]**. Results are shown in **Figure 28.** Significant differences between colocalization Pearson's coefficients, illustrating colocalization between two compounds, were observed at young (on the 3rd day), adult (on the 12th day) and old stage (on the 19th day). Colocalization of biological macromolecules was compared under all experimental conditions during adulthood **(Fig 28)**. Colocalization is considered significant if the absolute value of Pearson's coefficient ranges between 0.5 and 1. Values below this level were then considered as non-significant, and values close to zero mean lack of correlation. Generally, carbonyls co-localize best with proteins **[104]**. Here the same result is observed at young stage of *glp-1* adulthood **(Fig 28a, first row)** whatever the conditions, i.e. at adult stage (12 days) in control and at old stage in 0.5 Gy recovery (7 $mGy.h^{-1}$, 3 days of irradiation) and 24 Gy (52 $mGy.h^{-1}$, 19 days of irradiation). However, at young life stages, low dose rate (7 $mGy.h^{-1}$) irradiation tends to display higher colocalization between carbonyls and proteins than high dose rate irradiation (52 $mGy.h^{-1}$) **(Fig 28a)**. In addition, all irradiations reduced significantly carbonyl and protein colocalization in the adult stage of nematodes life (12 days) compared to control. However, irradiated adult stage (12 days) manifested something never observed: there is no colocalization between carbonyls and proteins at high dose rate (52 $mGy.h^{-1}$, in recovery and long-radiation groups), and there is even a tendency of negative colocalization between proteins and carbonyls here. Finally, different stages also impact protein-carbonyl colocalization. Indeed, reaching the old stage (19 days), control nematodes show no correlation between carbonyls and proteins.

If carbonyls do not colocalize with proteins, they might colocalize with lipids or nucleic acids. Carbonyls and lipids have usually non-significant positive correlation which is confirmed by the result of Pearson coefficient <0.5 in the young stage of control nematode **(Fig 28a, second row, middle panel)**. In contrast, radiation seems to enhance the negative correlation (still weak as <-0.5) between carbonyls and lipids **(Fig 28a, second row, middle panel)**. This negative correlation is enhanced and becomes significant at adult stage (in both control and irradiated worms) and in old controls **(Fig 28a, second row, middle panel and Fig 28b, carbonyl and lipid panel)**. However, non-significant positive correlation is observed in old worms after irradiation. At young stage and for adult controls the same phenomenon is observed between lipids and proteins **(Fig 28a, second row, left panel)**. In

contrast, at the adult stage (12 days) after chronic irradiation at 52 $mGy.h^{-1}$ and for old controls, lipids and proteins show a positive correlation **(Fig 28a, second row, left panel and Fig 28b, protein and lipid panel),** while lipids and carbonyls have a negative one **(Fig 28a, second row, middle panel and Fig 28b, carbonyl and lipid panel)**. Nucleic acids could then be the second colocalization partner of carbonyls. Indeed, carbonyls colocalize positively with nucleic acids, but at young stage (0.5 Gy) and adult controls this has not been checked. Finally, nucleic acid-protein colocalization was examined **(Fig 28a, second row, right panel)**. Proteins and RNA usually do not colocalize (Pearson's coefficient close to 0), which is the case in our conditions except for the 7 $mGy.h^{-1}$ radiation, when irradiation occurred at the young stage, i.e. 0.5 Gy young and old nematodes **(Fig 28a, second row, right panel)**.

To conclude, positive colocalization between proteins and lipids at adult and old stage excludes colocalization with carbonyls **(Fig 28b)**. However, this phenomenon requires further investigations to be elucidated.

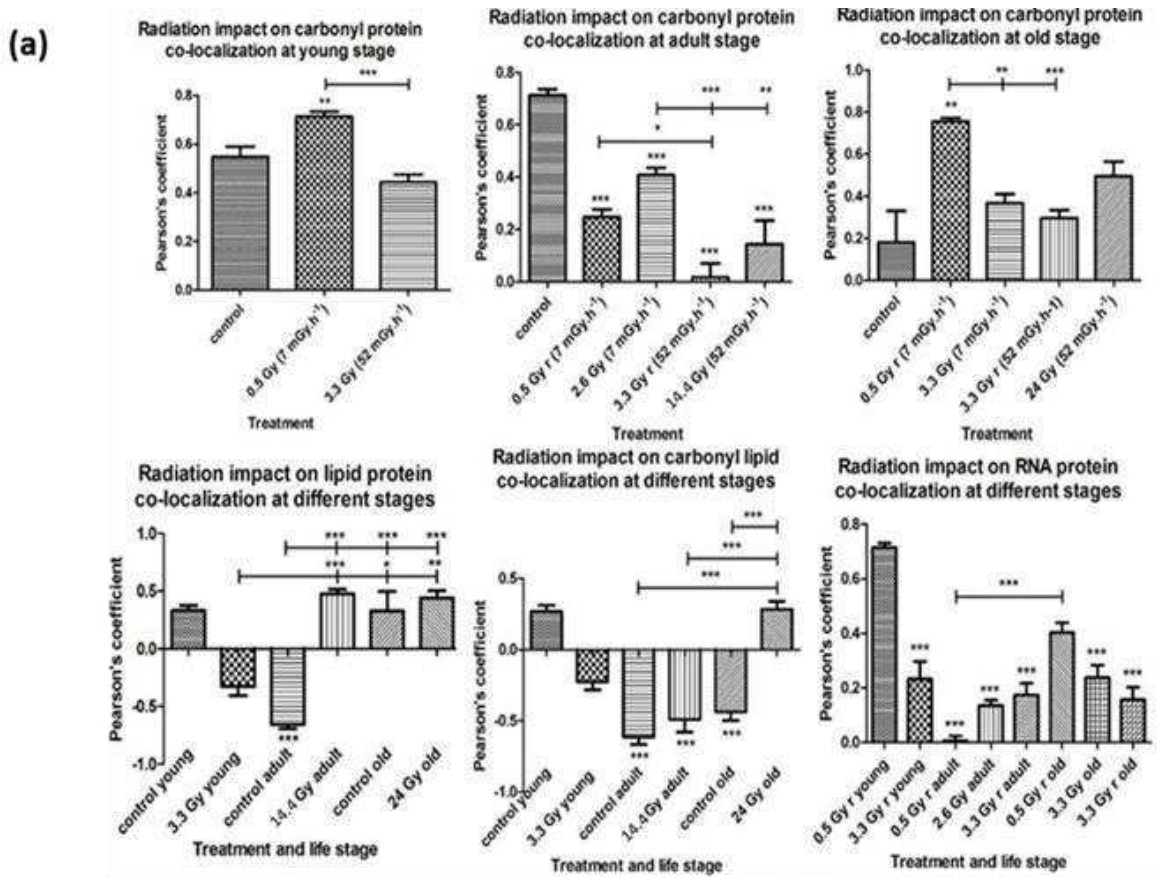


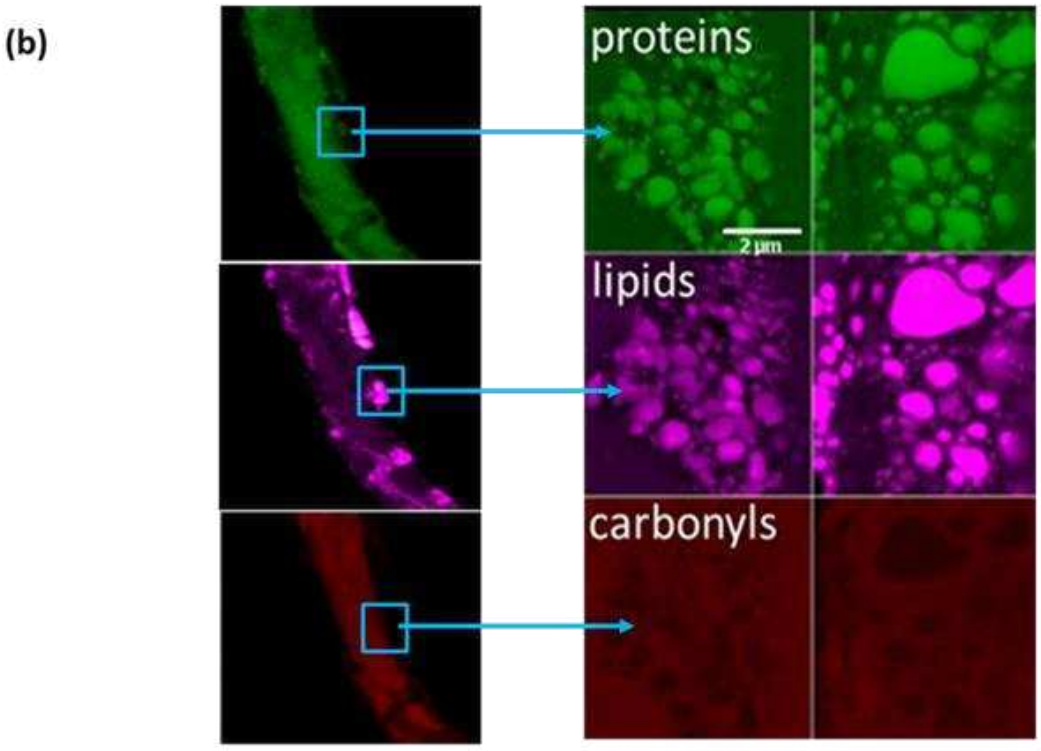


**Figure 28 – (a).** Impact of aging, radiation and recovery after radiation on colocalization between biomolecules in *C. elegans*. Colocalization was measured *via* Person's coefficient in ImageJ using JACoP plugging. Mean ± SE, n=15. Treatments with stars are significantly different (Tukey and Kruskal-Wallis tests; * < 0.05; **<0.01; ***<0.001). **(b)** Impact of aging on biomolecular colocalization in control old stage of *C. elegans*. Biomolecules were visualized *in situ* with the confocal microscope. Blue squares represent zoom zones that were magnified on the right side. Scale bar is 2 µm.

# PART VI: DISCUSSION

Discussion part will be centered on different results obtained; it will start with the new methodology we have developed **[104]**, continue with the case study of bacterial death and end with *C. elegans* aging.

Starting with the methodology, carbonylation has been used for decades as a biomarker of oxidative stress but also as a hallmark of many diseases, such as cancer **[215]** and many age-related diseases **[216]**. Carbonyl content in proteins, DNA and lipids has mostly been revealed by carbonyl derivatization with hydrazine or hydrazide compounds in cell extracts. RNA carbonylation has not yet been investigated.

Protein carbonylation, measured in extracted proteins, was shown to correlate with cellular and organism's death caused by radiation and aging **[10]**. However, the sequestration of carbonylated proteins in detergent-insoluble aggregates causes uncertainty in the quantification of protein carbonyls. Furthermore, such analysis (i) lacks the detection of heterogeneous level and distribution of carbonyls among cells and organs and (ii) does not allow for a simultaneous search for correlation between death and oxidative damage to other macromolecules, e.g. DNA, RNA and lipids.

As listed in **Table 10** for comparison with the method described in this paper, *in situ* analysis of the distribution of carbonyls and biological macromolecules (proteins, DNA, RNA and lipids) at the level of entire organisms has already been used. These methods relied on different dyes used for carbonyl and biomolecular detection and its labeling procedure (fixation – or not – of the organisms, choice of medium and concentrations of the dye (dye c), binding kinetics of the dyes and specificity of labeling) on different samples.

Regarding *in situ* carbonylation, as seen in **Table 10**, the methodology has been developed to ensure the best signal for a minimum background. First, the choice of Cy5 hydrazide (Cy5 Hz) for carbonyls derivatization **(Table 10)** (excited at 646 nm and emitting at 664 nm) ensures low auto-fluorescence background because only a few endogenous molecules emit fluorescence significantly when excited above 600 nm. Other advantage of this Hz probe are: its use at pH 7, which minimizes other chemical changes in target biomolecules of carbonylation, its good water solubility and its ability to reach lipids **[192]** and proteins **[181]**; hydrazine can reach DNA **[217]**. Moreover, the concentration of Cy5 Hz is 1-3 µM which is over 100 times lower than in a previous report **[192]**. This concentration allows accurate detection of UVC-induced carbonyls with a lowered background noise (i.e. higher sensitivity). Indeed, as the reaction

between hydrazide and carbonyls can yield side-products, reduced hydrazide concentration has been used and reaction time has been minimized. In addition, instead of PFA fixation followed by permeation, we used only permeabilization with 40 % isopropanol due to its efficacy. This has resulted in lower basal carbonylation (i.e. higher sensitivity) compared with the use of PFA **(Table 10)**, which is an external source of aldehyde **[194]**. Finally, *in situ* carbonylation detection assay has already been reduced from a few days **[193]** to 3 hours **[192]**, while our method requires only 15 to 30 minutes.

Regarding biomolecules and multiplexing methodology, this is a first article that shows direct *in situ* protein labeling **(Table 10)**, without any immunodetection steps needed to be performed. This can enable future research to visualize the protein level *in situ*. The same applies for RNA; its specific staining in cells has already been made *via in situ* hybridization fluorescence **[218]**, but RNA has not yet been visualized in total *in situ*. Therefore, this is the first paper that shows a level of RNA *in situ* at the organism level. In addition, previous studies of acute or chronic stress have focused on one or few molecular signals, e.g. DNA, lipids or proteins, but simultaneous localization of key biological macromolecules was missing. For *C. elegans* staining, DMSO or DMF **[219]** were often used to penetrate worm cuticle and diffuse inside its body, while we used alcohol which was found polyvalent towards all dyes, ensuring also the water-solubility and efficient labeling of lipids. In addition, isopropanol increased the sensitivity of the molecular probes as compared to water solubilization, due to a better permeation of *C. elegans*.

Regarding the results of carbonyl distribution associated with specific macromolecules within the body of *C.elegans,* after UVC irradiation, the spatial distribution of carbonyls over the *C. elegans* soma is coherent with previous research **[193]**, as well as the nearly perfect spatial correlation of carbonyls with proteins, and the moderate one with DNA, RNA or lipid fraction. Indeed, the carbonylation signal in nucleus is probably due to DNA bases, *e.g.* cytosine, guanine and thymine, containing carbonyl groups in their chemical structure as already proved **[217]**. Carbonylation is not supposed to increase after UV radiation, because most of the DNA damages in that case are pyrimidine dimers **[220]**. The same demonstration can be done with RNA, containing the same bases as DNA, except thymine which is replaced by uracil whose chemical structure only differs from one methyl group, thus having the same oxidative

status. A similar correlation of carbonylation and nucleic acids was expected in RNA and DNA, as shown by our data. The higher correlation of carbonylation and RNA in eggs than in worms can be due to higher abundance of RNA in eggs than in adult worms, as already published **[221]**. The slight lipid carbonylation was also observed after UV radiation, as in paraquat-treated cells **[192]**. This distribution of carbonyls over biomolecules draws attention to proteins as the main target of oxidative damage under our conditions. Moreover, this can be correlated with mortality and morbidity as observed in bacteria **[5]** and invertebrates **[91]**. In addition, colocalization between carbonyls and proteins is lower in the egg than in the worm. This can raise the possibility of a better anti-oxidant protection in the egg than in *C. elegans* soma, as it was already demonstrated that there is a reset of a protein carbonylation during reproduction in *C. elegans* **[193]**.

Finally, regarding the application of this *in situ* total carbonyl labeling methodology to assess carbonylation induction, as we have obtained a good correlation between carbonyls signal and UV light exposure time, there is no suspected loss due to protein extraction or migration through the gel **[14]**. Interestingly, the *in situ* method seems to allow the detection of protein carbonylation in protein aggregates; although aggregates make protein carbonyls less accessible to the dye, they could be partly stained *in situ* showing distinct foci. However, variability between nematodes within each condition seems important regarding the scan results. This can be either due to heterogeneity of dose delivering or due to a large number of worm analysed by this method. Indeed, worm population, even if chronogenic (an isogenic population with the same age), was synchronized over 3h but can present some difference in their initial carbonylation level and their susceptibility to produce some.

Thanks to its simplicity, our new carbonyl staining method can easily be implemented in any laboratory using standard equipment – depending on the application. The researcher can use low throughput imaging techniques (confocal, epifluorescence microscopes, etc.) or throughput fluorescence quantification techniques (Typhoon scanner, microplate readers, etc.).

In conclusion, we provide a simple-to-use protocol that permits sample preparation in a short amount of time and provides opportunity to take quantitative "snapshots" of the body-wide carbonyl distribution across major macromolecules, e.g. hypodermal and acidic lipids, RNA, DNA and proteins, in *C. elegans*. This procedure

enables monitoring of oxidative effects of noxious environmental conditions, as well as aging and disease on the whole animal scale *via in situ* carbonylation assessment.

The fundamental supposition of this thesis project is that radiation (ionizing and UV) is: (1) an environmental factor of aging and morbidity and (2) a biological mimic of aging *via* the similarity of cellular oxidative damage inflicted by ROS which is produced either by metabolism or by radiations. In the face of the formidable complexity of human aging and age-related diseases, we opted to use the most studied and simplest biological models to study cellular damage and cell death (*E. coli*) and organismal damage and aging (*C. elegans*).

Although bacterial death by UV radiation is the most extensively studied cell death phenomenon, we explore here the proximal cause and the time of cell death. We measured lethal UV dose of 100 $J.m^{-2}$ for *E. coli* based on CFU counting the following day. This dose was used acutely, on the ice during 100 s, with the effective dose rate of 1 $J.m^{-2}$. First, we wanted to test if depletion of DNA repair activity during the post-irradiation period caused death. To begin to assess possible effects of partial loss of repair activity on DNA, we monitored for 2 hours mutation rate and repair *in vivo* in *E. coli* with labeled MutL repair protein **[160]**, after lethal UV dose. Post-incubation period of 2 hours was set up based on preliminary data and on prior knowledge that after irradiation it takes 1 to 3 hours for protein neosynthesis and DNA repair **(Cvjetan et al, unpublished communication)**. Based on the number of MutL-YFP foci monitored during 2 h after irradiation, DNA repair eliminated 90-99% of DNA lesions detected by MMR. Although DNA repair proteins are required for UV resistance **[128]**, solely induced expression of DNA repair proteins is not sufficient for cell survival. The death took place despite efficient DNA repair.

Therefore, we have decided to test another potential biomarker of bacterial death induced by radiation that was repeatedly correlated with death, i.e. protein carbonylation **[5, 10, 222].** Simultaneously, we monitored the levels of proteins, lipids and DNA **[104]**. Protein carbonylation has reached a peak in 2 h after UV radiation. We have some indications that protein level is also potentially increasing, which corresponds with the post-irradiation time necessary for protein neosynthesis **(Cvjetan et al, unpublished communication)**. This increase of PC 2 h post-irradiation could be potentially explained by reduced anti-oxidant protection. Finally, deinococcal organisms with extreme resistance to UVR have increased anti-oxidant protection, which consists

largely of small cytosolic molecules (scavengers) and different proteins of anti-ROS defense **[5, 124]**. These molecules act as an anti-oxidant shield which neutralizes ROS. We have also observed changes in lipid levels and distribution after UVR. Finally, it seems that spatiotemporal changes of lipid droplets took place at bacterial edges. Those changes include brighter signal and bigger droplets 2 h after radiation. This could indicate membrane dilatation and rupture that induces membrane permeabilization and cell death. Lipid homeostasis is already correlated with the death of gram-negative bacteria **[223]**. Presumably, the key to survive is to avoid the stochasticity of membrane disintegration (permeation) that yields the leakage of key metabolites and electrolytes into the medium that stops entire metabolism. Nevertheless, for this conclusion additional studies of metabolites and electrolytes are necessary. We have noted remarkable changes in DNA during the post-irradiation time. DNA level is increased, while present more centrally and condensed, compared to the time point just after irradiation. Responding to irradiation, *E. coli* might prematurely enter metabolically, a quasi-stationary phase. This process resembles radiation-induced premature aging, i.e. cell senescence ensuing DNA damage signal as cells reach the end of their replicative lifespan *in vitro* or *in vivo* **[224]**.

The verdict – survival or death – occurs here, with UVC dose of 100 $J.m^{-2}$, within first 2 hours after radiation. The question is what makes the crucial difference for the minority of surviving cells clonally growing in the same medium having received a rather homogeneous radiation dose. It turns out that protein damage can be more critical than DNA damage because the latter is reparable by proteins and not *vice versa*. In other words, the fate of DNA (information) and proteins (function) depends on residual protein activity (remaining after radiation damage) necessary to trigger the cell recovery processes **[10, 222]**. DNA damage without protein damage **[5]** is much less lethal than protein damage without DNA damage **[141]**.

Now, this research presents further arguments that protein damage is the key target in cellular morbidity and mortality associated with UVC radiation. Preserved proteome can repair even highly damaged DNA and turn over considerable amounts of oxidized proteins. It appears that the failure of the proteome fraction responsible for the quality of the entire proteome (e.g. ribosomes, chaperons and the relevant proteases) **[141]**, is the primary cause of radiation-induced cell death in *E. coli*. Because proteins

repair DNA damage, function (proteins) rather than information (DNA) is the primary target of radiation-induced cell death.

Understanding aging is of fundamental interest in biology and medicine **[45]**, since aging and aging-related diseases (e.g. cancer and degenerative diseases) cause about 90% of deaths in developed countries. The key questions are: (i) what are the causes of aging and age-related diseases, (ii) what is the basic chemistry that triggers aging and associated diseases, (iii) which cellular mechanisms are responsible for the development of particular age-related diseases and (iv) how do the environment and life style affect aging and diseases.

Aging studies with *C. elegans* established that IIS (insulin/IGF1 signaling) and reproduction affect longevity through distinct mechanisms with a common DAF-16 mediator. Recruiting different signaling mechanisms (DAF-16, SKN-1/Nrf, oleic acid, lipase, etc.), germline ablation is enhancing immune defense, proteostasis and stress resistance. Notably, fat metabolism is profoundly altered in response to germline ablation **[225]**. We intended to explore how chronic gamma irradiation impacts sterile *glp-1 C. elegans* macromolecular damage and lifespan.

Herein, we show that *glp-1* lifespan is significantly shortened after several regimens of radiation treatments. Biochemical study of radiation-induced accelerated aging was investigated by focusing particularly on protein damage, i.e. protein carbonylation, previously shown to be correlated with aging and ionizing radiation **[5, 12]**. Carbonylation turned out to be a good biomarker of aging since old nematodes display consistently a progressive increase in accumulated protein carbonylation, in agreement with previous aging studies **[207, 226]**. However, chronic low-dose radiation treatment of *C. elegans* gave a rather unexpected result: radiation reduces carbonylation regardless the dose or duration of irradiation. All tested irradiation conditions reduce lifespan and global cellular carbonylation. Old non-irradiated nematodes (control) display the highest carbonylation levels. Carbonylation decrease by radiation could be contributed by an increased proteasomal activity of germline ablated *glp-1* worms that display highly increased caspase, trypsin, and chymotrypsin-like proteasome activities **[227]**. Chymotrypsin-like proteasomal activity is known to be induced by chronic irradiation **(Dubois et al, 2018 submitted)**. In addition, 26S proteasome regulators that reduce proteotoxic stress, e.g. rpn-6.1, have already been found upregulated following a constant mild heat stress at 25°C **[227]**. In *wt* nematodes, protein carbonylation level has

been found quite stable after chronic irradiation with an increasing proteasomal activity **(Dubois et al, 2018 submitted)**. As it was proposed **[228]** that carbonylation partially takes place in mitochondria, the relevant difference between both models could be the higher mitochondrial number in N2 than in Glp-1 (without germ cells).

Radiation also induced lipid catabolism in our experimentation, whatever the dose or the dose rate. Lipids are very important signaling molecules which constitute the cell membrane and form comprehensive energy storage. Lipid homeostasis is involved in endocrine signaling of longevity. It was already reported that germline ablation in worms alters lipid metabolism and affects longevity. Different long-lived mutants, e.g. *glp-1* mutant, have a higher level of lipids compared to *wt*. These lipids are initially dedicated to reproduction, e.g. yolk with high lipid storage vitellogenin, which does not take place in sterile mutants. In *wt* animal, they are placed in oocytes and embryos, whereas in sterile mutants (e.g. *glp-1*) they are distributed along the body cavity. SKN-1 is a nuclear protein that was reported to orchestrate lipid catabolism and increased proteasome activity in long-lived mutants **[82]**. Due to the mutation in *glp-1* gene, *C. elegans* overexpresses triglyceride lipase Lipl-4 and fatty acid desaturases. This induces autophagy, lipophagy and desaturation into healthier lipid status **[229]**. In the previous study it was shown that fatty acid desaturation, and therefore fat composition, is altered in germline-less animals **[225]**. On the other hand, our results show that lipid catabolism induced by radiation of *glp-1* nematode correlates with reduced longevity closer to *wt* nematode. To conclude, fat composition and fat content together could induce a beneficial or detrimental effect on longevity. However, lipid destruction, *via* radio-induced lipid peroxidation for instance, could mimic the lipid consumption like in *wt* nematodes and induce a standard process of aging.

Unexpectedly, we observed changes in biomolecular colocalization during radiation and aging, especially between lipids, proteins and carbonyls. From our observations and publication, among all biological macromolecules, carbonyls colocalize mostly with proteins **[104]**, from weak to strong. However, adult staged nematodes (12 days old) that were subjected to any of radiations regimens, showed no correlation between carbonyls and proteins. Furthermore, this phenomenon re-occurred in control nematodes after 7 days, but this time at old stage (19 days old). By verifying other biomolecular colocalization (carbonyls-proteins, carbonyl-lipids, carbonyls-nucleic acids, proteins-lipids, proteins- nucleic acids), some hypotheses

related to these results are: (i) the formation of “hydrophobic lipoproteins” because proteins and lipids colocalize without colocalization with carbonyls); ii) loss of homeostasis of chaperones (aggregases versus disaggregases); and (iii) loss of carbonylation observed due to stimulated autophagy and/or proteolysis. There is a 7 days delay in control sample compared to radiation treatments to form this new structure. This phenomenon appears sooner with irradiated worms, as they have a shorter lifespan with decreased lipid and carbonyl levels from beginning compared to control.

All these preliminary observations suggest that changes in protein structure, carbonylation and lipid structures and levels could be used as a potential marker of irradiation and aging. Finally, precise experimental design is necessary to verify potential biomolecular conformational changes.

# PART VII: CONCLUSIONS AND OUTLOOK

Although genetic factors play key roles in the regulation of organismal longevity and death, PTMs are also important in active processes of aging and death. A non-physiological PTM is carbonylation with the potential as relevant biomarker, due to its biological (phenotypic) effects. Stadtman singled out PC as a biomarker of oxidative damage and aging in 1992 **[12]**, while nowadays PC level shows correlation with age-related diseases (e.g. cancer) and mortality as their suspected cause **[5]**.

My conclusions and perspectives on three projects based on three initial questions and/or hypothesis are as follows:

(i) Project 1: The development of a method of *in situ* multiplex labeling, allowing visualization of carbonyl groups overlaid upon key cellular macromolecular species (protein, DNA, RNA and lipids) at the level of the whole organism (*C. elegans*) **[104]**. This is a semi-quantitative (comparative) method which means there are no SI units (e.g. nmol of carbonyls per mg of proteins) but rather arbitrary units based on fluorescence intensity. Nevertheless, this *in situ* method is suitable for comparison of carbonyl induction or reduction and validated by *in vitro* quantification that includes protein extraction followed by carbonyl labeling **[15]**. Regarding protein and RNA quantification, we did not yet make *in vitro* measurements in parallel. The method was validated also on other organisms, i.e. *E. coli* and *Tardigrade* in multiplex and carbonyl *in situ* labeling, respectively.

(ii) Project 2: Protein carbonylation is a biomarker and likely the cause of bacterial cell death by UV light. Since radiation induced-bacterial cell death was consistently correlated with protein carbonylation level **[5]**, we have monitored DNA damage and mutation rate and biomolecule (carbonyls, proteins, lipids, and DNA) levels after UV irradiation of *E coli*. We have shown that, following lethal UV exposure, most of the damage/mutations are repaired within 2 hours, while protein carbonylation remained significantly increased. In addition, we observed significant increase in protein and lipid levels. Furthermore, lipid pattern was changed from homogenous to heterogeneous pattern, which could be due to membrane alterations followed by cell death.

(iii) Project 3: As expected **[12]**, protein carbonylation was found to be a biomarker of aging of a sterile nematode mutant. However, against expectations chronic gamma irradiation decreased the level of carbonylation; this is not yet understood. The robust increase in protein carbonylation during aging is conserved regardless of

radiation, i.e. even though radiation reduced PC in young stage nematode, the same worm in old stage will display increased PC. Remarkably, we found that change in lipid metabolism is a biomarker of aging of a sterile nematode mutant and of its exposure to gamma radiation. In addition, we confirm in *C. elegans* that exposure to ionizing radiation (IR) significantly shortens the lifespan **[209]** whatever the dose and/or dose rate. One of the next challenges is to determine how chronic radiation impacts lifespan and lipid levels and pattern in other species. Moreover, it would be interesting to test whether the results of shortening the lifespan would be obtained even with shorter exposition in specific developmental stages, e.g. diakinesis. *Glp-1* regulates somatic and germline growth and differentiation; the loss of function in *glp-1* mutants induces lifespan expansion involving transcription factor such as Daf 2, Daf 12 and Daf 16, also involved in IIS pathway **[12]**. Irradiation can then play a role on one of those pathways. This puzzling result hints at still unelucidated mechanisms of stress response and protection against radiation damage, involving also Daf 16 transcription factor. In this case effects could be due to (a stimulation of) increased protection against radiation damage and/or increased clearance of damaged proteins – otherwise the lethal effect of chronic radiation would be more severe, wouldn't it? Well, finding the answer to this question will require a new project.

# PART VIII: ABSTRACT

**ROLE OF PROTEIN AND DNA DAMAGE IN BIOLOGICAL RESPONSE TO RADIATION AND AGING**

All key biological macromolecules are susceptible to carbonylation – an irreparable oxidative damage with deleterious biological consequences. Carbonyls in proteins, lipids and DNA from cell extracts have been used as a biomarker of oxidative stress and aging, but formation of insoluble aggregates by carbonylated proteins sometimes precludes their quantification. Since carbonylated proteins can correlate with morbidity and mortality, we have developed an *in situ* detection of total proteins, DNA, RNA, lipids and carbonyl groups at the level of the whole organism of the nematode *C. elegans*. The method enabled us to show that after UV irradiation, carbonylation colocalizes mainly with proteins, and was applied to improve the knowledge of mechanisms of *E. coli* cell death and *C elegans* aging.

There is a growing body of evidence that carbonylation could be the root cause of cell death and aging. To explore this possibility, we have monitored in *E. coli* DNA damage and protein carbonylation after UVC irradiation. A method that detects in real time all emerging mutations, allows the exclusion of mutations as the leading cause of UVC-induced cell death. The recovery process of DNA is nearly complete within two hours after irradiation, while UVC-induced protein carbonylation remains doubled. Our new method reveals that UVC induces also an increase in lipid levels and changes in lipid pattern which could indicate membrane permeabilization. Since cell death by membrane disintegration follows the increase in protein carbonylation, we have concluded that cell function (proteome activity) is the primary target in cell death. This is not surprising given the fact that all cellular structures and functions (e.g., DNA and membrane integrity) depend on proteome activity.

Moreover, we applied this method to explore the effects of chronic ionizing radiation of *C. elegans* on oxidative damage to its proteins. To follow the lifespan of rapidly reproducing animals after irradiation we used a conditional sterile *glp-1* mutant. Our results confirmed that: (i) increase in protein carbonylation with *C. elegans'* age establishes carbonylation as a good biomarker of aging and (ii) low-dose chronic ionizing radiation reduces the lifespan of sterile *C. elegans* whatever the dose/dose rate tested. However, there is also a rather unexpected result of reduced carbonylation after irradiation which could be explained by increased activity of proteasome in the germline ablated *glp-1* worms. In addition, radiations induced a decrease in lipid levels, whatever

the dose or the dose rate. Fat composition and fat content together could induce a beneficial or detrimental effect on longevity. All these findings are of particular importance. These parameters could become predictive biomarkers of biological consequences of radiation and aging.

In conclusion, our new procedure enables us to monitor carbonylation in *E. coli* during death and in the nematode *C. elegans* during its life cycle, including the egg stage, through all the stress and aging. That opens up a possibility that the method might be applied for *ex vivo* diagnostic detection of oxidative carbonylation in the samples of human biopsies.

# PART IX: SAŽETAK

# ULOGE OŠTEĆENJA PROTEINA I DNK U BIOLOŠKOM ODGOVORU NA ZRAČENJE I STARENJE

Biološke makromolekule su osjetljive na oksidaciju, na primjer karbonilaciju proteina koja je nepopravljivo oštećenje s pogubnim biološkim posljedicama. Budući da korelira s oksidativnim stresom i starenjem, upotrebljava se kao biomarker. Karbonilacija se događa i na ostalim biološkim makromolekulama, a osim toga karbonilirani proteini stvaraju unutarstanične agregate, što pridonosi otežanoj kvantifikaciji karboniliranih proteina. Također, svi postupci koji uključuju ekstrakciju proteina mogu prouzročiti gubitak karboniliranih proteina. Budući da postoji jasna povezanost između karboniliranih proteina, staničnog morbiditeta i smrti te da su karbonilirani proteini mogući uzrok navedenog, pojavila se potreba za vjernom kvantifikacijom i lokalizacijom na nivou stanica i tkiva. Zato smo, koristeći odgovarajuće fluorescentne molekule, razvili metodu *in situ* detekcije ukupnih proteina, DNK, RNK, lipida i karbonilnih skupina na razini cijelog organizma nematode *C. elegans*. Pokazali smo da nakon UV zračenja karbonilacija kolokalizira uglavnom s proteinima, a ova metoda je također primijenjena za poboljšanje znanja o mehanizmu smrti kod bakterije *E. coli* i starenju nematode *C. elegans*.

Postoji sve veći broj dokaza da bi karbonilacija također mogla biti i uzrok stanične smrti. Da bismo istražili ovu mogućnost, pratili smo oštećenje DNK i karbonilaciju proteina kod bakterije *E. coli* nakon UV zračenja. Metoda koja u realnom vremenu otkriva sve nove mutacije i oštećenja DNK, omogućuje isključivanje mutacija kao vodećeg uzroka stanične smrti izazvane UV zračenjem. Proces oporavka DNK je završen unutar dva sata nakon zračenja, dok se razina karbonilacije proteina inducirana zračenjem udvostruči. Naša nova metoda kod ozračenih bakterija također otkriva povećanje razine lipida i promjene u njihovom uzorku koje bi mogle ukazivati na povećanu propusnost membrane. Budući da stanična smrt prati porast karbonilacije, zaključujemo da je stanična funkcija (aktivnost proteoma) primarna meta smrti stanica. Ova spoznaja ne iznenađuje budući da stanične strukture i funkcije (kao što su npr. integritet genoma i membrana) ovise isključivo o aktivnosti proteina.

Naša metoda je također korištena za istraživanje učinaka kroničnog ionizirajućeg zračenja na životni vijek nematode *C. elegans*. Za praćenje životnog vijeka nematoda poslije zračenja smo koristili uvjetni sterilni *glp-1* mutant. Naši rezultati potvrđuju sljedeće: (i) karbonilacija je opravdan biomarker starenja budući da stare nematode

pokazuju višu razinu karbonilacije od mladih, što je očekivano i sukladno brojnim ranijim istraživanjima starenja, te (ii) kronično ionizirajuće zračenje niskim dozama smanjuje životni vijek sterilnih nematoda bez obzira na ispitivanu dozu/stopu doze. Međutim, kronično zračenje pokazalo je neočekivano smanjenje razine karbonilacije koje se može objasniti povećanom aktivnošću djelovanja proteasoma kod sterilnih nematoda. Zračenje je također izazvalo povećanje razine lipida kao odgovor na starenje te lipidni katabolizam kao odgovor na zračenje (također bez obzira na dozu). Konačno, sadržaj lipida i njihov udio mogu izazvati blagotvorno ili štetno djelovanje na dugovječnost. Ovi parametri mogu postati prediktivni biomarkeri bioloških posljedica zračenja i starenja.

U konačnici, ova metoda omogućuje praćenje karbonilacije u pojedinačnim stanicama–te prilikom stresa, starenja i bolesti tijekom cijelog životnog ciklusa nematode *C. elegans*, uključujući i stadij jajeta. Navedeno otvara put primjeni metode na *ex vivo* modelu odnosno na mogućnosti dijagnostike oksidativne karbonilacije na uzorcima ljudskih tkiva.

# REFERENCES

1. Dahm, R., *Discovering DNA: Friedrich Miescher and the early years of nucleic acid research.* Human Genetics, 2008. **122**(6): p. 565-581.
2. Holtzman, N.A., et al., *Predictive genetic testing: from basic research to clinical practice.* Science, 1997. **278**(5338): p. 602-5.
3. Pesec, M. and T. Sherertz, *Global health from a cancer care perspective.* Future Oncol, 2015. **11**(15): p. 2235-45.
4. Reisz, J.A., et al., *Effects of ionizing radiation on biological molecules--mechanisms of damage and emerging methods of detection.* Antioxid Redox Signal, 2014. **21**(2): p. 260-92.
5. Krisko, A. and M. Radman, *Protein damage and death by radiation in Escherichia coli and Deinococcus radiodurans.* Proc Natl Acad Sci U S A, 2010. **107**(32): p. 14373-7.
6. Kiang, J.G., R. Fukumoto, and N.V. Gorbunov, *Lipid Peroxidation After Ionizing Irradiation Leads to Apoptosis and Autophagy*. Lipid Peroxidation. 2012.
7. Beck, S.E., et al., *Comparison of UV-Induced Inactivation and RNA Damage in MS2 Phage across the Germicidal UV Spectrum.* Appl Environ Microbiol, 2016. **82**(5): p. 1468-1474.
8. Jaenisch, R. and A. Bird, *Epigenetic regulation of gene expression: how the genome integrates intrinsic and environmental signals.* Nat Genet, 2003. **33 Suppl**: p. 245-54.
9. Chondrogianni, N., et al., *Protein damage, repair and proteolysis.* Mol Aspects Med, 2014. **35**: p. 1-71.
10. Radman, M., *Protein damage, radiation sensitivity and aging.* DNA Repair (Amst), 2016. **44**: p. 186-92.
11. Nystrom, T., *Role of oxidative carbonylation in protein quality control and senescence.* EMBO J, 2005. **24**(7): p. 1311-7.
12. Stadtman, E.R., *Protein oxidation and aging.* Science, 1992. **257**(5074): p. 1220-4.
13. Bosshard, F., et al., *Protein oxidation and aggregation in UVA-irradiated Escherichia coli cells as signs of accelerated cellular senescence.* Environ Microbiol, 2010. **12**(11): p. 2931-45.
14. Augustyniak, E., et al., *Validation of protein carbonyl measurement: a multi-centre study.* Redox Biol, 2015. **4**: p. 149-57.
15. Pyr Dit Ruys, S., J.M. Bonzom, and S. Frelon, *Benchmarking of protein carbonylation analysis in Caenorhabditis elegans: specific considerations and general advice.* Free Radic Biol Med, 2016. **99**: p. 364-373.
16. Sansare, K., V. Khanna, and F. Karjodkar, *Early victims of X-rays: a tribute and current perception.* Dentomaxillofac Radiol, 2011. **40**(2): p. 123-5.
17. Kudriashov Iu, B., *[Main principles of radiobiology].* Radiats Biol Radioecol, 2001. **41**(5): p. 531-47.
18. Grammaticos, P.C., *Pioneers of nuclear medicine, Madame Curie.* Hell J Nucl Med, 2004. **7**(1): p. 30-1.
19. Bolus, N.E., *Basic review of radiation biology and terminology.* J Nucl Med Technol, 2001. **29**(2): p. 67-73; test 76-7.
20. Park, S.H. and J.O. Kang, *Basics of particle therapy I: physics.* Radiat Oncol J, 2011. **29**(3): p. 135-46.
21. Parisot, F., et al., *Étude mécaniste des effets transgénérationnels des radiations ionisantes alpha et gamma chez Daphnia magna*. 2015: éditeur inconnu.
22. Donya, M., et al., *Radiation in medicine: Origins, risks and aspirations.* Glob Cardiol Sci Pract, 2014. **2014**(4): p. 437-48.
23. Mehta, *Health risks of low level radiation exposures: a review.* Ind J Nucl Med., 2005. **20**: p. 29-41.
24. Suntharalingam N, P.E.B., and Hendry, J H, *Basic radiobiology.* Review of Radiation Oncology Physics, 2003: p. 399-401.
25. Goodhead, D.T., *Mechanisms for the biological effectiveness of high-LET radiations.* J Radiat Res, 1999. 40 Suppl: p. 1-13.
26. Bachi, A., I. Dalle-Donne, and A. Scaloni, *Corrections to Redox proteomics: chemical principles, methodological approaches and biological/biomedical promises.* Chem Rev, 2015. **115**(9): p. 3677.
27. Zhong, H. and H. Yin, *Role of lipid peroxidation derived 4-hydroxynonenal (4-HNE) in cancer: focusing on mitochondria.* Redox Biol, 2015. **4**: p. 193-9.
28. Pouget, J.P., et al., *Introduction to radiobiology of targeted radionuclide therapy.* Front Med (Lausanne), 2015. **2**: p. 12.
29. Strigari, L., et al., *Authors' reply to: Radiobiology as a basic and clinical medical science: what the physicists have forgotten.* Tumori, 2016. **102**(1): p. e9.
30. *The 2007 Recommendations of the International Commission on Radiological Protection. ICRP publication 103.* Ann ICRP, 2007. **37**(2-4): p. 1-332.
31. Hinton, T.G., et al., *Radiation-induced effects on plants and animals: findings of the United Nations Chernobyl Forum.* Health Phys, 2007. **93**(5): p. 427-40.

32. Harrison, F.L.A., S.L. , *Taxonomic and developmental aspects of radiosensitivity.* Digital Library, digital.library.unt.edu; crediting UNT Libraries Government Documents Department., 1996.
33. Garnier-Laplace, J., et al., *Are radiosensitivity data derived from natural field conditions consistent with data from controlled exposures? A case study of Chernobyl wildlife chronically exposed to low dose rates.* J Environ Radioact, 2013. **121**: p. 12-21.
34. *1990 Recommendations of the International Commission on Radiological Protection.* Ann ICRP, 1991. **21**(1-3): p. 1-201.
35. Howard, B.J. and C.M. Larsson, *The ERICA Integrated Approach and its contribution to protection of the environment from ionising radiation.* J Environ Radioact, 2008. **99**(9): p. 1361-3.
36. Larsson, C.M., *The FASSET framework for assessment of environmental impact of ionising radiation in European ecosystems--an overview.* J Radiol Prot, 2004. **24**(4A): p. A1-12.
37. Copplestone, D., J. Hingston, and A. Real, *The development and purpose of the FREDERICA radiation effects database.* J Environ Radioact, 2008. **99**(9): p. 1456-63.
38. Garnier-Laplace, J., et al., *A multi-criteria weight of evidence approach for deriving ecological benchmarks for radioactive substances.* J Radiol Prot, 2010. **30**(2): p. 215-33.
39. Wambersie, A., P. Smeesters, and J. Fruhling, *[Exposure to ionizing radiation: radiobiological effects and pathogenesis. 1].* Rev Med Brux, 1996. **17**(1): p. 27-38.
40. Garnier-Laplace, J., et al., *Issues and practices in the use of effects data from FREDERICA in the ERICA Integrated Approach.* J Environ Radioact, 2008. **99**(9): p. 1474-83.
41. Morgan, W.F. and W.J. Bair, *Issues in low dose radiation biology: the controversy continues. A perspective.* Radiat Res, 2013. **179**(5): p. 501-10.
42. Roh, J.Y., et al., *Ecotoxicity of silver nanoparticles on the soil nematode Caenorhabditis elegans using functional ecotoxicogenomics.* Environ Sci Technol, 2009. **43**(10): p. 3933-40.
43. Jha, A.N., *Ecotoxicological applications and significance of the comet assay.* Mutagenesis, 2008. **23**(3): p. 207-21.
44. Holliday, R., *Understanding ageing.* Philos Trans R Soc Lond B Biol Sci, 1997. **352**(1363): p. 1793-7.
45. Hsin, H. and C. Kenyon, *Signals from the reproductive system regulate the lifespan of C. elegans.* Nature, 1999. **399**(6734): p. 362-6.
46. Holliday, R., *Aging and the decline in health.* Health, 2010. **2**(6): p. 5.
47. Uno, M. and E. Nishida, *Lifespan-regulating genes in C. elegans.* NPJ Aging Mech Dis, 2016. **2**: p. 16010.
48. Schrodinger, E., *What is life?* Cambridge University Press. 1944, Cambridge.
49. Hayflick, L., *Intracellular determinants of cell aging.* Mech Ageing Dev, 1984. **28**(2-3): p. 177-85.
50. Hekimi, S., et al., *Molecular genetics of life span in C. elegans: how much does it teach us?* Trends Genet, 1998. **14**(1): p. 14-20.
51. Cumming, E., *New thoughts on the theory of disengagement.* Int J Psychiatry, 1968. **6**(1): p. 53-67.
52. Lemon, B.W., V.L. Bengtson, and J.A. Peterson, *An exploration of the activity theory of aging: activity types and life satisfaction among in-movers to a retirement community.* J Gerontol, 1972. **27**(4): p. 511-23.
53. Harris, B.N. and W. Saltzman, *Effects of aging on hypothalamic-pituitary-adrenal (HPA) axis activity and reactivity in virgin male and female California mice (Peromyscus californicus).* Gen Comp Endocrinol, 2013. **186**: p. 41-9.
54. Koltover, V.K., *Free Radical Timer of Aging: from Chemistry of Free Radicals to Systems Theory of Reliability.* Curr Aging Sci, 2017. **10**(1): p. 12-17.
55. Zs-Nagy, I., *Aging of cell membranes: facts and theories.* Interdiscip Top Gerontol, 2014. **39**: p. 62-85.
56. Short, K.R., et al., *Decline in skeletal muscle mitochondrial function with aging in humans.* Proc Natl Acad Sci U S A, 2005. **102**(15): p. 5618-23.
57. Bjorksten, J. and H. Tenhu, *The crosslinking theory of aging--added evidence.* Exp Gerontol, 1990. **25**(2): p. 91-5.
58. Kozina, L.S. and A.V. Arutjunyan, *Editorial: Denham Harman - Pioneer of the Free Radical Theory of Aging.* Curr Aging Sci, 2017. **10**(1): p. 2.
59. Harman, D., *Aging: a theory based on free radical and radiation chemistry.* J Gerontol, 1956. **11**(3): p. 298-300.
60. Richardson, R.B., *Ionizing radiation and aging: rejuvenating an old idea.* Aging (Albany NY), 2009. **1**(11): p. 887-902.
61. Johnson, H.A., *Age and Sensitivity to Radiation Life Shortening.* Radiat Res, 1964. **23**: p. 19-25.

62. Johnson, T.E. and P.S. Hartman, *Radiation effects on life span in Caenorhabditis elegans.* J Gerontol, 1988. **43**(5): p. B137-41.
63. Caratero, A., et al., *Effect of a continuous gamma irradiation at a very low dose on the life span of mice.* Gerontology, 1998. **44**(5): p. 272-6.
64. Upton, A.C., et al., *Some delayed effects of atom-bomb radiations in mice.* Cancer Res, 1960. **20(8)Pt2**: p. 1-60.
65. Calabrese, E.J. and L.A. Baldwin, *The effects of gamma rays on longevity.* Biogerontology, 2000. **1**(4): p. 309-19.
66. Little, M.P., *Cancer and non-cancer effects in Japanese atomic bomb survivors.* J Radiol Prot, 2009. **29**(2A): p. A43-59.
67. Loseva, O., et al., *Chronic Low Dose Rate Ionizing Radiation Exposure Induces Premature Senescence in Human Fibroblasts that Correlates with Up Regulation of Proteins Involved in Protection against Oxidative Stress.* Proteomes, 2014. **2**(3): p. 341-362.
68. Zhikrevetskaya, S., et al., *Effect of Low Doses (5-40 cGy) of Gamma-irradiation on Lifespan and Stress-related Genes Expression Profile in Drosophila melanogaster.* PLoS One, 2015. **10**(8): p. e0133840.
69. Maupas, E., *Modes et formes de reproduction des nématodes*. 1900.
70. Wood, W.B., *1 Introduction to C. elegans Biology*. 1988. 1988.
71. Corsi, A.K., B. Wightman, and M. Chalfie, *A Transparent Window into Biology: A Primer on Caenorhabditis elegans.* Genetics, 2015. **200**(2): p. 387-407.
72. Fielenbach, N. and A. Antebi, *C. elegans dauer formation and the molecular basis of plasticity.* Genes & Development, 2008. **22**(16): p. 2149-2165.
73. Lin, K., et al., *daf-16: An HNF-3/forkhead family member that can function to double the life-span of Caenorhabditis elegans.* Science, 1997. **278**(5341): p. 1319-22.
74. Brenner, S., *The genetics of Caenorhabditis elegans.* Genetics, 1974. **77**(1): p. 71-94.
75. Bargmann, C.I., *Beyond the connectome: how neuromodulators shape neural circuits.* Bioessays, 2012. **34**(6): p. 458-65.
76. Tissenbaum, H.A., *Using C. elegans for aging research.* Invertebrate Reproduction & Development, 2015. **59**(sup1): p. 59-63.
77. Kaletsky, R. and C.T. Murphy, *The role of insulin/IGF-like signaling in C. elegans longevity and aging.* Disease Models & Mechanisms, 2010. **3**(7-8): p. 415-419.
78. Johnson, S.C., P.S. Rabinovitch, and M. Kaeberlein, *mTOR is a key modulator of ageing and age-related disease.* Nature, 2013. **493**(7432): p. 338-345.
79. Robida-Stubbs, S., et al., *TOR signaling and rapamycin influence longevity by regulating SKN-1/Nrf and DAF-16/FoxO.* Cell metabolism, 2012. **15**(5): p. 713-724.
80. Lakowski, B. and S. Hekimi, *Determination of life-span in Caenorhabditis elegans by four clock genes.* Science, 1996. **272**(5264): p. 1010-3.
81. Back, P., B.P. Braeckman, and F. Matthijssens, *ROS in aging Caenorhabditis elegans: damage or signaling?* Oxid Med Cell Longev, 2012. **2012**: p. 608478.
82. Steinbaugh, M.J., et al., *Lipid-mediated regulation of SKN-1/Nrf in response to germ cell absence.* Elife, 2015. **4**.
83. Hosono, R., *Sterilization and growth inhibition of Caenorhabditis elegans by 5-fluorodeoxyuridine.* Exp Gerontol, 1978. **13**(5): p. 369-74.
84. Mitchell, D.H., et al., *Synchronous growth and aging of Caenorhabditis elegans in the presence of fluorodeoxyuridine.* J Gerontol, 1979. **34**(1): p. 28-36.
85. Gruber, J., et al., *Deceptively simple but simply deceptive – Caenorhabditis elegans lifespan studies: Considerations for aging and antioxidant effects.* FEBS Lett, 2009. **583**(21): p. 3377-3387.
86. Austin, J. and J. Kimble, *glp-1 is required in the germ line for regulation of the decision between mitosis and meiosis in C. elegans.* Cell, 1987. **51**(4): p. 589-99.
87. Sakashita, T., et al., *Radiation biology of Caenorhabditis elegans: germ cell response, aging and behavior.* J Radiat Res, 2010. **51**(2): p. 107-21.
88. Schumacher, B., et al., *Translational repression of C. elegans p53 by GLD-1 regulates DNA damage-induced apoptosis.* Cell, 2005. **120**(3): p. 357-68.
89. Gartner, A., et al., *A Conserved Checkpoint Pathway Mediates DNA Damage–Induced Apoptosis and Cell Cycle Arrest in C. elegans.* Molecular Cell. **5**(3): p. 435-443.
90. Takanami, T., et al., *Hyper-resistance of meiotic cells to radiation due to a strong expression of a single recA-like gene in Caenorhabditis elegans.* Nucleic Acids Research, 2000. **28**(21): p. 4232-4236.

91. Krisko, A., et al., *Extreme anti-oxidant protection against ionizing radiation in bdelloid rotifers.* Proc Natl Acad Sci U S A, 2012. **109**(7): p. 2354-7.
92. Lee, S.-J., et al., *A Werner syndrome protein homolog affects C. elegans development, growth rate, life span and sensitivity to DNA damage by acting at a DNA damage checkpoint.* Development, 2004. **131**(11): p. 2565-2575.
93. Bailly, A.P., et al., *The Caenorhabditis elegans homolog of Gen1/Yen1 resolvases links DNA damage signaling to DNA double-strand break repair.* PLoS Genet, 2010. **6**(7): p. e1001025.
94. Buisset-Goussen, A., et al., *Effects of chronic gamma irradiation: a multigenerational study using Caenorhabditis elegans.* J Environ Radioact, 2014. **137**: p. 190-197.
95. Buisset-Goussen, A., et al., *Effects of chronic gamma irradiation: a multigenerational study using Caenorhabditis elegans.* J Environ Radioact, 2014. **137**: p. 190-7.
96. Barth, J., *[Johann Wilhelm Ritter (1776-1810) and the discovery of ultraviolet irradiation 185 years ago].* Hautarzt, 1987. **38**(5): p. 301-3.
97. Beukers, R. and W. Berends, *Isolation and identification of the irradiation product of thymine.* Biochim Biophys Acta, 1960. **41**: p. 550-1.
98. Hockberger, P.E., *A History of Ultraviolet Photobiology for Humans, Animals and Microorganisms¶.* Photochemistry and Photobiology, 2002. **76**(6): p. 561-579.
99. Ikehata, H., T. Mori, and M. Yamamoto, *In Vivo Spectrum of UVC-induced Mutation in Mouse Skin Epidermis May Reflect the Cytosine Deamination Propensity of Cyclobutane Pyrimidine Dimers.* Photochem Photobiol, 2015. **91**(6): p. 1488-96.
100. D'Orazio, J., et al., *UV radiation and the skin.* Int J Mol Sci, 2013. **14**(6): p. 12222-48.
101. Diffey, B.L., *The risk of squamous cell carcinoma in women from exposure to UVA lamps used in cosmetic nail treatment.* British Journal of Dermatology, 2012. **167**(5): p. 1175-1178.
102. Silva, A.A., *Outdoor Exposure to Solar Ultraviolet Radiation and Legislation in Brazil.* Health Phys, 2016. **110**(6): p. 623-6.
103. Bykov, V.J. and K. Hemminki, *Assay of different photoproducts after UVA, B and C irradiation of DNA and human skin explants.* Carcinogenesis, 1996. **17**(9): p. 1949-55.
104. Kuzmic, M., et al., *In situ visualization of carbonylation and its co-localization with proteins, lipids, DNA and RNA in Caenorhabditis elegans.* Free Radic Biol Med, 2016. **101**: p. 465-474.
105. Diffey, B.L., *Sources and measurement of ultraviolet radiation.* Methods, 2002. **28**(1): p. 4-13.
106. Roy, C.R., H.P. Gies, and S. Toomey, *The solar UV radiation environment: measurement techniques and results.* Journal of Photochemistry and Photobiology B: Biology, 1995. **31**(1): p. 21-27.
107. Soderberg, P.G., R. Michael, and J.C. Merriam, *Maximum acceptable dose of ultraviolet radiation: a safety limit for cataract.* Acta Ophthalmol Scand, 2003. **81**(2): p. 165-9.
108. Hijnen, W.A., E.F. Beerendonk, and G.J. Medema, *Inactivation credit of UV radiation for viruses, bacteria and protozoan (oo)cysts in water: a review.* Water Res, 2006. **40**(1): p. 3-22.
109. Morton, R.A. and R.H. Haynes, *Changes in the ultraviolet sensitivity of Escherichia coli during growth in batch cultures.* J Bacteriol, 1969. **97**(3): p. 1379-85.
110. Lucas, R.M. and A.L. Ponsonby, *Ultraviolet radiation and health: friend and foe.* Med J Aust, 2002. **177**(11-12): p. 594-8.
111. de Laat, A., J.C. van der Leun, and F.R. de Gruijl, *Carcinogenesis induced by UVA (365-nm) radiation: the dose-time dependence of tumor formation in hairless mice.* Carcinogenesis, 1997. **18**(5): p. 1013-20.
112. Bandurska, H., J. Niedziela, and T. Chadzinikolau, *Separate and combined responses to water deficit and UV-B radiation.* Plant Sci, 2013. **213**: p. 98-105.
113. Marionnet, C., et al., *Diversity of biological effects induced by longwave UVA rays (UVA1) in reconstructed skin.* PLoS One, 2014. **9**(8): p. e105263.
114. Santos, A.L., et al., *Wavelength dependence of biological damage induced by UV radiation on bacteria.* Arch Microbiol, 2013. **195**(1): p. 63-74.
115. Ravanat, J.L., T. Douki, and J. Cadet, *Direct and indirect effects of UV radiation on DNA and its components.* J Photochem Photobiol B, 2001. **63**(1-3): p. 88-102.
116. Daly, M.J., et al., *Protein oxidation implicated as the primary determinant of bacterial radioresistance.* PLoS Biol, 2007. **5**(4): p. e92.
117. Zhang, M., L. Wang, and D. Zhong, *Photolyase: Dynamics and electron-transfer mechanisms of DNA repair.* Arch Biochem Biophys, 2017.
118. Jung, T., A. Höhn, and T. Grune, *The proteasome and the degradation of oxidized proteins: Part II – protein oxidation and proteasomal degradation.* Redox Biology, 2014. **2**: p. 99-104.

119. Xiong, Y., et al., *Degradation of Oxidized Proteins by Autophagy during Oxidative Stress in Arabidopsis.* Plant Physiology, 2007. **143**(1): p. 291-299.
120. Battista, J.R., A.M. Earl, and M.J. Park, *Why is Deinococcus radiodurans so resistant to ionizing radiation?* Trends Microbiol, 1999. **7**(9): p. 362-5.
121. Daly, M.J., *Death by protein damage in irradiated cells.* DNA Repair (Amst), 2012. **11**(1): p. 12-21.
122. Bouthier de la Tour, C., et al., *The abundant and essential HU proteins in Deinococcus deserti and Deinococcus radiodurans are translated from leaderless mRNA.* Microbiology, 2015. **161**(12): p. 2410-22.
123. Storl, K., C. Mund, and H. Venner, *Repair defect mutants of Proteus mirabilis. II. Excision of pyrimidine dimers from the DNA of ultraviolet-irradiated P. mirabilis wildtype and UV-sensitive mutants.* Mol Gen Genet, 1973. **124**(3): p. 259-68.
124. Daly, M.J., et al., *Small-molecule antioxidant proteome-shields in Deinococcus radiodurans.* PLoS One, 2010. **5**(9): p. e12570.
125. Lockhart, J.S. and L.C. DeVeaux, *The essential role of the Deinococcus radiodurans ssb gene in cell survival and radiation tolerance.* PLoS One, 2013. **8**(8): p. e71651.
126. Paulino-Lima, I.G., et al., *Extremely high UV-C radiation resistant microorganisms from desert environments with different manganese concentrations.* J Photochem Photobiol B, 2016. **163**: p. 327-36.
127. Han, W., et al., *Characterization and role of a 2',3'-cyclic phosphodiesterase from Deinococcus radiodurans.* Biotechnol Lett, 2017. **39**(8): p. 1211-1217.
128. Blanchard, L., et al., *Conservation and diversity of the IrrE/DdrO-controlled radiation response in radiation-resistant Deinococcus bacteria.* Microbiologyopen, 2017. **6**(4).
129. Hekimi, S., et al., *Genetics of lifespan in C. elegans: molecular diversity, physiological complexity, mechanistic simplicity.* Trends Genet, 2001. **17**(12): p. 712-8.
130. Sinha, R.P. and D.P. Hader, *UV-induced DNA damage and repair: a review.* Photochem Photobiol Sci, 2002. **1**(4): p. 225-36.
131. Foresti, M. and B. Avallone, *Only complete rejoining of DNA strand breaks after UVC allows K562 cell proliferation and DMSO induction of erythropoiesis.* J Photochem Photobiol B, 2008. **90**(1): p. 8-16.
132. Eriksson, D. and T. Stigbrand, *Radiation-induced cell death mechanisms.* Tumour Biol, 2010. **31**(4): p. 363-72.
133. Moon, Y.J., S.I. Kim, and Y.H. Chung, *Sensing and responding to UV-A in cyanobacteria.* Int J Mol Sci, 2012. **13**(12): p. 16303-32.
134. Escherich, T., *The intestinal bacteria of the neonate and breast-fed infant. 1884.* Rev Infect Dis, 1988. **10**(6): p. 1220-5.
135. Kim, H.H., et al., *Characteristics of antibiotic-resistant Escherichia coli O157:H7 in Washington State, 1984-1991.* J Infect Dis, 1994. **170**(6): p. 1606-9.
136. Peekhaus, N. and T. Conway, *What's for dinner?: Entner-Doudoroff metabolism in Escherichia coli.* J Bacteriol, 1998. **180**(14): p. 3495-502.
137. Vieira-Silva, S. and E.P. Rocha, *The systemic imprint of growth and its uses in ecological (meta)genomics.* PLoS Genet, 2010. **6**(1): p. e1000808.
138. Blount, Z.D., *The unexhausted potential of E. coli.* eLife, 2015. **4**: p. e05826.
139. Blattner, F.R., et al., *The complete genome sequence of Escherichia coli K-12.* Science, 1997. **277**(5331): p. 1453-62.
140. Daly, M.J., *A new perspective on radiation resistance based on Deinococcus radiodurans.* Nat Rev Microbiol, 2009. **7**(3): p. 237-45.
141. Krisko, A. and M. Radman, *Phenotypic and genetic consequences of protein damage.* PLoS Genet, 2013. **9**(9): p. e1003810.
142. Ternovoi, N.K., *[Effect of interferon-inducing complex on thymidine 3H-labeling of DNA, RNA and proteins of marrow cells after total X-irradiation of mice].* Ukr Biokhim Zh (1978), 1978. **50**(1): p. 98-101.
143. Chakalova, L. and G. Russev, *Comparison of repair activity in different genomic regions.* Acta Biochim Pol, 1998. **45**(1): p. 173-81.
144. Shabalkin, I.P., et al., *Delayed Consequences of Changes in DNA Synthesis in Cells Exposed to Single Irradiation at the End of S Phase of the Mitotic Cycle.* Bulletin of Experimental Biology and Medicine, 2015. **159**(4): p. 572-575.
145. Tomezak, M., et al., *A biophysical model of cell evolution after cytotoxic treatments: Damage, repair and cell response.* J Theor Biol, 2016. **389**: p. 146-158.

146. Ivanov, V.A., et al., *[DNA repair in mammalian nerve cells. I. DNA synthesis in the neocortex of rats induced by gamma irradiation].* Tsitologiia, 1987. **29**(1): p. 73-8.
147. Korbelik, M., *Some aspects of the effect of ultraviolet radiation on animal cells (Serbocroatian).* Arhiv za Higijenu Rada i Toksikologiju, 1976. **27**(3): p. 243-263.
148. Defais, M., et al., *Induction kinetics of mutagenic DNA repair activity in E. coli following ultraviolet irradiation.* Molecular and General Genetics MGG, 1976. **148**(2): p. 125-130.
149. Manda, K., et al., *Radiation-induced cognitive dysfunction and cerebellar oxidative stress in mice: protective effect of alpha-lipoic acid.* Behav Brain Res, 2007. **177**(1): p. 7-14.
150. Dalle-Donne, I., et al., *Protein carbonylation in human diseases.* Trends Mol Med, 2003. **9**(4): p. 169-76.
151. Lim, Y.B., et al., *Proteomic identification of radiation response markers in mouse intestine and brain.* Proteomics, 2011. **11**(7): p. 1254-63.
152. Barrett, D.M., et al., *Inhibition of protein-tyrosine phosphatases by mild oxidative stresses is dependent on S-nitrosylation.* J Biol Chem, 2005. **280**(15): p. 14453-61.
153. Hong, M., et al., *Mechanism of genotoxicity induced by targeted cytoplasmic irradiation.* Br J Cancer, 2010. **103**(8): p. 1263-8.
154. Madian, A.G. and F.E. Regnier, *Proteomic identification of carbonylated proteins and their oxidation sites.* J Proteome Res, 2010. **9**(8): p. 3766-80.
155. Temple, A., T.Y. Yen, and S. Gronert, *Identification of specific protein carbonylation sites in model oxidations of human serum albumin.* J Am Soc Mass Spectrom, 2006. **17**(8): p. 1172-80.
156. Levine, R.L., *Carbonyl modified proteins in cellular regulation, aging, and disease.* Free Radic Biol Med, 2002. **32**(9): p. 790-6.
157. Figueroa-Gonzalez, G. and C. Perez-Plasencia, *Strategies for the evaluation of DNA damage and repair mechanisms in cancer.* Oncol Lett, 2017. **13**(6): p. 3982-3988.
158. Arutyunyan, R., et al., *Comet-FISH using peptide nucleic acid probes detects telomeric repeats in DNA damaged by bleomycin and mitomycin C proportional to general DNA damage.* Mutagenesis, 2004. **19**(5): p. 403-8.
159. Frelon, S., et al., *High-Performance Liquid Chromatography−Tandem Mass Spectrometry Measurement of Radiation-Induced Base Damage to Isolated and Cellular DNA.* Chemical Research in Toxicology, 2000. **13**(10): p. 1002-1010.
160. Elez, M., et al., *Seeing mutations in living cells.* Curr Biol, 2010. **20**(16): p. 1432-7.
161. Fernandez, J.L., et al., *Application of FISH for in situ detection and quantification of DNA breakage.* Cytogenet Cell Genet, 1998. **82**(3-4): p. 251-6.
162. Cortes-Gutierrez, E.I., et al., *Use of the DBD-FISH technique for detecting DNA breakage in response to high doses of X-rays.* Radiat Environ Biophys, 2014. **53**(4): p. 713-8.
163. Santos, C.R., et al., *Cloning and sequencing of a full-length sea bream (Sparus aurata) beta-actin cDNA.* Comp Biochem Physiol B Biochem Mol Biol, 1997. **117**(2): p. 185-9.
164. Glei, M., G. Hovhannisyan, and B.L. Pool-Zobel, *Use of Comet-FISH in the study of DNA damage and repair: review.* Mutat Res, 2009. **681**(1): p. 33-43.
165. Yang, Z.A., et al., *Comparative investigation on spindle behavior and MPF activity changes during oocyte maturation between gynogenetic and amphimictic crucian carp.* Cell Res, 1999. **9**(2): p. 145-54.
166. Pilch, D.R., et al., *Characteristics of gamma-H2AX foci at DNA double-strand breaks sites.* Biochem Cell Biol, 2003. **81**(3): p. 123-9.
167. Kuo, L.J. and L.X. Yang, *Gamma-H2AX - a novel biomarker for DNA double-strand breaks.* In Vivo, 2008. **22**(3): p. 305-9.
168. Hagiwara, Y., et al., *3D-structured illumination microscopy reveals clustered DNA double-strand break formation in widespread γH2AX foci after high LET heavy-ion particle radiation.* Oncotarget, 2017. **8**(65): p. 109370-109381.
169. Cucinotta, F.A., et al., *Biochemical kinetics model of DSB repair and induction of gamma-H2AX foci by non-homologous end joining.* Radiat Res, 2008. **169**(2): p. 214-22.
170. Redon, C.E., et al., *gamma-H2AX as a biomarker of DNA damage induced by ionizing radiation in human peripheral blood lymphocytes and artificial skin.* Adv Space Res, 2009. **43**(8): p. 1171-1178.
171. Hanasoge, S. and M. Ljungman, *H2AX phosphorylation after UV irradiation is triggered by DNA repair intermediates and is mediated by the ATR kinase.* Carcinogenesis, 2007. **28**(11): p. 2298-2304.
172. Lee, Y.-J., et al., *An in vivo analysis of MMC-induced DNA damage and its repair.* Carcinogenesis, 2006. **27**(3): p. 446-453.

173. Modrich, P., *Mechanisms and biological effects of mismatch repair.* Annu Rev Genet, 1991. **25**: p. 229-53.
174. Smith, J. and P. Modrich, *Mutation detection with MutH, MutL, and MutS mismatch repair proteins.* Proceedings of the National Academy of Sciences of the United States of America, 1996. **93**(9): p. 4374-4379.
175. Keller, R.J., et al., *Immunochemical detection of oxidized proteins.* Chem Res Toxicol, 1993. **6**(4): p. 430-3.
176. Carty, J.L., et al., *The effects of vitamin C supplementation on protein oxidation in healthy volunteers.* Biochem Biophys Res Commun, 2000. **273**(2): p. 729-35.
177. Wehr, N.B. and R.L. Levine, *Quantification of protein carbonylation.* Methods Mol Biol, 2013. **965**: p. 265-81.
178. Dalle-Donne, I., et al., *Protein carbonylation: 2,4-dinitrophenylhydrazine reacts with both aldehydes/ketones and sulfenic acids.* Free Radic Biol Med, 2009. **46**(10): p. 1411-9.
179. Mohanty, J.G., et al., *A fluorimetric semi-microplate format assay of protein carbonyls in blood plasma.* Anal Biochem, 2010. **400**(2): p. 289-94.
180. Tamarit, J., et al., *Analysis of oxidative stress-induced protein carbonylation using fluorescent hydrazides.* J Proteomics, 2012. **75**(12): p. 3778-88.
181. Baraibar, M., R. Ladouce, and B. Friguet, *Oxi-DIGE: A novel proteomic approach for detecting and quantifying carbonylated proteins.* Free Radic Biol Med, 2014. **75 Suppl 1**: p. S23.
182. Maisonneuve, E., et al., *Carbonylated proteins are detectable only in a degradation-resistant aggregate state in Escherichia coli.* J Bacteriol, 2008. **190**(20): p. 6609-14.
183. Dasgupta, A., et al., *Increased carbonylation, protein aggregation and apoptosis in the spinal cord of mice with experimental autoimmune encephalomyelitis.* ASN Neuro, 2013. **5**(1): p. e00111.
184. Glei, M. and W. Schlormann, *Analysis of DNA damage and repair by comet fluorescence in situ hybridization (Comet-FISH).* Methods Mol Biol, 2014. **1094**: p. 39-48.
185. Nagaso, H., et al., *Simultaneous detection of RNA and protein by in situ hybridization and immunological staining.* J Histochem Cytochem, 2001. **49**(9): p. 1177-82.
186. Zhang, Z., et al., *High urea and NaCl carbonylate proteins in renal cells in culture and in vivo, and high urea causes 8-oxoguanine lesions in their DNA.* Proc Natl Acad Sci U S A, 2004. **101**(25): p. 9491-6.
187. Colombo, G., et al., *Oxidative damage in human gingival fibroblasts exposed to cigarette smoke.* Free Radic Biol Med, 2012. **52**(9): p. 1584-96.
188. Dasgupta, A., J. Zheng, and O.A. Bizzozero, *Protein carbonylation and aggregation precede neuronal apoptosis induced by partial glutathione depletion.* ASN Neuro, 2012. **4**(3).
189. Oberbach, A., et al., *Free fatty acid palmitate impairs the vitality and function of cultured human bladder smooth muscle cells.* PLoS One, 2012. **7**(7): p. e41026.
190. Lazarus, R.C., et al., *Protein carbonylation after traumatic brain injury: cell specificity, regional susceptibility, and gender differences.* Free Radic Biol Med, 2015. **78**: p. 89-100.
191. Mukherjee, K., et al., *Detection of oxidative stress-induced carbonylation in live mammalian cells.* Free Radic Biol Med, 2015. **84**: p. 11-21.
192. Vemula, V., Z. Ni, and M. Fedorova, *Fluorescence labeling of carbonylated lipids and proteins in cells using coumarin-hydrazide.* Redox Biol, 2015. **5**: p. 195-204.
193. Goudeau, J. and H. Aguilaniu, *Carbonylated proteins are eliminated during reproduction in C. elegans.* Aging Cell, 2010. **9**(6): p. 991-1003.
194. Possanzini, M., et al., *Determination of low boiling aldehydes in air and exhaust gases by using annular denuders combined with HPLC techniques.* Chromatographia, 1987. **23**(11): p. 829-834.
195. Stiernagle, T., *Maintenance of C. elegans.* WormBook, 2006: p. 1-11.
196. Bernstein, J.A., et al., *A pilot study to investigate the effects of combined dehumidification and HEPA filtration on dew point and airborne mold spore counts in day care centers.* Indoor Air, 2005. **15**(6): p. 402-7.
197. Najafi, M., et al., *The mechanisms of radiation-induced bystander effect.* J Biomed Phys Eng, 2014. **4**(4): p. 163-72.
198. Zimmermann, T., *Spectral imaging and linear unmixing in light microscopy.* Adv Biochem Eng Biotechnol, 2005. **95**: p. 245-65.
199. Klapper, M., et al., *Fluorescence-based fixative and vital staining of lipid droplets in Caenorhabditis elegans reveal fat stores using microscopy and flow cytometry approaches.* J Lipid Res, 2011. **52**(6): p. 1281-93.

200. Saint-Ruf, C., et al., *Reliable detection of dead microbial cells by using fluorescent hydrazides.* Appl Environ Microbiol, 2010. **76**(5): p. 1674-8.
201. Cox, M.M. and J.R. Battista, *Deinococcus radiodurans - the consummate survivor.* Nat Rev Microbiol, 2005. **3**(11): p. 882-92.
202. Kapuscinski, J. and B. Skoczylas, *Fluorescent complexes of DNA with DAPI 4',6-diamidine-2-phenyl indole.2HCl or DCI 4',6-dicarboxyamide-2-phenyl indole.* Nucleic Acids Res, 1978. **5**(10): p. 3775-99.
203. Rochette, P.J., et al., *UVA-induced cyclobutane pyrimidine dimers form predominantly at thymine–thymine dipyrimidines and correlate with the mutation spectrum in rodent cells.* Nucleic Acids Research, 2003. **31**(11): p. 2786-2794.
204. Talukder, A.A. and A. Ishihama, *Dps Is a Stationary Phase-Specific Protein of <i>Escherichia coli</i> Nucleoid.* Advances in Microbiology, 2014. **Vol.04No.15**: p. 10.
205. Pletnev, P., et al., *Survival guide: Escherichia coli in the stationary phase.* Acta Naturae, 2015. **7**(4): p. 22-33.
206. Hansen, M., T. Flatt, and H. Aguilaniu, *Reproduction, Fat Metabolism, and Lifespan – What Is the Connection?* Cell metabolism, 2013. **17**(1): p. 10-19.
207. Stadtman, E.R., *Protein oxidation and aging.* Free Radic Res, 2006. **40**(12): p. 1250-8.
208. Rikans, L.E. and K.R. Hornbrook, *Lipid peroxidation, antioxidant protection and aging.* Biochimica et Biophysica Acta (BBA) - Molecular Basis of Disease, 1997. **1362**(2–3): p. 116-127.
209. Upton, A.C., et al., *Some Delayed Effects of Atom-Bomb Radiations in Mice.* Cancer Res, 1960. **20**(8 Part 2): p. 1-60.
210. Yasunari, T.J., et al., *Cesium-137 deposition and contamination of Japanese soils due to the Fukushima nuclear accident.* Proc Natl Acad Sci U S A, 2011. **108**(49): p. 19530-4.
211. Berman, J.R. and C. Kenyon, *Germ-Cell Loss Extends C. elegans Life Span through Regulation of DAF-16 by kri-1 and Lipophilic-Hormone Signaling.* Cell, 2006. **124**(5): p. 1055-1068.
212. Mancuso, M., et al., *Acceleration of atherogenesis in ApoE-/- mice exposed to acute or low-dose-rate ionizing radiation.* Oncotarget, 2015. **6**(31): p. 31263-71.
213. Maniere, X., et al., *High transcript levels of heat-shock genes are associated with shorter lifespan of Caenorhabditis elegans.* Exp Gerontol, 2014. **60**: p. 12-7.
214. Bolte, S. and F.P. Cordelieres, *A guided tour into subcellular colocalization analysis in light microscopy.* J Microsc, 2006. **224**(Pt 3): p. 213-32.
215. Martin, F.A., et al., *Hepatocellular carcinoma protein carbonylation in virus C and metabolic syndrome patients.* Free Radic Biol Med, 2014. **75 Suppl 1**: p. S40.
216. Barreiro, E. and S.N. Hussain, *Protein carbonylation in skeletal muscles: impact on function.* Antioxid Redox Signal, 2010. **12**(3): p. 417-29.
217. Luo, S. and N.B. Wehr, *Protein carbonylation: avoiding pitfalls in the 2,4-dinitrophenylhydrazine assay.* Redox Rep, 2009. **14**(4): p. 159-66.
218. Mannack, L.V., S. Eising, and A. Rentmeister, *Current techniques for visualizing RNA in cells.* F1000Res, 2016. **5**.
219. Hekimi, S., *A neuron-specific antigen in C. elegans allows visualization of the entire nervous system.* Neuron, 1990. **4**(6): p. 855-65.
220. Rochette, P.J., et al., *Pyrimidine (6-4) pyrimidone photoproduct mapping after sublethal UVC doses: nucleotide resolution using terminal transferase-dependent PCR.* Photochem Photobiol, 2006. **82**(5): p. 1370-6.
221. Ly, K., S.J. Reid, and R.G. Snell, *Rapid RNA analysis of individual Caenorhabditis elegans.* MethodsX, 2015. **2**: p. 59-63.
222. Krisko, A. and M. Radman, *Biology of extreme radiation resistance: the way of Deinococcus radiodurans.* Cold Spring Harb Perspect Biol, 2013. **5**(7).
223. Sutterlin, H.A., et al., *Disruption of lipid homeostasis in the Gram-negative cell envelope activates a novel cell death pathway.* Proc Natl Acad Sci U S A, 2016. **113**(11): p. E1565-74.
224. Rajarajacholan, U.K. and K. Riabowol, *Aging with ING: a comparative study of different forms of stress induced premature senescence.* Oncotarget, 2015. **6**(33): p. 34118-27.
225. Goudeau, J., et al., *Fatty acid desaturation links germ cell loss to longevity through NHR-80/HNF4 in C. elegans.* PLoS Biol, 2011. **9**(3): p. e1000599.
226. Adachi, H., Y. Fujiwara, and N. Ishii, *Effects of oxygen on protein carbonyl and aging in Caenorhabditis elegans mutants with long (age-1) and short (mev-1) life spans.* J Gerontol A Biol Sci Med Sci, 1998. **53**(4): p. B240-4.

227. Vilchez, D., et al., *RPN-6 determines C. elegans longevity under proteotoxic stress conditions.* Nature, 2012. **489**(7415): p. 263-8.
228. Aguilaniu, H., et al., *Asymmetric inheritance of oxidatively damaged proteins during cytokinesis.* Science, 2003. **299**(5613): p. 1751-3.
229. Ackerman, D. and D. Gems, *The mystery of C. elegans aging: an emerging role for fat. Distant parallels between C. elegans aging and metabolic syndrome?* Bioessays, 2012. **34**(6): p. 466-71.

# CURICCULUM VITAE

# Mira Kuzmić

*Curriculum Vitae*

*11 Avenue Calendal*
*13009 Marseille*
*fr +33 6 32 45 39 74*
*mira.kuzmic@gmail.com*

***Developer of innovative biomarker assays***

## Skills

| | |
|---|---|
| Biomarker assays | *in situ* detection of biomolecules (proteins, RNA, DNA and lipids) and carbonyls in whole organism **[see Kuzmic 2016 ]**, immunofluorescence, ELISA |
| Organisms | cancer cell lines, *C. elegans*, *Tardigrada*, *E. coli* |
| Protein analysis | protein electrophoresis (SDS –PAGE), western blot, dot blot, statistical analyses in GraphPad |
| Molecular biology | plasmid and chromosomal DNA isolation, DNA cutting, DNA ligation, transformation, siRNA, nucleic acids electrophoresis, PCR, conjugational transfer, transduction, transposition, RNA isolation, RT-PCR, qPCR |
| Imaging | standard fluorescence microscopy, confocal microscopy, spectral imaging |
| Languages | English (C1 Cambridge certificate), Slovenian (B2 Slovenian certificate), French (B1 Delf certificate), Croatian (native language) |

## Assay development (and corresponding publication)

Co-inventor of a multiplex technique to reveal carbonylation *in situ*, along with co-detection of other biomolecules (proteins, RNA, DNA and lipids). Published in:
**Kuzmic, M**., et al., *In situ visualization of carbonylation and its colocalization with proteins, lipids, DNA and RNA in Caenorhabditis elegans*. **Free Radic Biol Med**, 2016. 10(16): p. 31029-2.

## Education and work experience

| | |
|---|---|
| 2015-2017 | **Research 2** at Institute for Radiological Protection and Nuclear Safety, Cadarache, France with Sandrine Frelon.<br>Projects: Chronic gamma irradiation impact on aging of *C. elegans.* |
| 2011-2014 | **Research 1** at Mediterranean Institute for Life Sciences (MedILS), Split, Croatia with Miroslav Radman.<br>Projects: General carcinogenesis; Studies of mechanism of death in *E. coli*. |
| 2011 | **Graduated with Distinction in Biochemistry**, Faculty of Chemistry and Chemical Technology, Ljubljana, Slovenia.<br>Project: Role of *rmoA* gene in bacteria *E. coli*. |

## References

| | |
|---|---|
| Dr. Christelle Adam Guillermin | Researcher and Head of laboratory at Institute for Radiological Protection and Nuclear Safety;<br>phone: +33 4 42 19 94 01; e-mail: christelle.adam-guillermin@irsn.fr |
| Dr. Jacqueline Garnier Laplace | Head of Department on research and expertise on environmental risks at Institute for Radiological Protection and Nuclear Safety;<br>phone: +33 1 58 35 94 19; e-mail: jacqueline.garnier-laplace@irsn.fr |
| Prof. Merica Glavina-Durdov | Leader of doctoral study Biology of Neoplasms, School of Medicine, Split, Croatia. phone: +385 21 556 536; e-mail: merigdst@yahoo.co.uk |